Integrated Hydrological CFD Modelling Approach for Simulating Bacteria in Stormwater Ponds

by

Farzam Allafchi
BSc, Bu Ali Sina University, 2009
MSc, Malek Ashtar University of Technology, 2012

A Dissertation Submitted in Partial Fulfillment
of the Requirements for the Degree of

DOCTOR OF PHILOSOPHY

in the Department of Mechanical Engineering

Supervisory Committee

Integrated Hydrological CFD Modelling Approach for Simulating Bacteria In Stormwater Ponds

by

Farzam Allafchi
BSc, Bu Ali Sina University, 2009
MSc, Malek Ashtar University of Technology, 2012

Supervisory Committee

Dr. Caterina Valeo (Department of Mechanical Engineering)
Supervisor

Dr. Rustom Bhiladvala (Department of Mechanical Engineering)
Departmental Member

Dr. Tara Troy (Department of Civil Engineering)
Internal Member

Abstract

Reusing stormwater is a sustainable approach that a lot of cities around the world, including cities in Canada, are developing to improve local and regional water resources. For this purpose, water is typically withdrawn from stormwater ponds (large urban infrastructure that retain stormwater) and used for applications that require less than pristine water quality. However, the large size of these ponds along with the heterogeneity in water quality internally, make the withdrawal location from these ponds for reusable stormwater critically important. Also due to the large sizes of these ponds, collecting data throughout the pond to determine the optimal location for withdrawal is not practical. Modelling however, can provide a more practical means of studying contaminant distribution within the pond over time in order to identify the withdrawal location, among other valuable information. In this dissertation, a modelling approach was developed that simulates fate and transport of bacteria in stormwater ponds after rainstorm events. The model was run to simulate bacteria in the Inverness stormwater pond, which is a large T-shaped pond located in southeast of the City of Calgary, Alberta, Canada. The model has two components: a hydrological component and a Computational Fluid Dynamics (CFD) component. The hydrological component calculates the stormwater runoff of the subbasins of the catchment draining into the pond. The results were compared with collected data and good agreement was observed. Then, the results were fed to the CFD component as input in order to simulate the distribution of contamination brought in by the local hydrology.

The CFD component simulates the hydrodynamics of the pond 3-dimensionally. The model was run based on collected data from the pond and multiple versions of the model were developed with regard to free-surface and particulate-attached bacteria transport. In order to address a common issue with hydro-environmental models – being difficult to validate - the model was validated in two ways. First, an instrument was designed and built to measure fluid flow velocity magnitude and direction in the pond. Once calibrated, it was deployed to the pond and the flow field was measured at multiple locations for validation purposes. Second, a non-dimensional number was introduced allowing a comparison between the bacteria concentration data from collected data and that of modelling result in multiple locations of the pond. In both of the validations, good agreement with collected data was observed.

A volume of Fluid model and sediment transport model were integrated into the model, which allowed consideration of free-surface effects and for modeling wider range of bacteria, respectively. The model was used to identify the optimal location for water withdrawal for reuse. The middle of the pond, where the three wings join and near the surface, was located as the optimal location due to the lowest bacteria concentration.

In an attempt to improve the water quality in the optimal location, strategic tree planting on the north bank of the West wing was studied. It was shown that the trees can reduce the transport of bacteria from the most contaminated location to the withdrawal location. The model was also used to study the impact of some of the important assumptions and environmental factors, such as rain and wind, on bacteria distribution. Wind was found to play a crucial role in the bacteria distribution in the pond.

Table of Contents

List of Tables

List of Figures

Acknowledgments

First of all, I would like to thank my supervisor, Dr. Caterina Valeo for giving me the opportunity to pursue my PhD under her supervision. Dr. Valeo has been an ideal thesis supervisor offering me advice, support and most importantly encouragement. By her guidance and support throughout the last five years, she made this work possible. Dr. Valeo gave me enough independence to find the direction of my research, which I really appreciate. It took me a relatively long time to find the direction of the research, and her patience during that time was appreciable. I am extremely grateful that she took me on as a student and continued to have faith in me over the years.

I greatly appreciate Dr. jianxun He at the University of Calgary, for her great feedback and advice during my PhD. I have benefited greatly from her knowledge and meticulous editing.

I also gratefully acknowledge Alberta Innovates for funding this research, grant number RES#0030866, and the National Research Council of Canada (grant number CRDPJ 520869 – 17). This work would not have been possible without their funding.

Finally, I would like to thank Dr. N. Neumann at the University of Alberta for fund acquisition; Drs. A. Chu and D. Bethune at the University of Calgary for helping me with data collection; Drs. B. Moa and M. Rahimpour, at the University of Victoria, for helping me with parallel computing; Mr. G. Shirakov for helping with calibration experiment; Mr. B. Kent at the University of Victoria for IT issues; and finally I would like to thank my supervisory committee.

Dedication

This dissertation is dedicated to four beloved people who have meant and continue to mean so much to me. First and foremost, to my mother, whose support, encouragement and constant love have sustained me throughout my life.

Next, my father who was my inspiration to pursue my doctoral degree. Although he is no longer of this world, his memories continue to regulate my life.

Last but not least, I am dedicating this to my beloved sister and brother who supported me throughout the entire doctoral program. I am truly thankful for having you in my life.

1. Introduction

1.1 Background and motivation

More than half of the world's population lives in urban areas and the number is anticipated to increase to 68% by the year 2050 (United Nations, 2018). On the other hand, most of the world is anticipated to be exposed to water scarcity due to climate change (Gosling and Arnell, 2016). Depletion of water resources along with the population growth and climate change urges many regions in the world to think of alternative water sources for reuse, specifically for applications that require less than pristine water quality (He et al., 2008). Reusing stormwater is a water resources management plan that is used for overcoming water scarcity problems as well as contributing to climate change mitigation in cities (Rodríguez-sinobas et al., 2018). Therefore, stormwater retention ponds are one of the most viable sources of stormwater for large scale reuse. However, there are some human health concerns regarding stormwater quality, particularly over the pathogens associated with the stormwater (Lundy et al., 2018).

Waterborne pathogenic microorganisms are very diverse and thus difficult to quantify. Therefore, current microbiological water quality studies monitor fecal indicator bacteria (FIB). FIB lives in abundance in human and warm-blooded animals' intestine, and the FIB found in the aquatic environment originates from direct or indirect release of human and the animals' feces. FIBs are used as indictor for pathogenic microorganism presence in the aquatic environment because it is easier to test for them as compared to the pathogens (de Brauwere et al., 2014a). *E.coli* and fecal coliforms are considered to be heavily associated

with gastrointestinal outbreaks and thus, used as indicator bacteria to assess contamination levels in water (Wu et al., 2019).

Stormwater ponds have been considered for stormwater reuse at large scales. However, previous studies on the ponds show that they are heterogeneous with regard to bacteria concentration (He, 2009). Therefore, the optimal location for withdrawal would be the location with the lowest concentration of bacteria. This requires continuous or intermittent water quality monitoring of the pond water. However, assessing the bacteria levels through measurement is often not practical for a variety of reasons including accessibility, spatial scale, and the variability in each of the multitude of environmental factors that may affect bacteria and pathogen levels over space and time. A more cost-effective alternative is to develop a computational model to simulate bacteria in the ponds.

There are numerous models developed for simulating water quality of runoff water from watersheds (Vanaei et al., 2021; Shrestha and Wang, 2019). The models generally include fate and transport of FIBs. To be specific, they generally integrate a decay model into the hydrological models (de Brauwere et al., 2014a). Most of the models are 1- or 2-dimensional (Aguilera et al., 2018; Wang et al., 2018; Zheng et al., 2011; Babaeyan-Koopaei et al., 2003), which can be used as a cost effective method when 1- or 2-dimensional assumptions are reasonable. However, simulating bacteria inside a water body, such as stormwater ponds, requires a 3-dimensional model. There are only a few models that use Computational Fluid Dynamics (CFD) to simulate bacteria 3-dimensionally in water bodies. CFD models are relatively more computationally expensive. However, they provide a wider array of outcomes and possibilities that can be

used for engineering design, while avoiding the inaccuracies associated with 1- and 2-dimensional assumptions. Vergeynst et al. (2012) used CFD to simulate fate and transport of *E.coli* in stormwater ponds considering attachment of the bacteria and settling. However, the study neglected convection and mainly focused on fate and settling, which is valid only under certain circumstances. Shilton and Mara (2005) developed a 3-dimensional CFD model to investigate the efficiency of waste stabilization ponds. For this purpose, they incorporated a first order decay model (a commonly used fate model) with the CFD model and modeled a variety of ponds configurations. They were primarily interested in the bacteria concentration in the inlet and outlet, and fate was calculated based on the residence time calculated by CFD. Similarly, fecal coliform levels in waste stabilization ponds were simulated using 3-dimensional CFD models (Shilton et al. 2008; Shilton and Harrison, 2003; Shilton, 2000), which highlights the capability of CFD models for simulating fate and transport of bacteria in water bodies. In another study (Wu and Chen, 2011), a first order kinetic decay was also integrated into a CFD model to simulate the biological oxygen demand (BOD) in an anaerobic lagoon. Adopting a similar approach, BOD concentration at the outlet was calculated using the residence time.

Although crucial impact of wind on the flow field of water bodies was highlighted previously (Abbasi et al., 2016), all of the above mentioned studies neglected wind effects. In addition, all of the above mentioned models assumed steady state conditions, which may be a reasonable assumption only for certain problems. Simulating bacteria in stormwater ponds requires unsteady modeling due to change in inflow and outflow. Also, wind has to be taken into account.

The bacteria fate and transport models often face two main challenges. First, model verification is a challenge due to lack of data, and the models are often left without validation (de Brauwere et al., 2014a). Second, these type of models are among process-based models and have numerous assumptions. If the assumptions are left invalidated, it might lead to significant uncertainties in the results. It was found that the challenges that the models face are poorly investigated and needs to be studied more closely.

The hydrodynamic part of the hydro-environmental models plays an important role in the modelling outcome and needs to be validated. There are some instruments available for quantifying the flow field needed for validation. However, some of them are designed primarily for measuring relatively low speed flows, and thus, are only used to measure groundwater flow velocities (Labaky et al., 2009; Melville et al., 1985; and Guaraglia and Pousa, 2014). There are some other velocity meters that are meant to be used for surface water. For example, propeller-base velocity meters (Chen et al., 2016) for which the measuring range starts at a higher value than the usual flow velocity in large water bodies (Dalian Zero Instrument Technology Co., 2020). There are other velocity measuring methods such as Particle Image Velocimetry (PIV) and Acoustic Doppler Velocity meters (ADV) that are able to quantify flow fields in the velocity ranges of large water bodies. However, these are either unaffordable or too difficult to be used for research purposes. Therefore, no affordable and easy-to-use instrument was found in the market that can be used to quantify flow fields in a water body such as a stormwater pond for validation purposes.

1.2 Research objectives

The following research objectives have been identified based on the gaps in the literature reviewed in this dissertation:

1. *Develop a modelling approach to identify the optimal location in stormwater ponds for withdrawing stormwater for reuse.*

Although stormwater is being reused in several parts of the world, no study was found to investigate the withdrawal location of stormwater ponds. The first objective of this research is to develop a robust modelling approach that is able to simulate bacteria in stormwater ponds and identify the optimal location that has the lowest bacteria concentration. Stormwater ponds are highly heterogeneous in all directions and the model needs to simulate bacteria 3-dimensionally throughout the ponds internally. For this purpose, the model has to be given geometry data including catchment data and 3D geometry of the pond, rain and wind data, and the bacteria load entering the pond. Then, the model would apply the physics and a biological model to find the transport of bacteria and fate, respectively. The model results have to be analyzed at the end of the simulations in order to identify the optimal location.

2. *Improve the model to widen the range of bacteria that can be modelled as well as improving the water quality in the withdrawal location.*

The model needs to be improved further in order to account for a wider range of bacteria. To be specific, attachment of bacteria to sediment particles is going to be accounted for in

bacteria transport according to this objective. For this purpose, a sediment transport model needs to be integrated with the CFD component. Moreover, the water quality in the location that is determined as the optimal location for withdrawal can be improved.

3. *Develop a validation scheme for the model.*

Non of the previous models in the literature is properly validated. It was also noted that validating such models is challenging due to a lack of data. However, it is important to validate modelling studies. Therefore, an objective of this dissertation is to develop a method to validate the model with appropriate data given the scope of the model. The validation needs to be performed in multiple ways. Since the flow field in the ponds plays an important role in the hydrodynamics of the ponds, aspects of the field have to be validated. However, no affordable and easy-to-use device was found on the market that suits this application. Therefore, this objective includes designing, building, calibrating and validating an instrument to quantify flow field in stormwater ponds.

4. *Assess the impact of main assumptions and factors on the model.*

Since the model is process based and there is not enough data needed to avoid assumptions in all of the processes involved, several assumptions are involved in the modelling. Also, the model requires input with other data such as wind and rain data. The fourth objective of this dissertation includes assessing the sensitivity of modelling outcomes to the assumptions and data, and to make suggestions about how to apply the data with confidence when data are missing.

1.3 Dissertation outline

This is a manuscript style dissertation with each chapter a modified version of a journal article. Thus, each chapter includes its own introduction, literature review, methodology, results and conclusions. Chapter 2 presents the first version of the modelling approach, in which the fate and transport of *E.coli* in the stormwater pond after rain events was simulated. The hydrological component of the model is extensively discussed in this chapter. However, the component's results are used in the other chapters. The content modified in Chapter 2 was published in the following publication: Allafchi, et al. 2019. "An Integrated Hydrological-CFD Model for Estimating Bacterial Levels in Stormwater Ponds". *Water*, 11, 1016, doi.org/10.3390/w11051016.

Chapter 3 presents a modified version of the model, in which sediment transport and the effect of a free surface are included. The distribution of *E.coli* and fecal coliform in the Inverness pond were found in this chapter. The optimal location for withdrawal for reuse is also determined. Moreover, a method is proposed that can improve the water quality in the withdrawal location even further. The content modified to produce Chapter 3 was published in the following publication: Allafchi, et al. 2021. "A mechanistic model for estimating bacteria levels in stormwater ponds", In press with *Journal of Hydro-Environment Research*.

Chapter 4 focuses on an instrument that was designed and built to measure flow field velocity magnitude and direction in the range that is experienced in medium to large water bodies, particularly stormwater ponds. In this chapter, calibration and validation of the instrument are described and the results are analyzed. The validation was performed in the

Inverness pond, which was the test case for the modelling approach. The velocity field that was measured in multiple locations of the pond was later used in chapter 5 for the model validation. The content modified to produce Chapter 4 was published in: Allafchi, et al. 2020. “A Velocity Meter for Quantifying Fluid Flow Velocity Vectors in Large Water Bodies.” *Sensors*, 20, 7204; doi:10.3390/s20247204.

Chapter 5 assesses the model in different ways. First, the model is validated in two different ways. Then the impact of some of the principal assumptions of the model on the bacteria distribution is extensively discussed. Also, the model is evaluated to see if it is possible to find the optimal and the most contaminated location of the pond without having rain data. The impact of wind on the bacteria distribution is also discussed in this chapter. The content modified to produce Chapter 5 was published in: Allafchi, et al. 2021. “Influence of Environmental Factors in Hydrodynamic Modelling of Bacterial Distribution in Stormwater Ponds,” *Journal of Environmental Informatics Letters*, 5(2) 87-101.

Chapter 6 is the concluding chapter of this dissertation, which summarizes the findings and the novel contributions contributing to the field by the Candidate.

2. An Integrated Hydrological-CFD Model for Estimating Bacterial Levels in Stormwater Ponds

2.1 Introduction

In recent decades, stormwater has been considered as an alternative water source for reuse, specifically for applications that need less than pristine water quality. Reusing stormwater is more critical in water-scarce regions and regions where rainfall patterns and rainfall frequencies are changing (The City of Calgary Water Resources, 2011). Several regions are trying to reuse stormwater as a sustainable method of water resources management; thus, prompting research into the feasibility of reusing stormwater from a water quality perspective (He et al., 2008).

Although stormwater ponds are built with the primary objective of reducing runoff quantities in order to protect urban areas against flooding, they also improve the quality of stormwater as well (The City of Calgary Water Resources, 2011). The stormwater quality within a pond varies both spatially and temporally and is not only a function of the quality of the influent, but also a function of local hydrological conditions and on the pond's design (Ahilan et al., 2019; Clevenot et al., 2018). A water quality study of a very large stormwater pond in Calgary, Alberta, Canada, showed that the quality of stormwater in the pond observed over a three year period did meet the irrigation water quality requirements but only under certain circumstances (He et al., 2008). Thus, stormwater recycling with pond water often requires continuous or intermittent water quality monitoring of the pond water

in order to remain compliant with local regulations. Highly distributed water quality sampling in stormwater ponds is often impractical due to the sizes of these ponds and the cost. In addition, most ponds are not designed with reuse in mind and the extraction point is often located in an ad hoc fashion and possibly in a region of the pond which has higher pollution levels relative to the rest of the pond because of local hydrodynamic conditions. If retrofitting a pond with the intent to recycle the water, the municipality could undertake a water quality sampling program that collected samples distributed throughout the pond over a period of time in order to identify the optimum location for extracting the "cleanest" water in the pond (assuming there is no treatment of this water). A more cost effective alternative is to develop a physical model to estimate the bacteria level in the pond that incorporates the factors leading to bacterial contamination of stormwater in retention ponds.

Water quality is impaired when mobilized sources of contaminants are transported away from their original location by runoff and discharged in aquatic environments (Gorgoglione et al., 2018; Di Modugno et al., 2015). Fine particles are either detached from the soil or washed off an impervious surface (St-hilaire et al., 2016). Determining levels of pathogenic microorganisms is expensive and difficult due to their large diversity; and thus, microbiological water quality monitoring procedures often use fecal indicator bacteria (FIB). FIB are present in feces of human and warm-blooded animals in large numbers and can be easily detected (Borrego and Figueras, 1997). Total coliforms (TC) and fecal coliforms (FC) were considered the main group of FIB during the twentieth century. However, nowadays, *Escherichia coli* (*E.coli*) and intestinal enterococci (IE) are

enumerated and considered as FIB because some water related epidemiological studies have shown that they are better bacterial indicators for predicting sanitary risk (Leclerc et al., 2001; Tallon et al., 2005).

The aim of microbiological water quality monitoring of stormwater ponds is primarily to assess the level of fecal contamination in an aquatic system. This contamination varies spatially and temporally throughout the pond and therefore, very large data sets must be collected to enable an adequate understanding of contamination levels and the processes leading to the degree of pollution in the system. Collecting such a large data set is often intractable, and thus models are often the only feasible approach for gaining greater insight into aquatic ecosystem processes. Two main types of models have been proposed to estimate bacterial levels in aquatic environments: data driven models, which are also considered black box models, and process-based models (de Brauwere et al., 2014a).

Data driven models use statistical methods or computational intelligence and machine learning to relate the involved parameters to the state variables (input, internal and output variables) with only a limited number of assumptions about the physical behavior of the system. In contrast, process-based methods predict the FIB concentration based on the mathematical description of sources, sinks, and internal processes influencing FIB levels. The fundamental principle underlying process-based models is conservational equations. The most important factors influencing microorganism fate in the aquatic environment are (i) environmental parameters, and (ii) whether or not they are attached to particles (de Brauwere et al., 2014a). Few estimates of the percentage of particles with attached bacteria in any collected stormwater sample can be found in the literature. One study found up to

10-28% and 22-30% of fecal coliform and E.coli, respectively, were associated with suspended solids in stormflow samples at the mouth of a canal discharging water to a lake with brackish water (Anna et al., 2005). Another study found that 30-55% of both fecal coliform and E.coli were attached to sediment particles in stormwater samples (Characklis et al., 2005).

The fate and transport of bacteria depends heavily on the attachment to suspended solids. Attachment to sediment protects bacteria from some processes that may accelerate death and decay, such as sunlight and predation. Thus, any modelling should use different decay rates for bacteria attached to sediment vs. free-floating bacteria. For example, the decay rate of free-floating *E.coli* was considered to be twice that of *E.coli* attached to sediment in a study in the Scheldt drainage network in Belgium (Ouattara et al., 2013). In another study in the Blackstone River watershed in Massachusetts, the ratio of the decay rate of free-floating bacteria to attached bacteria was considered to be 4 (Wu et al., 2009). Some studies even assumed that attached pathogens did not decay at all (de Brauwere et al., 2014a).

The fate of bacteria is most commonly modeled by first order kinetic decay, and this first-order model was used to study the efficiency of waste stabilization ponds. Shilton, (2000) used a pulse tracer study incorporated with Computational Fluid Dynamics (CFD) to find the retention time of a waste stabilization pond in order to use the first order kinetic decay based on the retention time (Shilton, 2000). In another study on an anaerobic lagoon, decay was calculated based on the retention time resulting from CFD simulations (Wu and Chen, 2011). In both the study of the waste stabilization pond and the anaerobic lagoon,

the objective was only to study the inlet and outlet bacteria concentrations, and they neglected to consider variation within the body. Also, in both of the studies the simulation was assumed to be steady state. Therefore, the retention time, which did not change with time could be an indicator of bacteria concentration. Two other studies on waste stabilization ponds used tracers integrated with CFD simulations to study different configurations of baffles (Shilton and Harrison, 2003; Shilton and Mara, 2005). They implemented first order kinetic decay by a source term in the transport equation of the tracer. All of the above mentioned studies simulated the flow as steady state and neglected wind. The fluid flow and bacteria fate and transport in stormwater ponds are intrinsically unsteady. Also, the wind cannot be neglected. In addition, the main goal of the present study is to study bacteria concentration within stormwater ponds for the purposes of determining the optimal location at which water may be withdrawn for reuse – the optimal location is a location with the cleanest water and having the lowest level of bacteria concentrations.

In the present study, a comprehensive model was developed that integrates a hydrological model for a catchment draining to a stormwater pond, with a Computational Fluid Dynamics (CFD) model simulating the pond's hydrodynamics. The results of the hydrological model were used as inputs to the CFD simulation. The model results are validated against data collected at the pond. The overall goal of this chapter is to enhance knowledge of bacteria fate and transport in stormwater ponds. Furthermore, the developed modeling approach leading to this enhanced understanding may ultimately be used as a tool to evaluate the capacity for a stormwater pond as a candidate for reuse and/or the need

for the modification/retrofit. Also, it may provide designers and planners with guidance to define standards for stormwater reuse.

2.2 Materials

2.2.1 Study area

The City of Calgary is a semi-arid city in Alberta, Canada, with many stormwater ponds that are being considered as candidate sources of stormwater reuse for irrigating parkland and other public lands during the irrigation season (He, 2009). The Inverness pond is one of the largest stormwater ponds in Calgary and is located in southeast quadrant of the city. It contains approximately 23 5000 m^3 of water at the permanent water level. Seven inlets convey stormwater runoff from 415 ha of catchment area into the pond. Figure 2.1 shows the pond and the locations of the inlets and outlets. All of the inlets are submerged except for Culvert 417. Outlet O1 at the west wing of the pond is the main outlet of the pond and is a 1.5 m diameter concrete pipe. I4 inlet, located at the south wing, conveys water from the largest subbasin of the catchment, which is 257.97 ha. The second largest subbasin corresponds to I3 inlet with an area of 89.52 ha. Also, there are four sediment forebays located in front of I2, I3, I4 and I5 inlets. Table 2.1 shows the subbasin area and design parameters corresponding to each inlet.

2.2.2 Data collection

Over a three year data collection campaign, several data were collected within and around the pond. Water quality and flowrate data collected during several rain events in the 2007 irrigation season were taken at a skimming manhole located just upstream of the

I5 inlet. The water quality data included FIB level (*E.coli*, FC, and total coliform), Total Suspended Solid (TSS), turbidity, PH, and dissolved oxygen (DO) (He, 2009). Rainfall data in 5-minute intervals were acquired from the City of Calgary (rain gauge #26 located 1 km north of the study site in McKenzie Towne) and wind data were extracted from the Calgary International Airport. Five rain events documented in 2007 were used in this research. Three of these are lower intensity events leading to moderate flowrates (on May 28, August 26, and September 20), while the other two (June 6 and September 12) are high intensity events leading to large flowrates into the pond. The rain event data are tabulated in Table 2.2.

An autosampler with 24 pre-sterilized bottles was placed inside the skimming manhole and collected samples for bacteriological analysis once triggered by a rain gauge. The autosampler was programmed to collect 12 samples (2 bottles per sample) during long events, and less than 12 samples were analyzed for short duration events. The samples were collected at unequal intervals (3 to 50 minute intervals), and much attention was paid to collect samples more frequently in the early stages of the rain event in order to catch the first flush effect. The water samples were recovered right after rain events or very early the next morning in case rain events occurred at night. The samples were packed with ice and analyzed at the Alberta Provincial Laboratory for Public Health by assaying microorganisms using the membrane method (He, 2009).

Figure 2.1 Arial schematic of Inverness pond showing location of inlets and outlets (base map from Google Earth [50º54'39.4"N 113º57'46.2"W at white cross-hairs at centre], arrows and texts added by author)

Table 2.1 Inlet and outlet parameters of the Inverness stormwater pond

Inlet	I1	I2	I3	I4	I5	I6	I7	O1	O2
Subbasin area (ha)	2.74	4.68	89.52	257.97	15.3	13.04	18.48	outlet	outlet
Residential (%)	0	27	6.48	10.04	62	83	69	-	-
Commercial (%)	0	53	0.36	0	0	7	21	-	-
Industrial (%)	0	0	0	0	0	0	0	-	-
Parks and Institution (%)	0	20	1.8	1.54	38	10	8	-	-
Major Transport Infrastructure (%)	0	0	0.36	23.97	0	0	2	-	-
Newly graded (%)	100	0	40	36.22	0	0	0	-	-
Farm (%)	0	0	52	28.22	0	0	0	-	-
Sediment Forebay	no	yes	yes	yes	yes	no	no	no	no
Invert elevation (m) from PWL[1]	-	2.44	2.12	2.83	2.11	2.48	1.86	2.80	2.80

[1] Permanent Water Level

Table 2.2 Rainfall data of the events in 2007

Date	Rainfall Depth (mm)	Start of the Event	Duration
May 28	4.8 mm	11:05 PM (May 27)	2 hr
June 6	31.8 mm	5:55 AM	7 hr 10 min
August 26	12.3 mm	9:25 AM	5 hr 55 min
September 12	30 mm	1:05 PM	7 hr 45 min
September 20	4 mm	8:00 PM	1 hr 40 min

2.3 Methods

The model is comprised of a hydrological component that simulates stormwater runoff feed into the CFD, which simulates the hydrodynamics and predicts the bacteria levels within a water body. The modeling approach is formulated in a way in which *E.coli* are primarily discharged into the pond through contaminated stormwater runoff (water fowl droppings from the surface are not considered) and *E.coli* concentrations are affected by biological fate of *E.coli* and pond hydrodynamics, which are in turn affected by meteorology and pond bathymetry. Studies in the literature have revealed that the concentration of bacteria is highly dependent on land use - in particular, the percentage of imperviousness (Mallin et al., 2000). Developed areas, which have more impervious areas, have elevated increases in *E.coli* concentrations in runoff (Chen and Chang, 2014) as opposed to less developed areas. In order to provide insight into the relationship between landuse and bacteria concentration in runoff, bacteria concentrations were measured during storms in different watersheds with different landuses (Schoonover and Lockaby, 2006). They demonstrated the variability in fecal coliform concentrations for different landuses. In the present study, the fraction of bacteria in stormflow corresponding to each landuse

was calculated using the findings of Schoonover and Lockaby, 2006. However, here, all of the landuses except for newly graded land and farm land were considered as urban. Thus, by knowing the fraction of bacteria that could be generated from the area draining into inlet I5, bacteria load of different inlets was estimated based on the measured data of inlet I5.

2.3.1 Hydrological model, calibration and validation

The Hydrologic Modeling System (HEC-HMS 4.2.1) (U.S. Army Corps of Engineers. Hydrological Modeling System HEC-HMS, User's manual 2016) was used to simulate stormwater runoff generated by each subbasin and drained into the pond in storm events. In the HEC-HMS, the Soil Conservation Service (SCS) curve number (CN) loss method (Mockus, 1972), which is a very common method for runoff estimation (Teegavarapu and Chinatalapudi, 2018) is adopted. The SCS-CN model considers precipitation excess as a function of cumulative precipitation, soil cover, land use, and antecedent moisture. Precipitation excess is estimated by Equation (2-1):

$$P_e = \frac{(P - I_a)^2}{P - I_a + S} \qquad (2\text{-}1)$$

where P_e is the accumulated rainfall excess (mm) at time t; P is accumulated rainfall depth (mm) at time t; S is the potential maximum retention (mm); and I_a is the initial abstraction (mm), where $I_a = 0.2S$. Here, S is a function of the CN, which is a function of watershed characteristics, and is calculated by Equation (2-2) (U.S. Army Corps of Engineers. Hydrologic Modeling System HEC-HMS, Technical Reference Manual 2000):

$$S = \frac{25400 - 254CN}{CN} \qquad (2\text{-}2)$$

The CN number of each subbasin was initially estimated based on the land uses within each subbasin. The time step of the HEC-HMS model was set at 5 minutes. The runoff at I5, measured in the event on June 6, was employed to adjust the initial CN of this subbasin aiming to reproduce the runoff well. Accordingly, the CN of other subbasins was modified using the difference between the adjusted CN number for I5 subbasin and its initial CN.

2.3.2 CFD simulations

This chapter adopted Reynolds averaged Navier Stokes (RANS) equations as follows:

$$\rho\left[\frac{\partial \bar{u}_i}{\partial t} + \frac{\partial}{\partial x_j}(\bar{u}_i \bar{u}_j)\right] = -\frac{\partial p}{\partial x_i} + \rho\frac{\partial}{\partial x_j}\left(\upsilon\frac{\partial \bar{u}_i}{\partial x_j}\right) - \frac{\partial}{\partial x_j}\left(\rho\overline{u_i' u_j'}\right) \qquad (2\text{-}3)$$

with the velocity decomposed into mean velocity and velocity fluctuation ($u_i = \bar{u}_i + u_i'$), where

$$\bar{u} = \frac{1}{T}\int_0^T u dt \qquad (2\text{-}4)$$

and T is period of time (s); ρ is density (kg/m^3); t is time; p is pressure (pa); υ is kinematic viscosity (m^2/s); and x_j are the axes of the Cartesian coordinate system, and i,j = 1,2,3 are indices indicating the three axes in the coordinate system. The term $-\rho\overline{u_i' u_j'}$ is called Reynold's stress term (Graebel, 2007). Since the popular k-ε turbulence model has been successfully applied to simulate water body flow fields (Abbasi et al., 2016; Shilton et al.,

2008) in this study the *k-ε* turbulence model (Launder and Sharma, 1974) was used to calculate the Reynold's stress terms. The turbulence model is not detailed here. The fundamentals of CFD and turbulence modeling can be found in Versteeg and Malalasekera Versteeg and Malalasekera (1995).

Kunkel et al. (2013) studied the attachment of *E.coli* to particles in stormwater. The study showed that *E.coli* appeared to attach predominantly to fine particles (< 4μm), while further study on attachment to smaller particles was recommended. Another study on the attachment of *E.coli* showed that most of them attached to particles smaller than 2 μm (Muirhead et al., 2006). The City of Calgary characterizes the particles in stormwater and suggests the settling velocity of 0.00592 (mm/s) for small particles (< 10 µm) (The City of Calgary Water Resources, 2011). Using Stokes relation for settling velocity (Stokes, 1851), the settling velocity of finer particles (< 2 µm) can be estimated using:

$$w_s = \frac{g(\rho_p - \rho_w)}{18\rho_w \upsilon} d_p^2 \quad (2\text{-}5)$$

where w_s is settling velocity (m/s); ρ_p and ρ_f are particle and fluid density (kg/m^3), respectively; d_p is particle diameter (m); g is gravitational acceleration (m/s^2). This relation is valid for small Reynolds numbers (Re < 1) (Gu et al., 2017). With regard to the settling velocity of small particles, this condition is certainly satisfied in the Inverness pond (The City of Calgary Water Resources, 2011). The calculated settling velocity for the very fine particles (< 2μm) is 0.001 mm/s using the Stokes relation. This suggests that the attached bacteria settle less than 9 cm in 24 hours. Therefore, it was assumed that all the bacteria (i.e. free-floating and attached *E.coli*) remain in the water column during the simulation. Accordingly, bacteria (both attached and free-floating bacteria) were modeled as passive

scalars, which are massless particles that do not affect the physical properties of the flow field.

The passive scalar transport equation was solved for the transport of both free-floating and attached *E.coli*. The transport equation for a passive scalar, ϕ_i, is:

$$\frac{\partial}{\partial t}\int_V \rho\phi_i dV + \oint_A \rho\phi_i v.dA = \oint_A j_i.dA + \int_V S_{\phi_i} dV \quad (2\text{-}6)$$

where t is time (s); V is volume (m^3); A is area (m^2); i is the component index; j_i is diffusion flux ($kg/m^2 \cdot s$); and S_{ϕ_i} is source term ($kg/m^2 \cdot s$).

The fate of bacteria has been modeled using a negative value for the source term in the passive scalar transport equation in previous studies on waste stabilization ponds (Shilton and Harrison, 2003; Shilton and Mara, 2005. This approach is, however, not appropriate for stormwater ponds due to two reasons. Firstly, the flow field and bacteria transport in stormwater ponds are intrinsically unsteady; thus, the location and strength of the sources cannot be determined. Secondly, bacteria concentrations in some spots of stormwater ponds are very low, so a general source, representing decay over the entire domain, might cause negative bacteria concentrations which is not physically feasible. Therefore, in this chapter the transport of bacteria was calculated with Equation (2-6), while the fate of bacteria was modeled separately.

A finite volume discretization scheme was used to discretize Equations (2-3) and (2-6), and the turbulence model equations over the domain to solve the flow field and the concentration of passive scalar. Then, a field function implements the first-order kinetic decay (Equation (2-7)) for the free-floating portion of bacteria and adds the concentrations

of both attached and the remaining free-floating bacteria at each computational cell. Characklis et al., (2005) found that 30-55% of bacteria attach to sediments in stormwater, whereas the other study (Bai and Lung, 2005) applied a higher value in the range (50%). Therefore, in this chapter it was assumed that 50% of bacteria are attached to sediments and do not decay. Decay is calculated using Equation (2-7).

$$N = N_0 \exp(-\mu t) \quad (2\text{-}7)$$

where N and N_0 are the number of indicator bacteria at time t and at t=0, respectively; and μ is the decay rate (s^{-1}) (Chick, 1908). The decay rate of *E.coli* was calculated with the following relationship that has been used in several studies (Ouattara et al., 2013; de Brauwere et al., 2014b) in the literature:

$$\mu = k_{20} \frac{e^{\left(-\frac{(T-25)^2}{400}\right)}}{e^{\left(-\frac{25}{400}\right)}} \quad (2\text{-}8)$$

where k_{20} is the decay rate of *E.coli* at 20^{o}C and T is water temperature (^{o}C). A value of 1.25×10^{-5} s^{-1} was proposed for k_{20} of *E.coli* in the water column; average measured data was used for temperature in this chapter.

2.3.2.1. Boundary and Initial Conditions

The effect of wind on the flow field is not negligible considering the size of the study pond. Since the wind vector is not stationary with time, a dynamic boundary condition of wind on the pond surface was defined. The effect of wind was applied as a velocity vector on the top layer of the pond. The velocity of the top layer of the pond was calculated from the wind velocity based on the experimental data from a study by Banner and Peirson

(Banner and Peirson, 1998), which measured velocity at the top layers of water bodies under windy conditions.

The boundary condition of the inlets was set as the "velocity inlet" with parameters changing with time including velocity and *E.coli* concentration. A time variable boundary condition was also defined which linearly interpolated the value of bacteria concentration and velocity between the interval that data were collected. "Pressure outlet" and "stationary wall" were set as the boundary conditions for the outlets and the bottom of the pond, respectively.

A steady state simulation in no storm conditions and with an average wind was simulated and its result (flow field) was used as the initial condition for the main simulations. The main simulation is unsteady. Using the steady simulation's results also accelerated the convergence. The unsteady simulations started one hour before the storm in order to let the flow field form based on the real wind data before the storm.

2.4 Results and Discussions

2.4.1. Hydrological modeling performance

The hydrological model was manually calibrated with the measured data in inlet I5 on June 6 and then validated on four other events: May 28, August 26, September 12, and September 20. During the calibration, the error in the total volume of water between prediction and observation was adopted to evaluate model performance, as the total volume of water entering the pond is considered to be the key factor that determines bacteria loading.

The CN number for the subbasin draining to I5 was calculated to be 11% less than the initially calculated CN value in the calibration of the June 6 event. Noting this, all other CN numbers were decreased by 11%. Table 2.3 shows the CN numbers for the different subbasins before and after calibration of the model. Lag time was also calibrated at the same time, and a 30 minute lag time was found to be optimal. In addition, an attempt was made to calibrate initial abstraction; however, the default setting ($I_a = 0.2S$) resulted in the lowest error, and was therefore left unchanged. Figures 2.2 – 2.5 show the modeled and observed hydrographs for the validation events for subbasin I5. The Nash-Sutcliffe model efficiency (NSE), which is a reliable criterion for assessing the goodness of fit of hydrological models (McCuen et al., 2006), and the error in total volume for all events, are tabulated in Table 2.4. The calibrated CNs (Table 2.3) were then used to model other subbasins.

Table 2.3 Curve numbers of the different subbasins draining to the Inverness pond inlets

	I1	**I2**	**I3**	**I4**	**I5**	**I6**	**I7**
Estimated CN	91	86.49	87.33	87.99	78.34	81.21	83.39
Calibrated CN	80.99	76.97	77.72	78.31	70	72.27	74.21

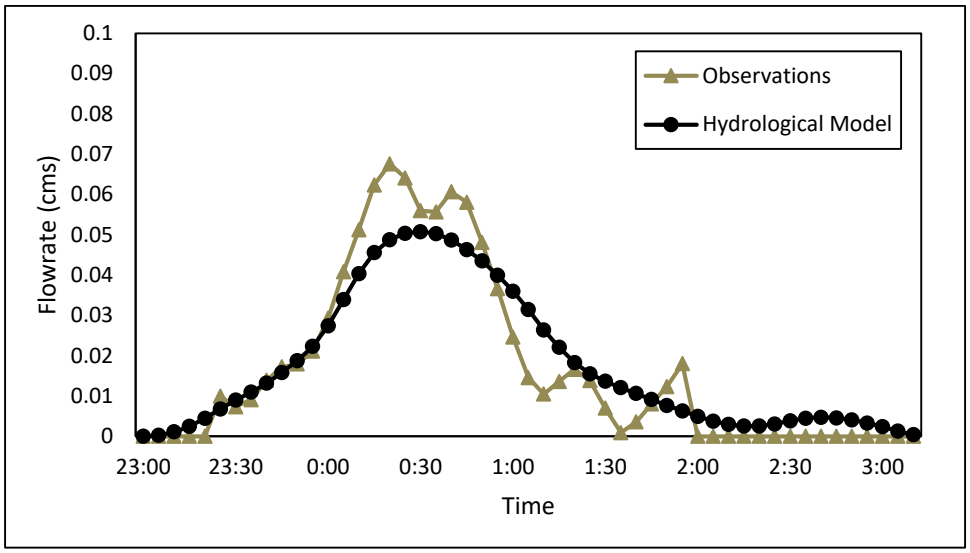

Figure 2.2 Modeled and observed hydrographs at I5 inlet of storm event on May 28

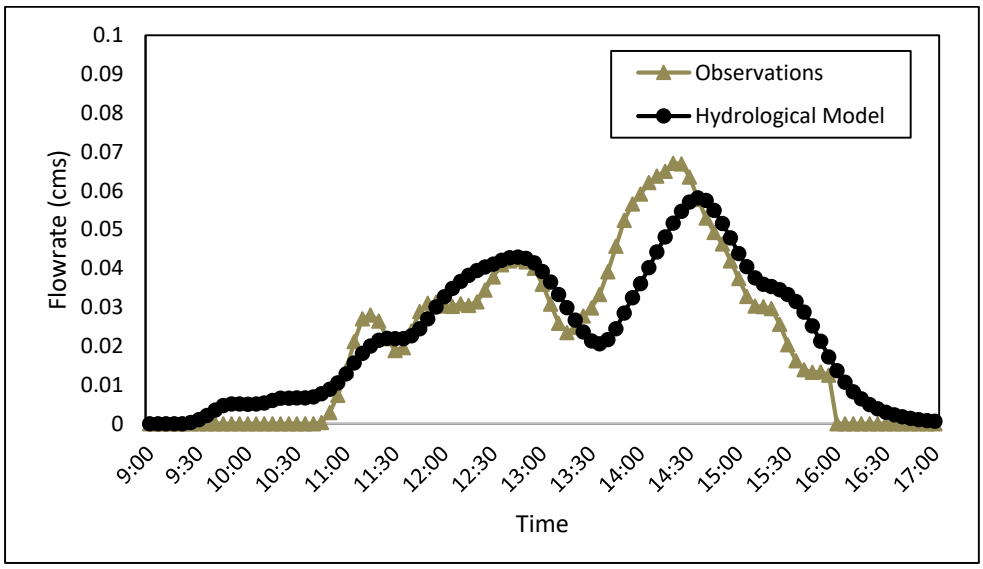

Figure 2.3 Modeled and observed hydrographs at I5 inlet of storm event on August 26

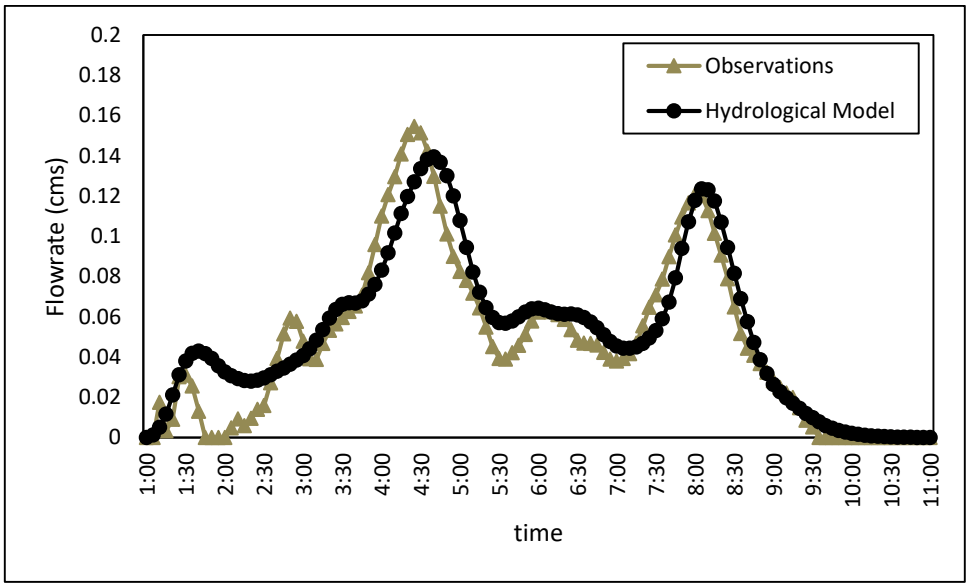

Figure 2.4 Modeled and observed hydrographs at I5 inlet of storm event on September 12

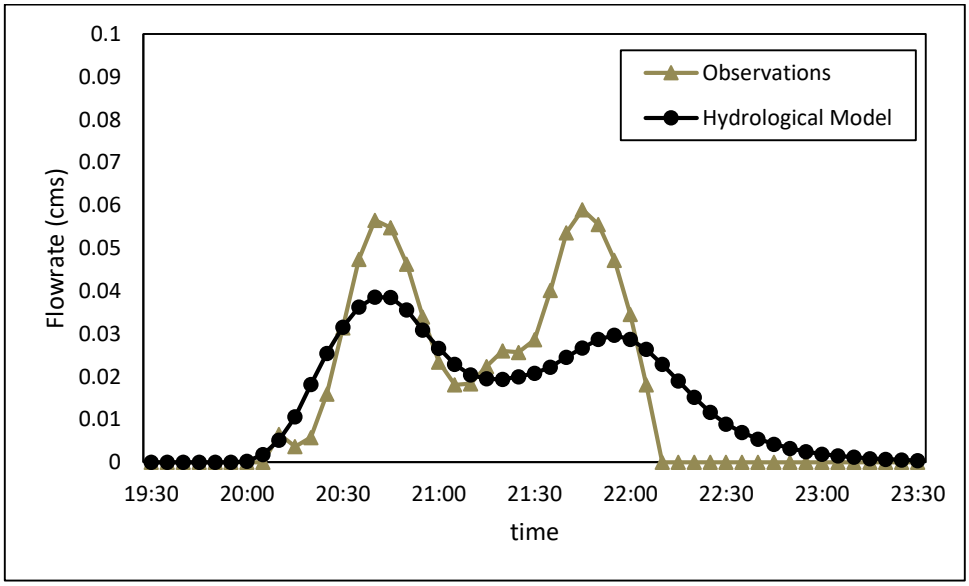

Figure 2.5 Modeled and observed hydrographs at I5 inlet of storm event on September 20

Table 2.4 Model performance in model calibration and validation. The event on June 6 is the calibration event and all others are validation events

Event	Total volume error	Nash-Sutcliffe efficiency (NSE)
June 6	4.8%	0.89
May 28	2.8%	0.92
August 26	4.1%	0.81
September 12	7.4%	0.86
September 20	-7.3%	0.66

Results show good agreement between the modeled and measured data. In all of the events except for September 20, the model slightly overestimated the total volume but the total volume error is less than 10%. The underestimation of the total volume for the event on September 20 may be due to the excessive moisture in the soil resulting from heavy rains that fell prior to the event; thus, potentially leading to greater runoff generation. However, the Nash-Sutcliffe efficiency in all of the modeled events is reasonable.

2.4.2 CFD Simulations

The simulation results for the event on August 26 are detailed and discussed in this section as an example. The concentrations of *E.coli* on the surface of the pond at different time steps after the rain event are shown in Figure 2.6. As time passes, bacteria entering from the inlets redistribute in the pond. The flow field was affected by the inlet velocities for the first few hours after the events, but afterwards, the wind is the only parameter affecting the flow field.

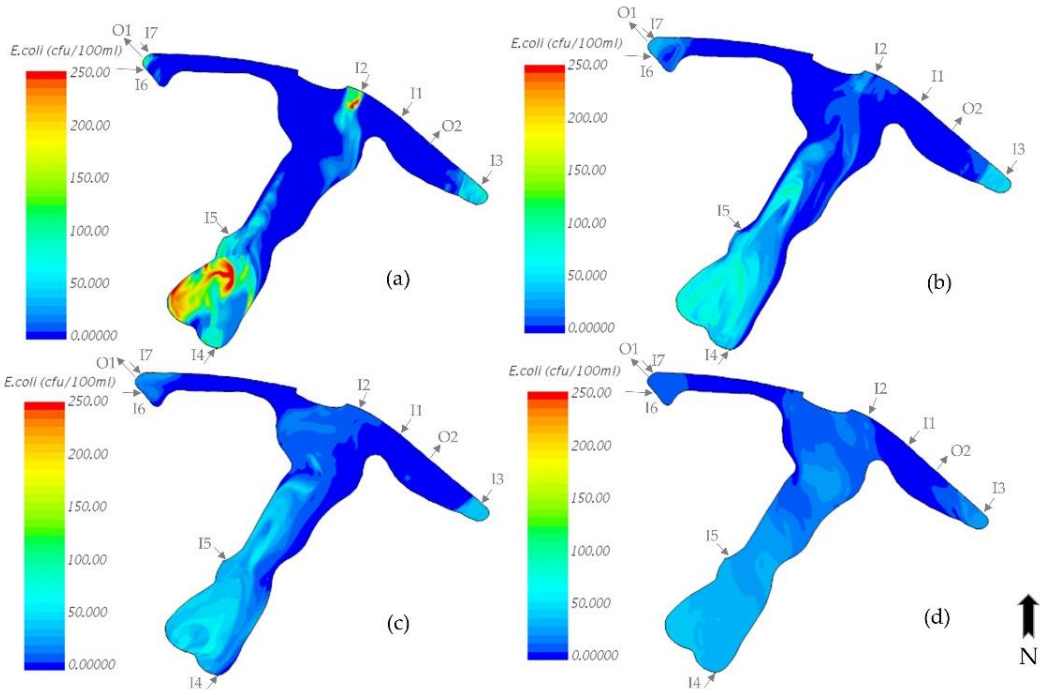

Figure 2.6 Contours of *E.coli* concentration (cfu/100mL) on the surface of the Inverness pond on a) August 26 at 5pm, b) August 26 at 11pm, c) August 27 at 5am, and d) August 27 at 11am

The bacteria concentrations in the South wing of the pond are greater as compared with the other two wings (the East and West wings). There are two inlets (I5 and I4) in the south wing. The *E.coli* concentration is higher in the stormwater runoff entering the pond from inlet I5 than all other inlets; while bacteria loading from I4 is highest as it drains the largest area (Table 2.1). For example, the *E.coli* concentration in the storm runoff from I5 on August 26 at 2 pm (during the storm) was 2,100 cfu/100mL, while the storm runoff from I4 had a concentration of 1,038 cfu/100mL. However, the flowrate of the inlets at that time were 0.045 m^3/s and 0.39 m^3/s for the I5 and I4 inlets, respectively. Therefore, more bacteria mass enters the pond from inlet I4 even though the concentration of bacteria is greater in I5. Also, a relatively large amount of bacteria enters the pond from inlets I3, I7

and I6, but most of the bacteria coming from I7 and I6 immediately exit the pond through outlet O1, because these two inlets are in proximity to the outlet. Therefore, they do not have a significant effect on the bacteria level in the pond. In general, inlets I4, I3 and I5 have the most significant effect on the bacteria levels in the pond.

Figure 2.7 shows the vertical profile of *E.coli* distribution in the pond at six hours after the end of the storm. It reveals that the bacteria concentration also changes with depth. As illustrated in Figure 2.7, the maximum concentration of *E.coli* on the surface barely reaches 90 cfu/100mL. However, the maximum *E.coli* concentration is more than 120 cfu/100mL at 2 m depth. Also, the bacteria in the middle of the pond (where the three wings join) is less distributed at the bottom compared to the surface. The reason is that the direction of wind had been NE and NNE for the last few hours, so the bacteria escaping from the sediment forebay of inlet I2 could reach the other side where the south wing and the west wing join. In contrast, there is a current flow toward the NE and NNE directions at the bottom simply because of mass conservation. This current potentially brings clean water close to the I2 sediment forebay. There is also a downwelling near the bank of the middle of the pond where the south and the west wings join. Generally, wind will cause differences in *E.coli* distribution in different layers of the water column. *E.coli* data collected at different depths on five random days between the year 2006 and 2007 (He et al., 2008) reveal that bacteria concentration changes with depth. However, these data did not show any specific trend, and this is likely an indication of the influence of multiple environmental conditions on the bacteria distribution at various depths.

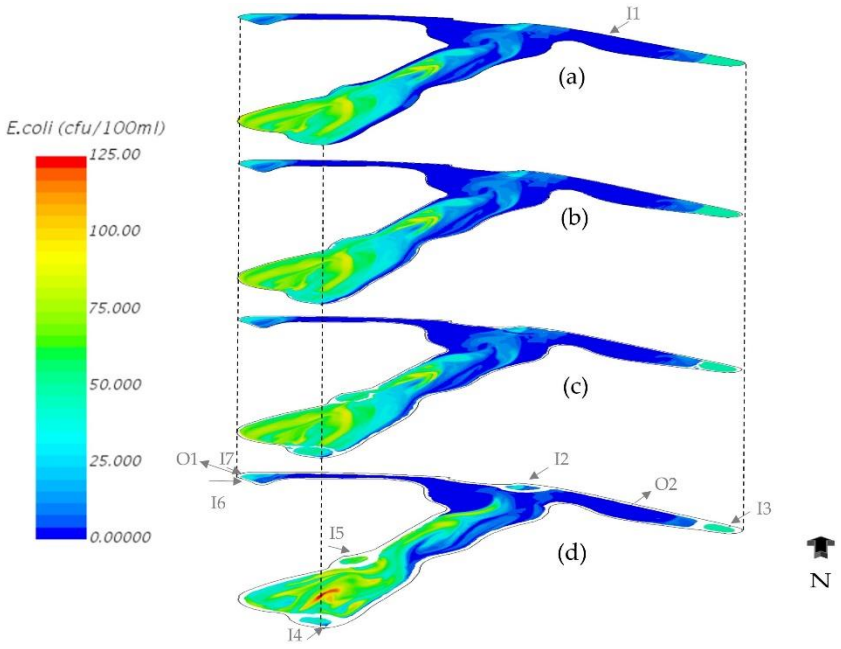

Figure 2.7 The vertical profile of *E.coli* concentration on August 26 at 11pm a) on the surface, b) at 0.5 m below the surface, c) at 1 m below the surface, and d) at 2 m below the surface

The sediment forebay corresponding to I3 was full of bacteria at all depths after the event (Figure 2.7). The sediment forebay was able to retain bacteria many hours after the event, which resulted in keeping the East wing relatively clean as compared with the South wing. Figure 2.8 magnifies the contours of *E.coli* concentration near the sediment forebays at the surface on August 27 at 2 am. It also confirms that the sediment forebay of I3 outperforms the forebay of other inlets. As illustrated in Figure 2.8, the concentration of *E.coli* in the sediment forebays of inlets I4 and I5 appears to be similar or even slightly less than that in the region outside the forebays. This reveals that the bacteria entering these forebays during the storm was promptly discharged out of the forebays and consequently increased the *E.coli* concentration in their nearby regions.

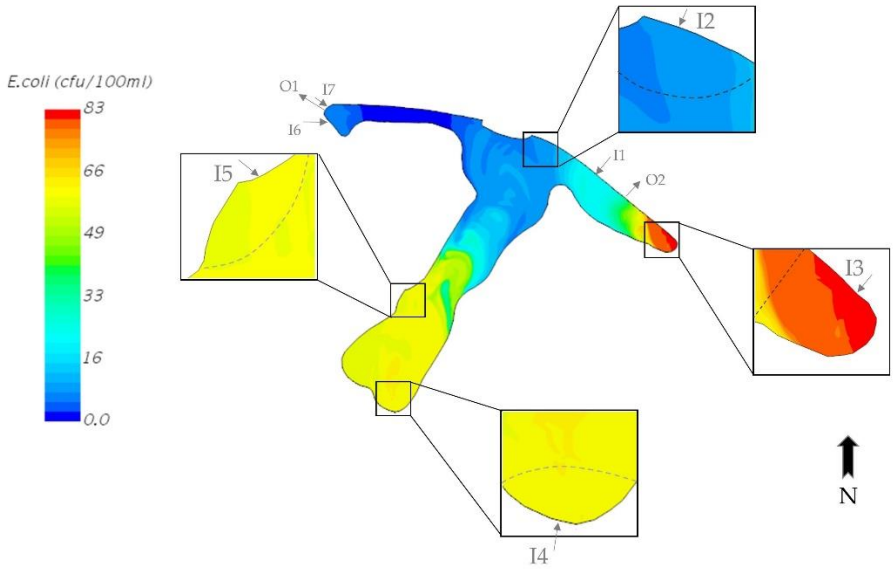

Figure 2.8 *E.coli* distribution on the surface Aug. 27 at 2am (9 hours after the end of the storm)

The design of sediment forebays, such as their configuration and size, determines their efficiency in trapping bacteria. Figure 2.9 shows streamlines coming out from the inlets and spreading throughout the pond during the storm. The streamlines from I4 continue straight out of the forebay, which means the bacteria are transported into the pond. One reason is that the size of the forebay is not large enough to fit a circulation proportional to the high flowrate of the I4 inlet. Another reason may be the configuration of the inlet and sediment forebay. The direction of the streamline from I4 and the corresponding sediment forebay are perpendicular to each other (i.e. they are in front of each other), so the water jet coming out of the inlet can easily escape the forebay without circulating. The situation is the same in the sediment forebays corresponding to the inlets I2 and I5. However, their size is proportional to their flowrate. The sediment forebay corresponding to the inlet I3

has the best configuration, since the direction of steamlines coming out of the inlet is parallel to the forebay. Thus, the bacteria coming from the inlet has no way but to circulate and in the long term they die, which keeps the East wing relatively clean. Also, the size of the forebay is large enough to fit two large eddies.

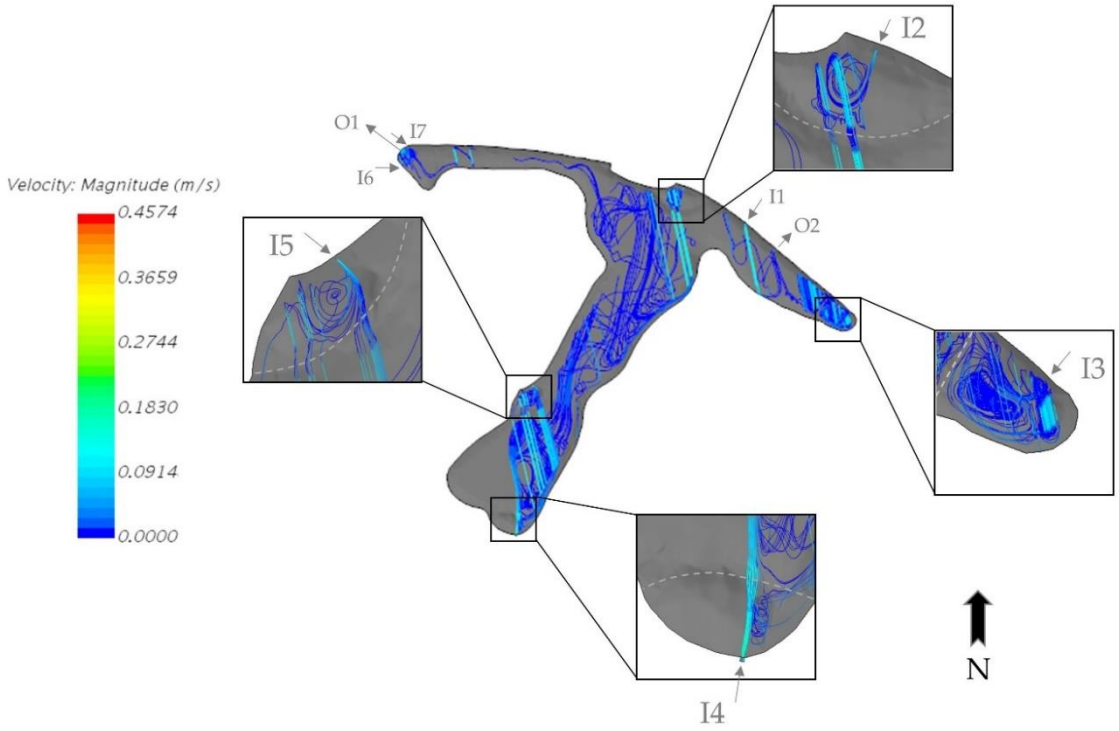

Figure 2.9 Velocity streamlines on August 26 at 3pm (during the storm)

During the data collection campaign surface grab samples were collected from 6 different sites at the pond over several days (He et al., 2008). All of the samples were collected at an average depth of 15 cm. One of the sample collection days was after a day with heavy rain. On September 10, 2005, 68 mm of rain fell and on the next day water samples were collected from the six sites. Although much greater rain fell on September 10, 2005 than in the simulated events from 2007, it provides an interesting case for validation due to the

dominant effect of rain on the bacteria distribution. The initial bacteria level in the pond before an event can influence the final bacteria levels after an event, particularly for small, low rainfall events. However, for high rainfall events, the majority of bacteria is transported into the pond with the storm runoff, and the initial bacteria level is a far smaller proportion of the total bacteria level. In this chapter, it was assumed that initial bacteria level was negligible, and only the effect of the storm was studied. Thus, the modelling results can be compared with collected data on September 10, 2005. Although it was noted that due to a lack of data it is difficult to validate the process-based FIB methods thoroughly (de Brauwere et al., 2014), a comparison was done between the different events using a non-dimensional number. The non-dimensional number was computed as the ratio of *E.coli* concentration at a site to the maximum *E.coli* concentration among all of the six sites at a certain time. Thus, the non-dimensional number at the site where *E.coli* concentration is a maximum is one. The number was calculated for the individual modeled events, and then the average was taken for each site. Figure 2.10 shows the non-dimensional number at the six sites for the measured data and the average of the simulated events with its variation range. Simulation results show a good agreement with the measured data in recognizing hot spots (spots with high concentration of bacteria) and spots with the lowest level of bacteria. The variation in the non-dimensional number in the East and West wings are higher than that in the South wing and in the middle of the pond. This may be due to a stronger influence from meteorological factors such as wind and rain at the tip of the east wing and the tip of the West wing. On the other hand, the low variation in the calculated data in the south wing and their high values show that the South wing always has the

highest bacteria levels in the pond. Therefore, it is not recommended to extract water for reuse from the South wing.

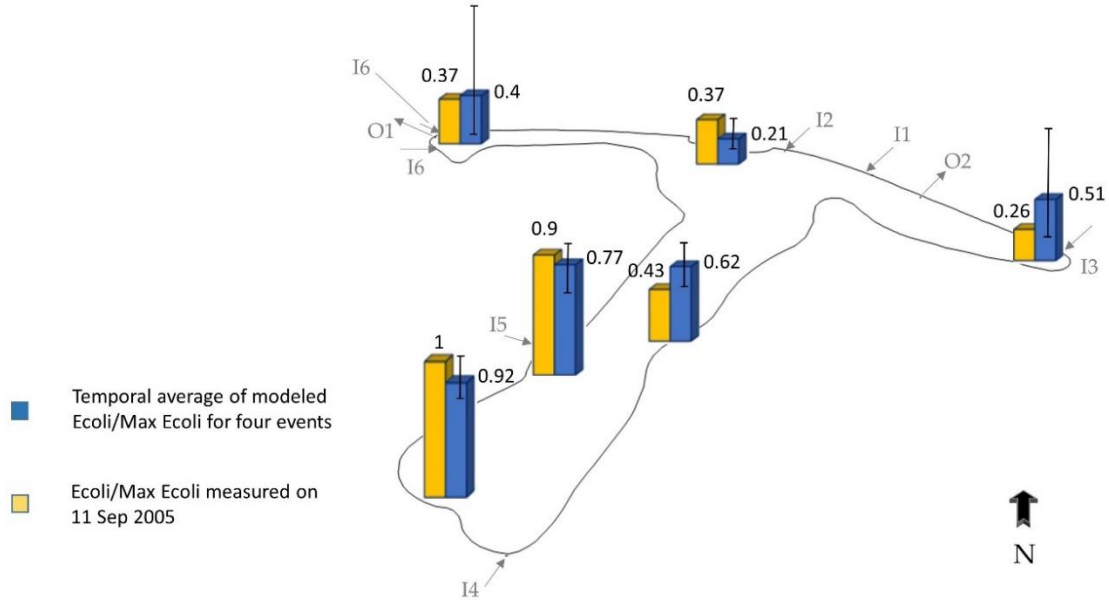

Figure 2.10 Non-dimensional *E.coli* concentraion 15 cm below the surface

Also, both measured and calculated data show that the middle of the pond, where the three wings join, has the lowest level of bacteria among the six sites; this site is a reliable spot for water extraction due to low concentrations of bacteria and low variability in the calculated data. There were no collected data for the middle of the West wing; however, simulation results show that this spot has the lowest *E.coli* concentrations in the pond. Therefore, the middle of the West wing can be considered as a potential location for water extraction as well. However, more data should be collected from the entire pond for a more comprehensive validation. In addition, further modelling studies after rain events are recommended when more data are available. More experimental and modeling studies need

to be conducted in order to study the effect of sedimentation on bacteria transport in the pond, which was assumed to be negligible in this chapter.

2.5 Conclusions

An integrated hydrological-CFD model was developed to simulate bacteria concentrations within the Inverness stormwater pond in Calgary, Alberta, in order to locate the best (cleanest) locations within the pond to extract water for potential reuse. The model was calibrated at one inlet with observed flowrate data in order to estimate the flow rates and bacteria levels at other inlets. The flowrate and bacteria concentration at the inlets were implemented as boundary conditions for an unsteady CFD simulation to determine the distribution of bacteria in the pond. The bacteria concentration distribution in Inverness pond was simulated both during and after four rain events using the integrated model. Results showed a good agreement with collected data from six different points in the pond, indicating that the model can be successfully used to model fate and transport of bacteria in stormwater ponds. It was found that wind plays a crucial role in forming the flow field in the pond, which affects the bacteria distribution. In addition, one of the sediment forebays, located in the east wing of the pond, successfully trapped large amounts of bacteria until death occurred. However, other sediment forebays were found ineffective. The middle of the west wing was found to be the best location for extracting water, because it showed the lowest levels of bacteria during the simulation of the pond both in, and after, the events.

3. A Mechanistic Model for Estimating Bacteria Levels in Stormwater Ponds

3.1 Introduction

About 55% of the world population (7.7 billion (PRB, 2020)) lives in urban areas and the number is projected to increase to 68% by 2050 (United Nations, 2020). An exacerbating problem along with the world population growth is the depletion of water resources (Goonetilleke et al., 2017). Therefore, stormwater is increasingly recognized as a valued alternative water resource (Hamdan, 2009). Stormwater has been successfully reused in the USA, UK, and Sweden for outdoor, domestic and irrigation purposes (Zhang et al., 2015). However, there are still some human health concerns regarding stormwater quality, particularly over the pathogens associated with the stormwater (Lundy et al., 2018).

The large variety of waterborne pathogenic microorganisms makes them difficult and expensive to quantify. Instead, current microbiological water quality monitoring procedures are based on the concept of fecal indicator bacteria (FIB). These indicators are groups of bacteria that originate from either direct or indirect release of human and warm-blooded animal feces into aquatic environments. FIB concentrations are used as indicators for the presence of pathogenic organisms (Wu et al., 2019) because FIB are easier to detect due to their presence in higher numbers compared to waterborne pathogens (de Brauwere et al., 2014a).

Although fecal indicator bacteria are much more readily detectable, it is still very costly to collect a highly distributed set of data (with respect to time and space) from large water bodies. Therefore, models are considered a more practical alternative for estimating bacteria level distributions in large water bodies. For example, Shilton (2000) developed a full 3-dimensional Computational Fluid Dynamics (CFD) model to study the treatment efficiency of waste stabilization ponds for treating Biological Oxygen Demand (BOD) and Fecal Coliform (FC), which is a commonly used FIB. Wu et al. (2011) used the same method to study the BOD removal of an anaerobic lagoon. In both of the studies, conservation equations were numerically solved in order to find the residence time, and then the first-order kinetic decay was implemented to calculate bacteria and/or BOD reduction in the water bodies. In several other studies on waste stabilization ponds (Shilton and Harrison, 2003; Shilton et al., 2008) the transport of bacteria was modelled as a passive scalar by the general transport equation, and then the decay was modelled under the assumption that bacteria concentration is uniform over the water bodies. In all these studies, the conservation equations were solved for steady state, which is feasible for waste stabilization ponds but not for stormwater ponds because their inflows and outflows vary significantly during storm events. Furthermore, the uniform bacteria concentration is not applicable for stormwater ponds as bacteria are in fact heterogeneously distributed over stormwater ponds as water in such water bodies are not often completely mixed. A most recent study by Allafchi et al. (2019) applied an unsteady model for simulating the distribution of *Escherichia coli* (*E.coli*) in a stormwater pond after storm events. In this study, *E.coli* was modelled as a passive scalar, and thus, the settling of particle-attached

bacteria was neglected. As *E.coli* also attach to particles (Muirhead et al., 2006), this approach could over predict *E.coli* concentrations in the water column if settling is neglected. In addition, the change in water surface elevation was neglected in the study which can adversely affect the estimation of bacteria concentration. Many previous works on the 3-dimensional hydro-environmental models (e.g. Shilton, 2000; Shilton and Harrison, 2003; Shilton et al., 2008; Wu and Chen, 2011) neglected the change in water surface as well.

Generally, there are two primary processes, namely fate and transport, governing the concentration of bacteria in an aquatic environment (Jeong et al., 2019). The fate of bacteria is modelled with the generally accepted first-order kinetic decay model, while the environmental parameters are the driving factors, in particular temperature (de Brauwere et al., 2014a). The bacteria transport is simulated using the transport equation. It has been well acknowledged that bacteria exist in water bodies in two different states: free-floating and particle-attached (Pachepsky and Shelton, 2011). A study by Characklis et al. (2005) revealed that an average of 30-55% FC and *E.coli* attach to particles in stormwater. Attachment to particles not only increases the settling velocity of bacteria but also protects bacteria from sunlight, predators, chemicals and other environmental factors that increase the mortality of bacteria (Wang et al., 2018). In some studies, it is even assumed that the particle-attached bacteria never die (de Brauwere et al., 2014a). However, in other studies it was assumed that the decay rate of particle-attached bacteria is 50% of the decay rate of free-floating bacteria in a drainage network (Ouattara et al., 2013) and assumed to be 25% in the Blackstone River watershed in Massachusetts, US (Wu et al., 2009).

With regard to fluid dynamics affecting transport, wind has been demonstrated to play a crucial role in the fluid circulation and pollutant transport in water bodies, such as Lake Taihu, China (Wu et al., 2018), two interconnected urban lakes in Central Finland (Juntunen et al., 2019) and stormwater ponds (Andradóttir and Mortamet, 2016). Whereas, canopy around water bodies could reduce wind velocity and in turn reduce the shear stress over the water surface and thereby reduce pollutant transport. Among the canopy characteristics influencing the shear stress and velocity profile over the water surface, such as aerodynamics roughness and porosity, canopy height is found to be the most prominent influential factor (Markfort et al., 2010). Apart from wind, the inflow and/or outflow that lead to variations in the water body's water surface levels during and after storm events, should be taken into consideration in order to better capture the flow field. In tracking interfaces in interfacial flows, Volume of Fluid (VOF) is an efficient and robust method (Seric et al., 2018), and has been successfully used in many interfacial flow problems (Rodriguez et al., 2004; Wu et al., 2018).

The literature shows that the free-floating and particle-attached bacteria, which operate differently with regard to transport and decay in the water column, have not been modelled separately in 3-dimensional hydro-environmental models that have been developed thus far. In addition, the effect of the change in water surface on the fluid flow field has often been ignored as the water surface is fixed in the models. These effects make the simulation of bacteria complicated and thus, the literature uses models that have not included these effects. But in this chapter, the issues were addressed by integrating sediment transport with a fully 3-dimensional CFD model that takes into account the transport of particle-

attached bacteria. In addition, a surface tracking model, namely VOF, is employed to handle the effect of the free water surface. The decay of the free-floating and particle-attached bacteria were modelled separately. The developed model was validated in a case study conducted for the Inverness Stormwater Pond in Calgary, Alberta, Canada. The modelling results were applied to identify the optimal location for recycling stormwater for irrigation that requires low bacteria concentrations. In addition, the effect of the wind reduction by a canopy on bacteria transport and distribution was also explored.

3.2 Study material and methodology

3.2.1Site description and data collection

The Inverness Stormwater Pond is situated in the southeast quadrant of the City of Calgary. It has been considered as one of the candidate sites by the municipality for recycling stormwater for irrigation applications (requiring a water quality level below that of potable water). The pond has a capacity of 235,000 m^3 with an average depth of 3.10 m at the permanent water level. It has two outlets and seven inlets discharging stormwater runoff from a 415-ha urban residential catchment. Figure 3.1 shows the Inverness Stormwater Pond, its catchment, and the locations of inlets and outlets. The pond consists of three wings – South, East and West wings. The land use characteristics of the subbasins corresponding to the inlets are tabulated in Table 3.1.

Table 3.1 Land use characteristics of the subbasisns in the Inverness Stormwater Pond catchment

Inlet	I1	I2	I3	I4	I5	I6	I7
Subbasin area (ha)	2.74	4.68	89.52	257.97	15.3	13.04	18.48
Residential (%)	0	27	6.48	10.04	62	83	69
Commercial (%)	0	53	0.36	0	0	7	21
Industrial (%)	0	0	0	0	0	0	0
Parks and Institution (%)	0	20	1.8	1.54	38	10	8
Major Transport Infrastructure (%)	0	0	0.36	23.97	0	0	2
Newly graded (%)	100	0	40	36.22	0	0	0
Farm (%)	0	0	52	28.22	0	0	0
Sediment Forebay	no	yes	yes	yes	yes	no	no

During a data collection campaign from 2004 to 2007, hydroclimate (flow and precipitation) and water quality data (bacteria and sediment) were collected from the stormwater runoff discharging into the pond as well as the stormwater in the pond. Water samples were collected from 10-20 cm below the water surface at six locations (P1~P6) near the shore of the pond (Fig. 3.1) during the irrigation seasons. When sampling from the pond, no attempt was made to favour rain events; however, 7 out of 26 sampling days were within three days after rain events. For the stormwater runoff monitoring, the flow was continuously measured at the inlet (I5) and outlet (O1) at 5-minute time intervals (Fig. 3.1); while the precipitation was recorded at a 5-minute time interval by a tipping bucket rain gauge. The stormwater runoff samples were collected for water quality assay by an autosampler. The autosampler was installed in the manhole located before the inlet I5 and triggered by the rain gauge during rain events. The stormwater runoff sampling scheme was scheduled to collect more samples (namely at smaller time intervals) in the beginning of the events in order to catch the first flush effect. In each storm event, a maximum of 12

water samples could be collected. All water samples were transported to the University of Calgary's Civil Engineering Wastewater Laboratory for assaying total suspended solids (TSS) using the Standard Methods (APHA, 1998), and to the Provincial Laboratory for Public Health in Calgary for testing microorganisms including FC and *E.coli* using the membrane method. In addition, the bathymetric data and catchment data of the pond were acquired from the City of Calgary. Wind data were obtained from the weather station at the Calgary International Airport.

3.2.2 Methodology

In this chapter, it is assumed that fluid is incompressible and the biological movement of bacteria is negligible. Therefore, the transport of bacteria is only governed by fluid movement and sediment transport. More specifically, free-floating and particle-attached bacteria are assumed to be transported by the fluid particles or by the sediments, respectively. In other words, the free-floating bacteria are modelled as passive scalars that do not have any effect on the flow field and follow the fluid particles; whereas the settling of sediment-attached bacteria are to be taken into consideration. Turbulence is modelled with the renormalized k-ε turbulence model. The movement of the free surface is captured using VOF and the wind effect is also considered in the model. As for bacterial decay, the first order kinetic decay is implemented to model the fate of the free-floating and particle-attached bacteria (both FC and *E.coli*), separately.

3.2.2.1 Equations of Motion

In the Fractional Area/Volume Obstacle Representation method (FAVOR) (Savage and Johnson, 2001), the continuity equation for incompressible fluid is expressed as:

$$\frac{\partial(u_j A_j)}{\partial x_j} = \frac{R_s}{\rho} \qquad (3\text{-}1)$$

where j = 1,2,3 indicate three directions of 3D domains; u_j and A_j are the velocity and the fractional area open to flow in the three directions, respectively; R_s is a mass source term; and ρ is the density of the fluid.

The unsteady incompressible Reynolds-Averaged Navier-Stokes equations which represent momentum conservation is expressed as follows:

$$\frac{\partial u_k}{\partial t} + \frac{1}{V_F}\left(u_j A_j \frac{\partial u_k}{\partial x_j}\right) = -\frac{\partial P}{\rho \partial x_k} + G_k + f_k - \frac{R_s}{\rho V_F}(u_k - u_{sk}) \qquad (3\text{-}2)$$

where t is the time; k = 1,2,3 indicate different directions; V_F is the fractional volume open to flow; P is pressure; G_k is the body force; f_k represents viscous stresses for which a turbulence model is required for closure; and u_{sk} is the injection velocity of fluid. Here, the VOF equation is used to track the free-surface (Hirt and Nichols, 1981). In the VOF model, the grid is generated for the space which might not necessarily include water. However, in solving the VOF equation, the fill fraction of fluid can be found, and the free-surface of water is located by determining the cells that are partially filled with water.

$$\frac{\partial F}{\partial t} + \frac{1}{V_F}\left[\frac{\partial}{\partial x_j}(F A_j u_j)\right] = 0 \qquad (3\text{-}3)$$

here F represents the fraction of the cell filled with fluid. The VOF model can track the free-surface of water by identifying the partially full cells that were fully exposed to fluid.

The turbulence model is based on two equations for turbulent kinetic energy and its dissipation that are derived from the *k-ε* Re-Normalization Group (RNG) method.

$$\frac{\partial k_T}{\partial t} + \frac{1}{V_F}\left(u_i A_i \frac{\partial k_T}{\partial x_i}\right) = P_T + G_T + Diff_{k_T} - \varepsilon_T \qquad (3\text{-}4)$$

$$\frac{\partial \varepsilon_T}{\partial t} + \frac{1}{V_F}\left(u_i A_i \frac{\partial \varepsilon_T}{\partial x_i}\right) = \frac{C_{\varepsilon 1}.\varepsilon_T}{k_T}(P_T + C_{\varepsilon 3} G_T) + Diff_{\varepsilon_T} - C_{\varepsilon 2}\frac{\varepsilon_T^2}{k_T} \qquad (3\text{-}5)$$

where k_T and ε_T are turbulence kinetic energy and its dissipation, respectively; P_T and G_T are the production terms of turbulence kinetic energy and buoyancy; $Diff_{kT}$ and $Diff_{\varepsilon T}$ are diffusion of turbulence kinetic energy and its dissipation, respectively; $C_{\varepsilon 1}$ and $C_{\varepsilon 3}$ are constants equal to 1.42 and 0.2, respectively. However, $C_{\varepsilon 2}$ is calculated from turbulent kinetic energy and its production term (Flow Science Inc., 2018; Yakhot and Smith, 1992).

The above equations (3-1) – (3-5) are discretized with the Finite Volume Method (FVM) using an orthogonal structured mesh based on the FAVOR method. This method can eliminate the "stair-stepping" effect normally associated with rectangular grids (Savage and Johnson, 2001), as the generated grids take up not only the fluid, but also a larger area including some of the void regions above the water surface and the surrounding solid. Therefore, the FAVOR method can well represent the interfaces and obstacles with small surfaces connected together.

3.2.2.2 Sediment and attached bacteria transport

In the model, the transport of particle-attached bacteria is modelled based on sediment transport. The transport equation of sediments, and thus particle-attached bacteria, is expressed as:

$$\frac{\partial C_{s,i}}{\partial t} + \nabla.\left(u_{s,i}C_{s,i}\right) = \nabla.\nabla\left(DC_{s,i}\right) + C_{s,i}^{sor} \qquad (3\text{-}6)$$

where $C_{s,i}$ is the sediment mass concentration of species i; D is diffusivity; $u_{s,i}$ is the sediment velocity of species i; and $C_{s,i}^{sor}$ is the sediment source term. In the model, it is assumed that 1) the sediment grains are spherical; 2) the interaction of sediment grains with each other is negligible; and 3) diffusion of sediments is negligible compared to other terms. Therefore, the main velocity difference between the sediment grains and the fluid-sediment mixture is the settling velocity of the sediment grains ($u_{settling,i}$), which is in the direction of gravity. Therefore, the sediment velocity is calculated by $u_{s,i} = u_{f\text{-}s} + u_{settling,i}$ $c_{s,i}$, where $u_{f\text{-}s}$ is the velocity of the fluid-sediment mixture; and $c_{s,i}$ is the volumetric concentration of sediment species i, which can be calculated as $c_{s,i} = C_{s,i}/\rho_i$ and where ρ_i is the density of sediment species i (Flow Science Inc., 2018). The settling velocity of sediment of species i is calculated by Eq. (7), which is an empirical relation proposed by Soulsby (1997).

$$u_{settling,i} = \frac{\upsilon_f}{d_i}\left[\left(10.36^2 + 1.049d_{*,i}^3\right)^{0.5} - 10.36\right] \qquad (3\text{-}7)$$

where υ_f is kinematic viscosity of fluid; d_i denotes grain diameter of sediment species i; and $d_{*,i}$, the dimensionless grain diameter which is calculated with Eq. (3-8).

$$d_{*,i} = d_i\left[\frac{\rho(\rho_i - \rho)g}{\mu^2}\right]^{1/3} \qquad (3\text{-}8)$$

where ρ_i is density of sediment species i; g is the gravity acceleration constant; and μ is the dynamic viscosity of fluid.

Two indicator bacteria, namely FC and *E.coli*, were modelled in this work. In spite of the fact that FC are a bacteria set that contain *E.coli*, the two indicator bacteria were modelled as separate species for two reasons. First, separate data for FC and *E.coli* had already been collected in the field campaigns. Second, in the literature, various particle sizes were identified as the particle sizes that FC or *E.coli* each show preference for attachment. Therefore, both of the bacterial indicators were modelled separately to better assess the performance of the modelling approach through comparing model results with measured data. In the City of Calgary, sediments of urban stormwater runoff have been categorised into five species according to their sizes. The physical characteristics of each species are tabulated in Table 3.2. It has been reported that more than 90% of FC are associated with small particles in the range of 0.45-10 μm (Auer and Niemaus, 1993); while *E.coli* predominantly attach to particles smaller than 2 μm (Muirhead et al., 2006). In the model, *E.coli* are assumed to attach to the particles less than 2 μm; while FC attach to the particles of 2 – 10 μm. Therefore, the sediment type "a" (Table 3.2) is further divided into two sub-categories, namely 2 – 10 μm and < 2 μm, in order to quantify the sediment-attached FC and *E.coli*. The fractions of these two sub-categories are determined by linear interpolation by particle size. In each computation cell, the concentrations of particle-attached bacteria are then determined according to the concentrations of bacteria.

Table 3.2 Stormwater sediment characteristics in the City of Calgary (The City of Calgary Water Resources, 2011)

Sediment type	Size (μm)	Density (Kg/m^3)	Fraction %
a	<10	1500	23
b	10-20	2000	9
c	20-50	2500	13
d	50-150	2650	23
e	>150	2650	32

3.2.2.3 Free-floating bacteria transport

The transport of free-floating bacteria is described by Eq. (3-9), which is basically a general transport equation written based on FAVOR (Flow Science Inc., 2018).

$$\frac{\partial F_b}{\partial t} + \frac{1}{V_F}\left(u_j A_j \frac{\partial F_b}{\partial x_j}\right) = \frac{1}{V_F}\left[\frac{\partial}{\partial x_j}\left(A_j D \frac{\partial F_b}{\partial x_j}\right)\right] + F_b^{sor} \quad (3\text{-}9)$$

where F_b is the concentration of free-floating bacteria without decay; and F_b^{sor} is the source term. In the model, it is assumed that bacteria have the same density as the surrounding stormwater and no diffusion occurs (Wu and Chen, 2011).

3.2.2.4 Fate of Bacteria

The bacteria decay is calculated based on the first-order kinetic decay (Chick, 1908) at the end of each time step to find the concentration of bacteria.

$$C_t = C_0 \exp(-\eta t) \qquad (3\text{-}10)$$

where C_t and C_0 are the concentration of bacteria at the time of t and t=0, respectively; and η is the bacteria decay rate. The temperature is the dominant parameter affecting survival of bacteria (Wang et al., 2018). The decay rate of free-floating FC is calculated by Eq. (3-11).

$$\eta_{FC} = \eta_{20}\theta^{T-20} \qquad (3\text{-}11)$$

where η_{FC} is the decay rate of FC; T is temperature; η_{20} is the decay rate of FC at 20°C; and θ is a temperature correction factor. In urban stormwater studies, η_{20} =1.167×10^{-5} and θ =1.09 were used by Selvakumar et al., (2007) and these same values are used in this work.

The decay rate of free-floating *E.coli* is modelled by Eq. (3-12), which has been used in many studies (de Brauwere et al., 2014b; Beaudeau et al., 2001; Ouattara et al., 2013).

$$\eta_{E.coli} = k_{20}\frac{\exp\left[-\frac{(T-25)^2}{400}\right]}{\exp\left[-\frac{25}{400}\right]} \qquad (3\text{-}12)$$

where k_{20} is decay rate of *E.coli* at 20°C. In this chapter, similar to Ouattara et al. (2013), a value of 1.25×10^{-5} is used for k_{20}. In this model, half of the bacteria (both FC and *E.coli*) are assumed particle-attached (Wu et al., 2009), and their decay rates are 4 times less than those of free-floating bacteria.

Figure 3.1 The study site: (a) aerial view of the City of Calgary; (b) the catchment of the Inverness Stormwater Pond (the dark solid line – catchment boundary); and (c) the locations of inlets (I1~I7), outlets (O1 and O2), and sampling locations (P1~P6) in Inverness pond [50º54'39.55"N 113º57'48.4"W at the centre of the map]

3.2.3 Model settings and simulations

In the model, inlets and outlets are represented by disk-shaped mass and momentum sources allowing flow into and out of the water body. The inflow at inlets was obtained from a previous hydrological model developed for the stormwater pond (Allafchi et al., 2019) (explained in chapter 2) in which bacteria concentrations of inflows were estimated based on the measured data at I5 inlet. The very high expenses involved in the data collection campaigns resulted in the rainfall-runoff data being collected from only one inlet. Since highly urbanized areas are associated with higher concentrations of bacteria (Mallin et al., 2009; Selvakumar and Borst, 2006), the inlets discharging stormwater from highly urbanized areas play a more important role in the bacteria distribution of the pond. The I5 subbasin is highly urbanized, relatively speaking, and the manhole before I5 inlet was easily accessible. Therefore, the I5 inlet was chosen for data collection. Bacteria

concentrations in the other inlets were based on those measured in the I5 inlet using the ratio between bacteria concentration and landuse found by Schoonover and Lockaby (2006). Figure 3.2 shows the bacteria concentration in I3, I4 and I5 during the storm event that occurred on September 20, 2007. The one corresponding to I5 shows the measurement data. The flowrate of O2 was measured for the storm events, which was used for the associated mass and momentum source in the CFD model. The flowrate of O1 was found based on the size ratio of O1 and O2, and fed to the model. Sediment concentrations in inflow at all inlets was assumed to be the same as that measured at the I5 during the data collection campaign. At the water surface, the specified pressure equal to the atmospheric pressure was used as the boundary condition. The effect of wind on the flow field is represented by a shear stress at the water surface using Eq. (3-13).

$$\tau = \rho_{air} C_D \left|\vec{W}\right| \vec{W} \qquad (3\text{-}13)$$

where τ is the shear stress; ρ_{air} is the density of the air; $\vec{W}$ is the wind vector; and C_D is the drag coefficient, which is 0.0026 (Foreman and Emeis, 2010) in the model. The time step is determined to keep the Courant number less than unity (Flow Science Inc., 2018), but not exceed 0.25s. The permanent water level of the pond was selected as the initial condition for the water level. In addition, it is assumed that the initial concentrations of bacteria and sediment in the pond are zeros. In other words, the inflows from the inlets are considered as the only sources of bacteria and sediments in the modelling, and consequently, the fate and transport of bacteria discharging into the pond in rain events are investigated. Among the four rain events that were selected based on the availability of data (Allafchi et al., 2019), one event had high flowrates, which was not used for simulation

here due to high numerical costs. As a result, the simulation was conducted for three rain events in the year 2007 (Table 3.3) in the time period from half an hour before the start of the rain events to 24 hours after the end of the events. Irrigation is unnecessary during and right after (e.g., in 24 hours) rain events. Moreover, considering the high computational demand of the model, the simulation was performed up to 24 hours after storm events when possibly starting irrigation.

Table 3.3 Rainfall data of the stormwater events in 2007

Date	Rainfall Depth	Start of the Event	End of the Event
May 28	4.8 mm	11:05 p.m. (May 27)	1:05 a.m. (May 28)
August 26	12.3 mm	9:25 a.m.	3:20 p.m.
September 20	4 mm	8:00 p.m.	9:40 p.m.

Stormwater ponds are known to be thermally stratified (Song et al., 2013) in the summer months. Accounting for thermal stratification effects on bacteria distribution by a 3D model of the kind in this work would require an extreme increase in the amount of additional computational time required to run a simulation. But field work in the Inverness pond revealed that the pond was stratified diurnally; that is, the temperature varied vertically only in the daytime hours and this stratification gradually disappeared as the evening grew (He et al., 2015). Their study also observed that this daily cycle of stratification growth and diminishment was restricted to higher parts of the water column and seemed to have no effect on sediment resuspension or turbidity. Those results coupled with the extreme

increase in computational requirements led the authors in this work to assume that the water temperature in the pond is constant. Also, He et al.'s (2015) work suggested that the impact of thermal stratification on the water column mixing is smaller than the effect of mixing due to the discharged stormwater through inlets and outlets. The pond temperature was 20, 16 and 12.9^{o}C in the events on May 28, August 26 and September 20, 2007, respectively. These temperatures were determined based on the measured temperature.

In this chapter, two sets of simulations were conducted using the model. In the first set of simulations, the model was run for the three rain events to simulate the fate and transport of the bacteria in the stormwater pond. The results were used to identify the optimal location of the pond for withdrawal for reuse, namely the location of the lowest bacteria concentrations. In the second set of simulations, the model was employed to assess the potential influence of wind reduction (e.g., by canopy) at the north bank of the West wing, where relatively high bacteria concentrations were found from the first set of simulations. In other words, the effect of wind reduction on preventing the transport of highly contaminated stormwater from the West wing to the rest of the pond was evaluated. Due to the high computational cost, the simulation was conducted only for the West wing of the pond with the same settings as the first set of simulations but with the exception of the boundary condition for the cut side of this sub-portion. The cut side of this section, which separates the West wing from the rest of the pond, is now a boundary.

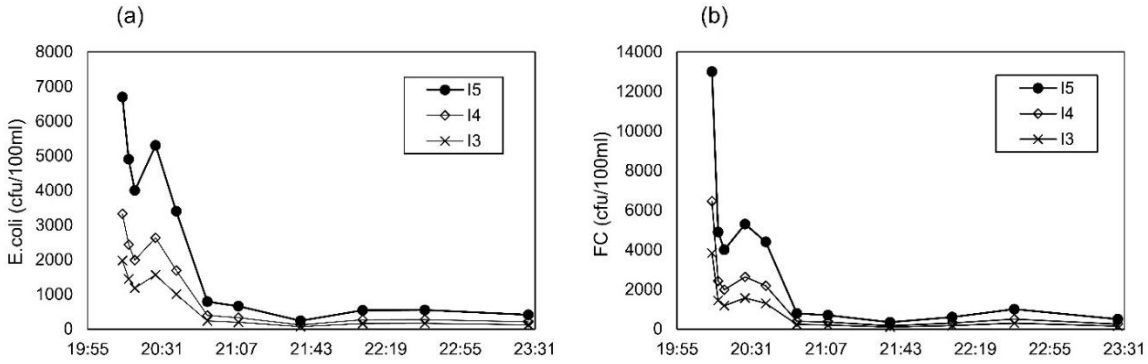

Figure 3.2 Bacteria concentration in inlet during the storm event on September 20, 2007

The velocity at this boundary is not uniform and varies with position and time, which makes it impractical to set a flux or velocity type boundary condition for the section at the cut. Instead, a time-varying specified pressure, which is equal to the water depth at the section, was used for the boundary condition at this section. The water depth at this section was obtained from the first set of simulations. To illustrate the effect of the canopy, the second set of simulations were run under the condition if the canopy reduced the north component of wind by 80% in speed. In fact, the reduction of wind speed by canopy is a function of the distance to the canopy. Manickathan et al. (2018) found that the wind speed behind a tree can change from 0 just behind the tree to 40% of the wind speed at a distance equal to 3 times the tree height. The exploration on the effect of canopy associated with distance is beyond the scope of this chapter. The effect of wind reduction by canopy on reducing pollutant transport was demonstrated by comparing the bacteria concentrations in the cases of with and without the canopy. All the simulations were run on 16 logical cores of a Xeon E5-2630 CPU for approximately 250 and 15 hours on average for the first and second sets of simulations, respectively, using the CFD commercial code FLOW-3D ®

(Version11.2) (Flow Science, 2019). It should be noted that the code was customized to calculate decay of bacteria.

3.3 Results and Discussions

3.3.1 Hydrological Performance of the Model

Inflow into the stormwater pond was monitored at Inlet I5 (Fig. 3.1), and the hydrological model was calibrated and validated for inflow at this inlet (Allafchi et al., 2019). In comparison to some of the other inlets, I5 drains a smaller subcatchment within the pond's total drainage catchment. However, landuse is critical in determining bacteria load and previous studies on the correlation between landuse and FIB showed that lands with high residential area are associated with higher concentrations of bacteria (Mallin et al., 2009; Selvakumar and Borst, 2006; and Schoonover and Lockaby, 2006). Thus, subcatchments with higher residential landuses play a more important role in the bacteria distribution in the pond; and therefore, I5 was selected for the data collection, and thus, the hydrological validation. Further validation of the model performance was performed using the CFD modelling results of the pond water level. For the CFD modelling, an orthogonal structured grid with 4 million computational cells was found sufficiently fine and the corresponding results are presented. Figure 3.3 shows the water surface elevation rise (relative to PWL) during and after the event on May 28, 2007 as an example. Regardless of the small fluctuations in the observed data, the model results show good agreement with the measured data in this storm event, as the calculated R^2 is 0.99. The calculated R^2 is 0.92 and 0.79 for storm events on August 26 and September 20 of 2007, respectively. As a

result, the model performs fairly well in simulating the hydrology and hydraulics of the catchment and the pond. In addition, it can be concluded that the hydrological model provides good inputs to CFD for the following simulation of bacteria transport and fate, and that the VOF method tracks the free surface quite well.

3.3.2 Spatial distribution of bacteria

The modelling results of the first set of simulations for *E.coli* concentration at the water surface after the storm event on September 20, 2007 at four time steps are shown in Fig. 3.4 as an example. Right after the storm event, the regions with high *E.coli* concentrations are concentrated around the inlets (Fig. 3.4a). The highly contaminated pond water around I4 gradually dispersed along the pond shore towards the north and west; *E.coli* from inlet I5 appeared to be transported towards the south; while *E.coli* from inlets I6 and I7 was transported along the West wing of the pond towards the east (Fig. 3.4b - 3.4c). A full 24 hours after the end of the storm event (shown in Fig. 3.4d), *E. coli* appeared to be transported towards the west half of the pond in the South wing, which is also where *E. coli* concentrations were higher than that in the east half of the pond. FIB originate directly or indirectly from the intestines of human and warm-blooded animals, so residential areas introduce relatively more bacterial loading. As a result, during the storm events, more bacteria loading was discharged into the pond through I4, I5, I6 and I7 located in the West and South wings compared to I1, I2 and I3 in the East wing. Subbasins I1 and I2 are very small compared to other subbasins and the primary land use type of subbasin I3 was non-residential. As a result, among the three wings (namely West, East and South wings) of the pond, overall the West and South wings showed to have relatively higher *E. coli*

concentrations, while the East wing had the lowest concentration. The subbasins on the west side of the pond had the highest residential densities in the entire catchment, so I6 and I7 discharged the most contaminated stormwater with respect to bacteria loading. I4 discharged the highest volume of stormwater because the subbasin corresponding to I4, which is the largest in the catchment, is more than 8 times the surface area of I6 and I7 combined. Moreover, the residential area in the I4 subbasin is larger than that of I5 and I6 combined. The South wing had the highest numbers of bacteria, but the bacterial numbers were diluted by higher discharges as compared to the West wing, which experienced the highest concentrations of bacteria. The distribution of FC (data not shown) in this storm event is similar to that of *E. coil*.

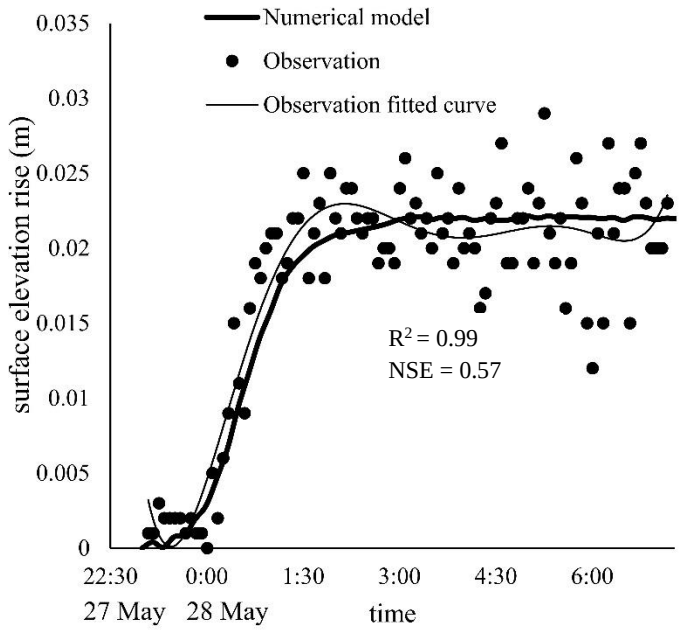

Figure 3.3 Simulated and measured water surface elevation rise during and after the storm event on May 28, 2007

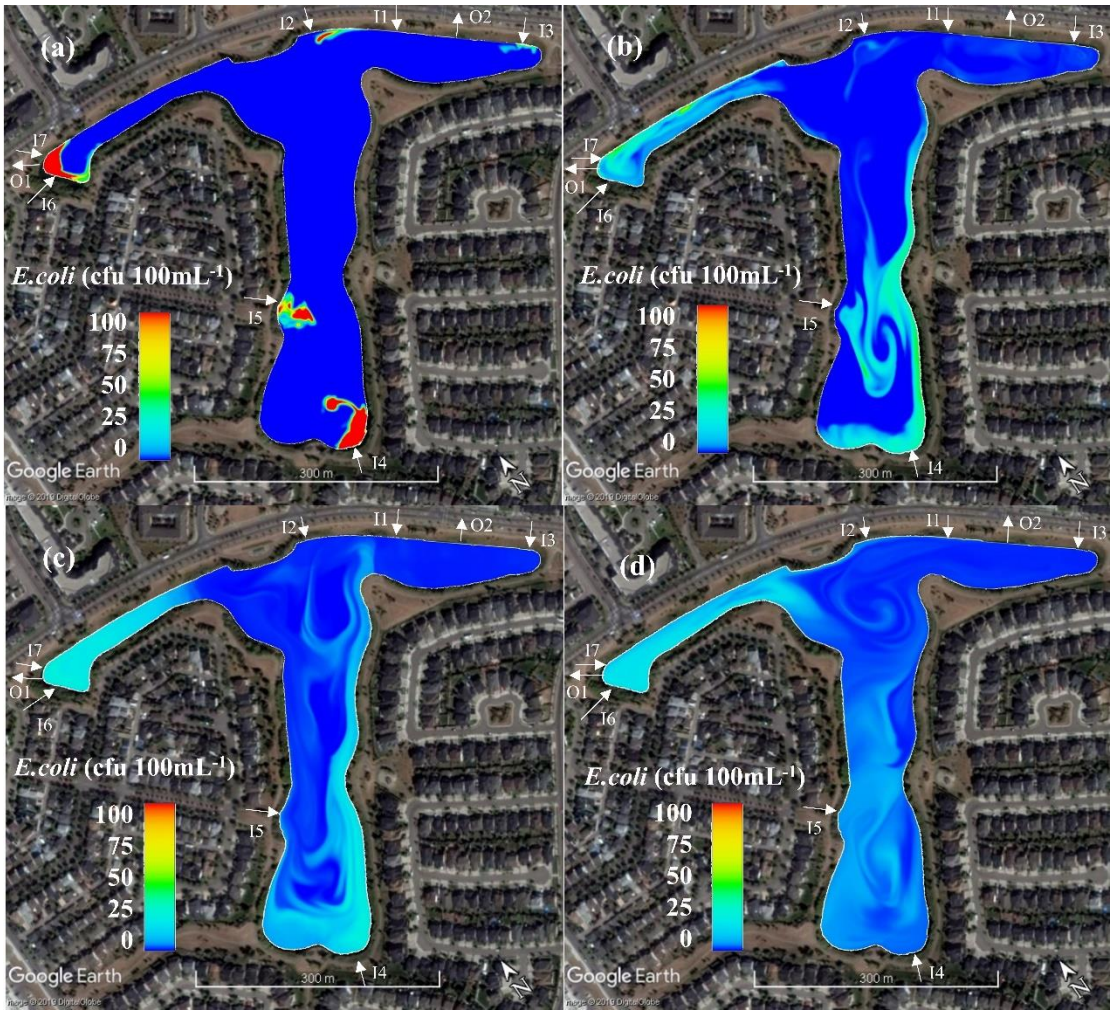

Figure 3.4 Modelled *E.coli* concentration on the surface of Inverness pond on a) September 20, 2007 at 9:40 pm, b) September 21, 2007 at 3:40 am, c) September 21, 2007 at 3:40 pm, and d) September 21, 2007 at 9:40 pm

As highlighted by de Brauwere et al., (2014a) the lack of data leads to challenges in validating mechanistic models and thus, are often neglected (Wu and Chen, 2011; Vergeynst, et al., 2012; Shilton and Mara, 2005). Similarly, the data used in this work was not necessarily collected in the most appropriate way for this type of work (the data

collection campaigns preceded this research) and consequently, the database is sparse at certain points in time. However, introducing a non-dimensional number enables a validation between model results and available data through a relative comparison as opposed to an absolute one. The modelled bacteria concentrations were compared with the measured ones in terms of their normalized values at the six sampling locations (15 cm below the water surface) of the pond. Modelled and measured bacteria concentrations were normalized with their highest concentrations of the six sampling locations in the corresponding modelling event (for modelled concentrations) and sampling events (for measured concentrations), separately. Note that the modelled bacteria concentrations at the end of modelling (namely at 24 hours after the end of storm events) were used to derive the modelled normalized concentrations for the comparison. Figure 3.5 displays the comparison of the averaged normalized modelled (over three modelling events) and measured (over the sampling events) bacteria concentrations at the six sampling locations. The normalized measured bacteria concentrations were derived for two cases: case 1 - by using all measured data (26 data points), and case 2 - by using the measured data collected on sampling days, when rain event(s) occurred within three days prior to the sampling days (7 data points out of the 26 in case 1). According to the measured concentrations (in both cases), among these six sampling locations, the best and least preferred locations for withdrawing stormwater from the pond for irrigation are located at P4 and P3, respectively. This is where smallest and largest average normalized values were calculated, respectively, for both *E.coli* and FC. Both cases agree on the best and least preferred locations, which shows the overall distribution of bacteria in the pond does not change substantially between

the time frames of the two cases. The modelling results both for *E.coli* and FC are in agreement with the measured data (in both cases) in this aspect. It should be noted that P4 is near the shore and close to inlet I2, which together can increase the risk of contamination of water in the withdrawal region. Therefore, at the water surface, the region where the three wings meet that is also away from the shore, has the lowest risk of contamination for reuse. When comparing the modelling results and measurements, for *E.coli*, the modelling results appear to be in better agreement with the measurements of Case 2 in 5 out of 6 locations (Fig. 3.5a). For FC, the measurements of Case 2 better match the modelling results in 4 out of 6 locations (Fig. 3.5b). The modelling results in general capture the spatial variation of bacteria concentrations at the water surface of the pond.

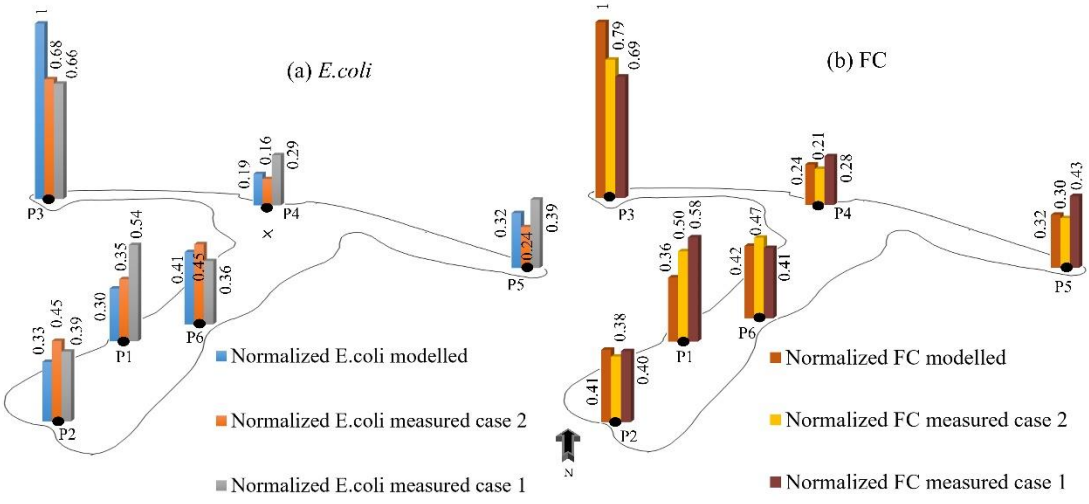

Figure 3.5 Comparison of modelled and measured average normalized concentrations of (a) *E.coli*; and (b) FC in the Inverness Stormwater Pond. The cross in (a) shows the position of the joint of the three wings.

In addition, Figure 3.6 shows the vertical distribution of FC in the middle of the withdrawal area (shown by a cross in Fig. 3.5a) at several time steps after the ends of the three rain events, respectively. Results for vertical distribution of *E.coli* in the area were similar to that of FC. Northeast wind occurring close to the end of rain event on August 26, 2007, transported stormwater that was freshly discharged from I2 to the middle of the pond. Regardless of that particular case, regions near the surface demonstrated the lowest bacteria concentrations in water column. Therefore, the region of the pond close to the water surface and in the middle of the pond is considered the optimal location for water withdrawal for reuse. It should be noted that the impact of extracting water on the bacteria distribution in the pond was not considered in this chapter. However, it is recommended to be investigated in future studies.

In this model, the VOF was employed to deal with water surface of the pond, and the mesh was generated in a way that allows the water surface elevation to vary. In addition, sedimentation of the sediment-attached bacteria was introduced into the current model. Compared to the model previously developed by Allafchi et al. (2019) for the same pond, in which the effects of water surface change and sedimentation of bacteria were neglected, differences in the spatial distribution of bacteria concentrations at the water surface are obvious. Results from this model show that among the three wings, the West wing was the most contaminated followed by the South wing. However, the results of the previously developed model (explained in chapter 2) found that the South wing is the most contaminated (Allafchi et al., 2019). The current model can capture the spatial distribution of both *E.coli* and FC near the water surface. In addition, the validation in the present work

was strengthened because modelling results were compared against the normalized concentrations derived from observations collected on 26 random days, plus 7 of these 26 random days that were found to be within three days of a rain event. In the results of a previous model version (see Allafchi et al., 2019) application, the previous model results were compared to normalized concentrations derived from observations only the day after an event. Therefore, it can be concluded that the inclusion of VOF and sedimentation of bacteria in the model has strengthened the appropriateness of the modelling in estimating bacteria concentration.

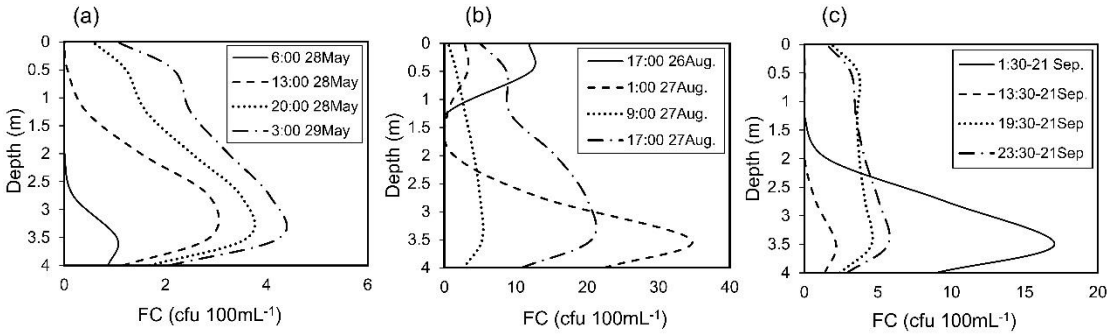

Figure 3.6 Vertical distribution of FC after the end of the rain events on (a) May 28, 2007; (b) August 26, 2007; and (c) September 20, 2007

O1 is located near I6 and I7, and thus a large portion of the discharged stormwater left the pond immediately through the outlet. It should be noted that in the beginning of a storm, stormwater is often more contaminated (Todeschini et al., 2019), but the flowrate of this outlet is relatively low. Hence, there is opportunity for the highly-contaminated stormwater discharged from the I6 and I7 inlets to distribute throughout the West wing, particularly if the wind accelerates the distribution.

3.3.3 Effect of Wind on Bacteria Transport

In the second set of simulations, the bacteria transport in the West wing of the stormwater pond was explored to illustrate the effect of wind mitigation on bacteria transport and its spatial distribution. The spatial distribution of *E.coli* concentration at the water surface for the entire pond, and the West wing only can be seen in Fig. 3.7a and 3.7b, respectively. The modelled results at 24 hours after the end of the rain event on September 20, 2007 are illustrated as an example. As shown in these figures, these two cases of modelling (the entire pond and only the West wing) yielded similar results as a similar spatial distribution pattern in *E.coli* concentration was observed in the West wing area in both figures. In addition, the difference in the bacteria concentrations between these two modelling cases was calculated as less than 10% for high concentration locations (along the south bank of the wing). Note that the second set of simulations has far less computational cost as compared to simulating the full pond. The success of this work suggests that it is feasible to simulate a particular sub-portion of a large pond when knowing the boundary conditions at the section of interest and particularly if simulating the whole pond is expensive.

Therefore, the effect of wind on bacterial transport was investigated using this modelling approach and focusing on the West wing. In general, north wind is dominant in the region. Hence, it was expected that planting a tree barrier on the north bank of the wing would be more effective to reduce/mitigate the bacteria transport (Fig. 3.7c) to other parts of the pond. In addition, for this stormwater pond, planting trees on the north bank of the West wing would have the advantage of not obscuring sun light, which can enhance bacterial decay (de Brauwere et al., 2014a). Note that the effect of a tree barrier on wind reduction

in fact depends on multiple factors including tree height and density. In this simulation, to illustrate the effect of wind reduction on the bacterial spatial distribution, the north component of wind was reduced by 80% in the simulation. Figure 3.7c presents the modelled bacteria distribution at the water surface at 24 hours after the end of the rain event on September 20, 2007. Different from the case with no wind reduction (Fig. 3.7b), this simulation (Fig. 3.7c) shows that wind reduction hinders the highly contaminated stormwater from traveling further east along the West wing to the east end of this wing. Figure 3.8 shows the flow field streamlines corresponding to Fig. 3.7b (without wind reduction) and 7c (with wind reduction). Comparing Fig. 3.8a and 3.8b, it can be concluded that the wind reduction not only decreased velocity magnitude but also changed velocity direction of the flow in the wing.

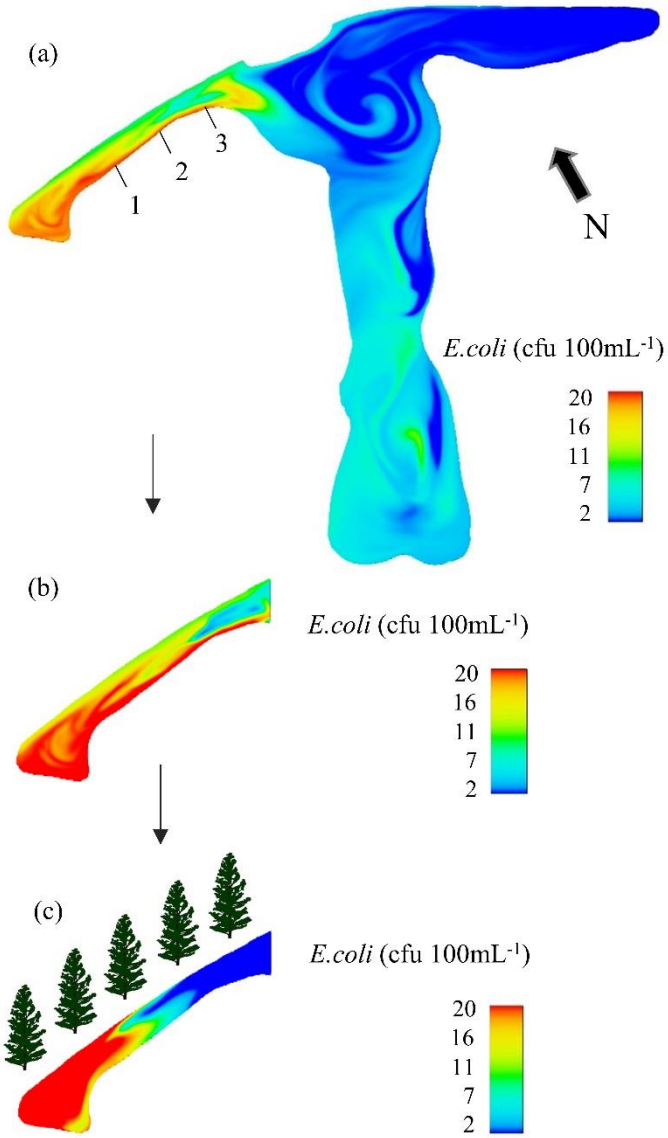

Figure 3.7 Modelled *E.coli* concentrations on the surface at 24 hours after the end of the event on September 20, 2007: (a) entire pond simulation; (b) only West wing simulation; (c) only West wing with 80% reduction of north component of wind

Furthermore, the temporal variations of *E.coli* and FC concentrations (at 10-minute time intervals) at three selected sites in the West wing (shown in Fig. 3.7a) after the September 20th event are shown in Figure 3.9 for the two cases of with and without wind reduction.

The transport of bacteria from the West wing to the rest of the pond occurred at the second 12-hour period after the event (Figure 3.4d) and the entire pond simulation results and the case without the trees agree well (see Figure 3.9). This suggests that simulating only the West wing can be used to study the transport of bacteria to the rest of the pond. The concentration of bacteria at all three sites decreased considerably when the effect of wind reduction was added. In particular, the effect of wind reduction on the decreases in both FC and *E.coli* concentrations appear to be more prominent at sites 2 and 3, where the concentrations at these two sites remained low. Since the primary source of bacteria in the wing is the inflow from I6 and I7 situated at the west end of the West wing, the reduction of bacteria concentrations at the east of the wing could be due to the reduction of flow velocity and thus, reduction of advection of bacteria towards the east. Similar results are obtained for the other two simulated events. It should be noted however, that the trees may also come with some adverse effects. For example, the increased concentration of bacteria might diffuse to the environment, or the trees might attract birds that may lead to increased fecal contamination in the area. Therefore, more research is recommended to investigate the impacts of the trees.

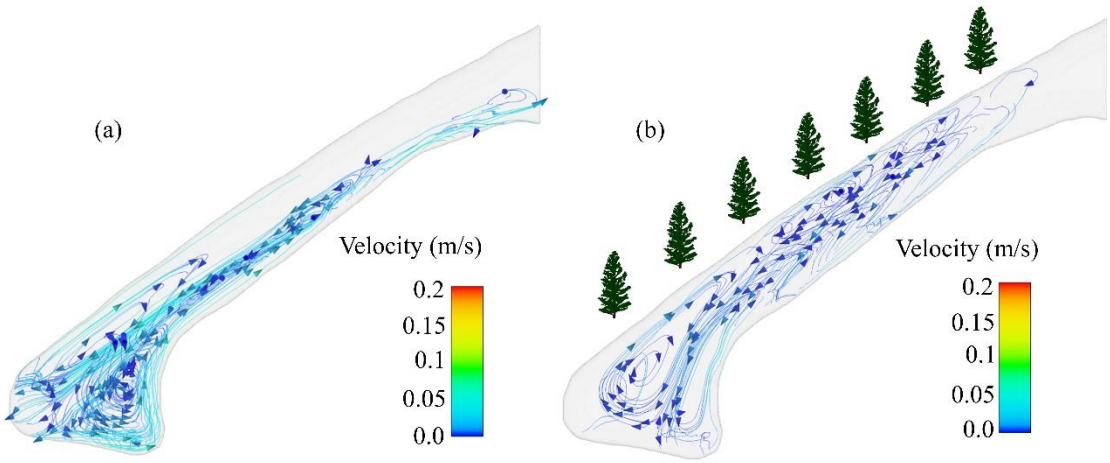

Figure 3.8 Flow field streamlines in the West wing at 24 hours after the end of the event on September 20, 2007: (a) without wind reduction and (b) with 80% reduction of north component of wind

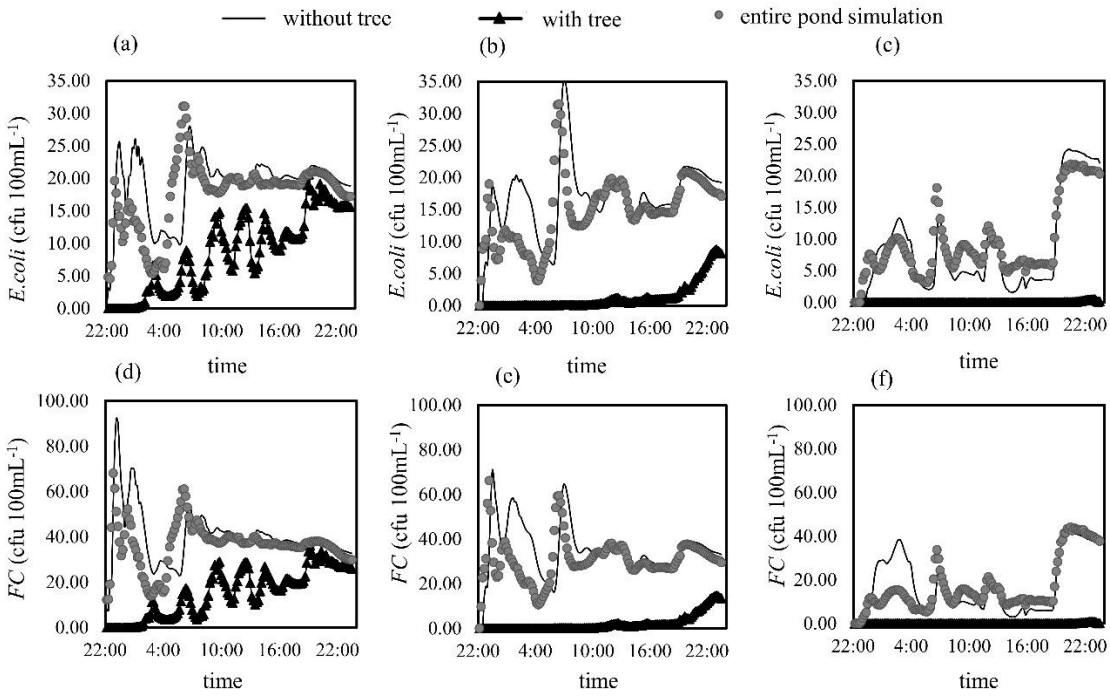

Figure 3.9 Temporal variations of bacteria concentrations after event on September 20, 2007: (a) *E.coli* at site 1, (b) *E.coli* at site 2, (c) *E.coli* at site 3, (d) FC at site 1, (e) FC at site 2, and (f) FC at site 3

3.3 Conclusion

A mechanistic model was developed for modeling the transport and fate of bacteria in water bodies. The model was fed by the inflows that were simulated by the hydrological model developed previously by Allafchi et al. (2019). Free-floating and particle-attached bacteria were modelled separately both for their fate and transport. In addition, the effect of water surface elevation change was taken into account using a VOF model coupled with a CFD model. The application of the model was illustrated by modelling bacteria concentrations in the Inverness Stormwater Pond located in Calgary, Alberta, Canada. The proposed model captured the post-storm, spatial distribution of bacteria at the pond water surface reasonably well with the data collected. The inclusion of the VOF for free water surface and settling of particulate attached bacteria might enhance the model performance, as the modeling results were in better agreement with field measurements when compared to the previous model (Allafchi et al., 2019). Implementing this model for the Inverness pond showed that the optimal location for water withdrawal from this pond was near the surface and at the middle of the pond (the joint of the three wings) because it had the lowest bacteria concentrations. In addition, the developed model was applied to illustrate the effect of wind reduction (e.g., by trees) on the transport and thereby on the spatial distribution of bacteria in the West wing, which was identified to have relatively high bacteria concentrations. To mitigate the transport of highly contaminated stormwater from the west end of the West wing into the pond water body, implementing a tree barrier against the wind was proposed. It could considerably reduce bacteria transport towards the east end of the West wing and thus, can reduce the public health risk due to reuse of the stormwater

withdrawn from the region, where the three wings meet. The model can be used to simulate bacteria fate and transport in medium to large-size water bodies such as stormwater ponds and waste stabilization ponds. Also, physical water quality improvement measures, such as strategic tree planting or baffles, can be studied in the future using the model.

Since 2007, the catchment characteristics for this pond have changed. In 2007, the major land use of the I3 subbasin was farm land and part of the land was under development for future residential areas. In addition, the land use in I4 subbasin has changed significantly since 2007 and it is likely that the amount of impervious area has increased for both subbasins and along with that, bacterial loading and inflow rates have increased. Thus, given the success of the model in the current work, an application of this model using more up-to-date catchment data is recommended to identify the current optimal location for water withdrawal given the changes in catchment land use.

4. A Velocity Meter for Quantifying Advection Velocity Vectors in Large Water Bodies

4.1 Introduction

Measuring streamflow velocity is an essential component in numerous applications and interests and several studies have been conducted to assess how flow velocity is measured in practice (Guaraglia and Pousa, 2014). Labaky et al. (2009) introduced the Point Velocity Probe (PVP), which estimates flow velocity based on the travel time of a saline tracer between an injector and two detectors. The tracer is detected by measuring the conductivity of fluid (mainly water). The injector and detectors are located on the surface of a cylindrical probe. Experimental tests revealed that the instrument is capable of measuring flow velocities between 5 and 98 cm per day (Labaky et al., 2009). Another instrument for water flow velocity measurement is called the Horizontal Heat Pulse Flowmeter (HHPF), which consists of a probe containing a heater surrounded by a circular array of thermistors. A heat pulse is generated by the heater and diffuses radially. If the medium is stagnant, a symmetric distribution of heat is expected. However, the water displacement causes some advection of heated water, thus, leading to an asymmetric distribution of heat. Therefore in this situation, there is a difference between temperatures read by thermistors. By calibrating temperature differences versus water velocity, the velocity can be estimated (Guaraglia and Pousa, 2014). Experimental results showed that HHPF can measure flow velocities between 3.5×10^{-8} to 3.5×10^{-5} m/s (Melville et al., 1985).

Colloidal borescope is another instrument for measuring flow velocity, consisting of magnifying lenses and miniature video cameras capable of observing natural particles in the flow. Using this method, both flow direction and magnitude can be measured. As particles pass beneath the lenses, a light source illuminates the particles. The video recorded by the camera is later analyzed to find the flow velocity. The best results with this instrument are obtained for particles moving with a rate below 12×10^{-3} m/s (Guaraglia and Pousa, 2014) and the total velocity range is below 25×10^{-3} m/s (REALtime Aquifer Services 2020). The velocity ranges of PVP, HHPF and colloidal borescope make them suitable for primarily groundwater applications and are not particularly suited for surface waters.

However, there are other types of velocimetry methods that are more suitable for surface flow measurement. For example, propeller-based velocity meters, in which the flow causes rotation in a small propeller that is facing the flow direction head-on. The velocity range of such velocity meters is larger than PVP, HHPF and colloidal borescope. However, the range starts at a relatively higher value because the flow should be strong enough to overcome the friction in the mechanical parts of the instrument. The velocity range of a typical propeller-based velocity meter, used in research studies (Chen et al., 2016) is between 0.07 and 7 m/s (Dalian Zero Instrument Technology Co. 2020). This range makes the propeller-based velocity meters mostly suitable for measuring flow velocity of relatively fast flowing rivers but not other water bodies such as lakes and ponds because the low end of the range of the device might be higher than the flow velocity experienced in most parts of a large water body.

On the other hand, Particle Image Velocimetry (PIV) is a global, quantitative method for monitoring fluid flow that yields a distribution of vectors over a plane or a volume (Rahimpour et al., 2018; Raffel et al., 2018). In this method, tracer particles, so-called seeds, are illuminated with a known frequency. The light scattered by the tracer particles is recorded by a camera in a sequence of frames and the displacement of particles between light images is calculated through sophisticated post-processing (Raffel et al., 2018). This method has been used extensively in various research projects; however, PIV requires multiple instruments for which the setup is time consuming and complicated.

Moreover, acoustic Doppler velocimetry is a robust method for measuring flow velocity components in different directions. The working principles of Acoustic Doppler Velocity meter (ADV) consist of Doppler phase analysis of the high-frequency signal backscattered from suspended particles. Commercial ADVs have an emitter in the center that transmits short acoustic pulses at a fixed frequency. The disseminated acoustic pulse collides with suspended particles or bubbles, reflects back and is sensed by receivers that focus on a common region of the fluid called the 'sampling volume.' The physical size of the sampling volume for a commercial ADV is a cylinder less than one cm in both length and diameter (SonTek, 2020). The flow velocity is estimated analyzing the phase change between two successive coherent signals. ADVs are sophisticated instruments, however, they are easy to operate and are extensively used in different hydraulic field and laboratory studies (Moeini et al., 2020). The operating velocity range of a commercial ADV is between 0.001 and 4 m/s (SonTek, 2020), which makes it useful for measuring flow velocities of rivers and other water bodies. However, they cost between 10K to 20K CAD, which makes it an

unaffordable tool for many research and engineering projects. In addition, the footprint of ADVs—the physical size of the sampling volume—is very small compared to other velocimetry methods.

Recent research into stormwater ponds includes developing a model that can estimate bacteria level, such as *E. coli*, in stormwater in order to improve Best Management Practices in Canada (Allafchi et al., 2019). In these types of studies, the majority of hydro-environmental modelling in the literature is not validated (Vergeynst et al., 2012; Sah et al., 2011; Wu and Chen, 2011). On the other hand, the importance of understanding the fluid flow field in such water bodies is highlighted (Allafchi et al., 2019). Therefore, in attempts to validate modelling with observations of flow field velocity in the field, no affordable velocity meter was found on the market that can be used to measure flow velocities in medium to large water bodies such as stormwater ponds. Therefore, a velocity meter was designed and built to address this need. The velocity meter or Dye Injection Velocity meter (DIV), is calibrated in a laboratory scale flume equipped with a PIV and further validated in a stormwater pond using an ADV. The method of dye injection was chosen for its simplicity, low cost and practical range of use. In terms of velocity range, the closest type of device to the DIV meter designed here is an ADV, however, the disadvantages associated with an ADV noted above make it less than ideal for the application of interest.

4.2 Materials and Methods

The DIV was designed and built in the Mechanical Engineering Machine Shop of the University of Victoria, Victoria, BC, Canada. The DIV has four main parts including an injector, a graduated plate, a camera and a structural frame holding the camera over the plate facing downward. The frame includes a pole and an arm with a clamp at the end to hold the camera. The pole is connected perpendicularly to the plate using a support beneath the plate. The operating principles involve injecting dye tracer into the flow and recording videos of the dye being transported by the flow. Electric red AmeriColor® soft gel paste was diluted in water with the ratio of 2 to 1000 mL. The dye is injected from a vertical injector protruding from the center of a graduated plate. The plate is graduated with multiple circles, sharing the same center and diagonal lines that concur at the center. Each two consecutive circles and diagonal lines are 1 cm radially and 15 degrees angularly distanced, respectively. Figure 4.1 shows a schematic of the velocity meter. A 1000TVL Sony CCD endoscope camera, which was originally used as a pipe inspection camera, was held downward above the injector and plate with an arm. Several LED lights, already attached to the camera, illuminate the plate. Using a 30 mL syringe, the dye is injected and the camera records the movement in a 50 frame per second video. The video is saved and later analyzed frame by frame on a computer. It is assumed that the dye reaches flow velocity within 2 cm of the injection point. Therefore, the flow velocity was estimated by dividing 0.16 m length by the time it takes for the dye to travel from the second innermost circle to the outermost circle, which is 18 cm in radius.

The target range of velocity that the DIV can measure was set to be between 0.01 m/s and 0.2 m/s. At this range of velocity the flow over the plate stays laminar and the boundary layer thickness is determined by Equation (4-1) (Kundu et al., 2016).

$$\delta = \frac{4.9\mathrm{L}}{\mathrm{Re}^{1/2}} \quad (4\text{-}1)$$

where δ is the boundary layer thickness; L is the length of the plate and equal to 0.36 m; and Re is the Reynolds number. The maximum boundary layer thickness, which occurs at the end of the plate with a flow velocity equal to the lower bound of the velocity range, is equal to 0.028 m. Therefore, protruding the injector 3 cm higher than the plate is assurance that the viscous effects due to the plate on the transport of the dye is negligible.

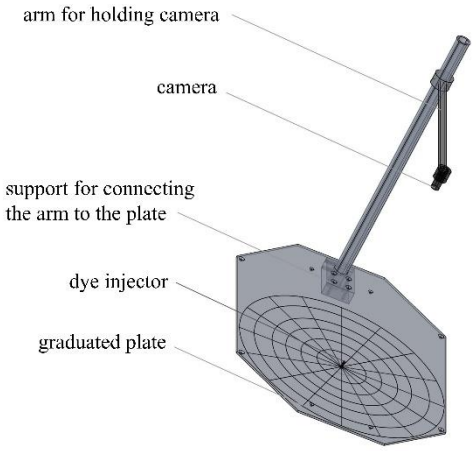

Figure 4.1 DIV and its components

4.2.1 Calibration Setup

The DIV meter was calibrated using a flow visualization flume equipped with a PIV system and located at the Fluid Mechanics Laboratory in the University of Victoria, Victoria, BC, Canada. The velocity operating range of the flume was not quite low enough for the test. Therefore, a 40 mm diameter flexible tube was placed near the injector and

discharged the flow generated by a COPBB5 SHURflo Pedestal Mount centrifugal pump run by a Parker MPP1003D1E-KPSN motor. The tube was placed behind the injector so that the middle of the tube and the tip of the injector were at the same height. In this way, the injected dye was subjected to the highest discharged velocity. Various flow rates and thus flow velocities, were obtained by changing the rotor speed. The plane of interest for the PIV was parallel to the graduated plate, at a height equal to that of the center of the tube and the injector's tip. Image shifting via a flat mirror was utilized for the PIV camera to overcome the optical restrictions. The mirror has an axial rotation around the *y*-axis at an angle of $\phi = 45°$ to prevent distortion. The camera field of view was set to capture the dye path in the middle to minimize any velocity shift (Oschwald et al., 1995). Furthermore, the main velocity component, which is parallel to the rotation axis of the mirror (y-direction) is expected to be less sensitive to velocity shifts (Zhang and Eisele, 1995). Moreover, the water level was set high enough to prevent any surface effects. Figure 4.2 demonstrates the calibration test setup configuration. The dashed line in the Figure shows how the image was shifted by the mirror. The PIV camera was situated beside the flume recording the images and the laser was next to it at a lower height. It should be noted that the mirror and its supporting parts were only used for the calibration test and they are not part of the DIV.

The PIV system consists of Davis LaVision 10.0.1 software utilized for raw image acquisition and calculations of velocity vectors. Particles with a mean diameter of 10 μm were illuminated by the Quantel Evergreen Nd:YAG 532 nm wavelength dual pulsed laser. The laser beam was expanded into a planar sheet that illuminated the data acquisition plane (DAP). Images of the DAP were recorded using a LaVision XS 6M camera equipped with

a lens with the focal length of 50 mm and a 532-nm narrow-band filter, at an acquisition rate of 13 Hz. The field of view of the images corresponded to the spatial domain was 160 mm × 80 mm. The resolution of raw image was 2752 pixels × 2200 pixels. The captured raw images were processed with a final interrogation window size of 64 × 64 pixels with 75% overlap applied throughout the multi-pass vector calculation process (LaVision GmbH, 2018). The spatial resolution of the resulting velocity vector field was 0.76 vectors/mm. Averaged velocity field was calculated by averaging 300 instantaneous velocity fields at each flow velocity. For the purpose of calibration, the PIV vectors from the averaged field were spatially averaged along a straight line between 2 and 18 cm far from the injector, respectively.

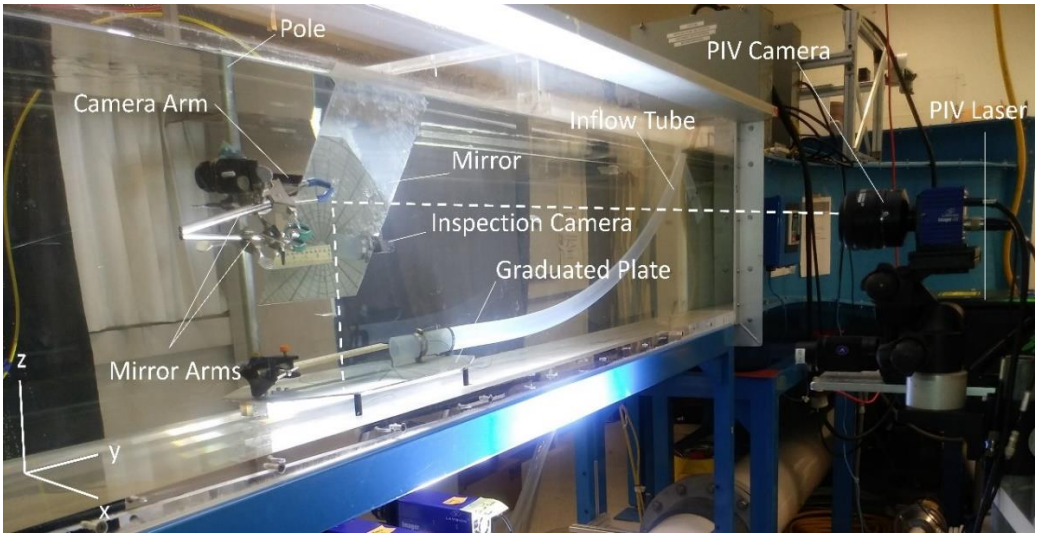

Figure 4.2 Calibration test setup at the Fluid Mechanics Laboratory, University of Victoria, Victoria, Canada.

4.2.2 Validation Setup

The DIV was deployed to the Inverness stormwater pond, Calgary, Canada, for validation tests. A structure was built to secure two canoes with a 1-m distance in between. The gap between the canoes was used to send the DIV down into the water. Four anchors were used to keep the boats in the data collection location. A heavy weight was sent to the bottom of the pond with a rope using a pulley attached to the structure. The rope was threaded through the pole of the DIV and tightened using the pulley. Figure 4.3 shows data collection locations and the validation tests' setup. The velocity meter was kept in place using another rope attached to the camera arm. Velocity data from two locations on August 27, 2020 and four locations on August 29, 2020 were collected using both the DIV and FlowTracker2®, which is a commercial ADV (SonTek, 2020). The characteristics of the data collection locations are tabulated in Table 4.1. The ADV recorded two samples per second and the velocity was calculated based on 80 collected samples.

Table 4.1 Characteristics of data collection points.

Location	Depth from Water Level (m)	Date and Time
P1	0.3	27 August 2020 12:50 p.m.
P1	0.6	27 August 2020 01:35 p.m.
P2	0.3	29 August 2020 11:04 a.m.
P2	0.6	29 August 2020 11:25 a.m.
P2	0.9	29 August 2020 11:45 a.m.
P3	0.3	29 August 2020 02:08 p.m.
P4	0.3	29 August 2020 04:30 p.m.

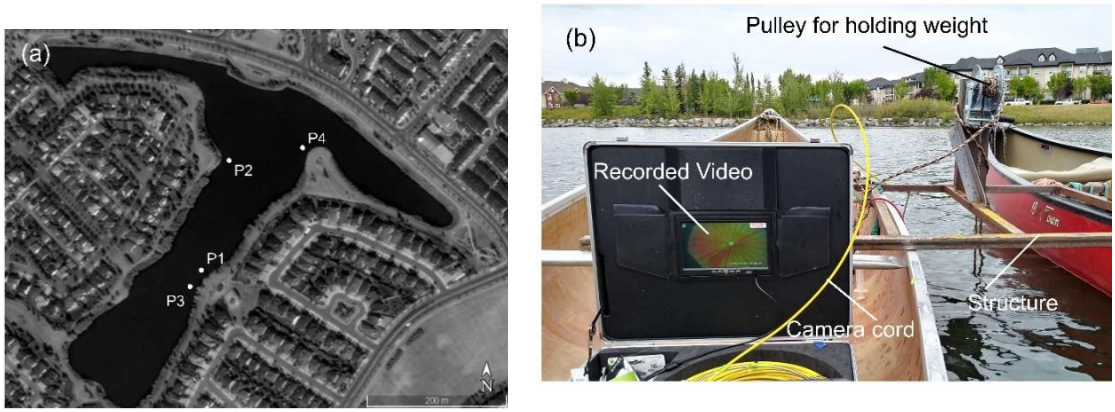

Figure 4.3 (a) Data collection locations in the Inverness pond (background photo extracted from Google Earth); (b) validation setup.

4.3 Results and Discussions

4.3.1. Calibration with the PIV

In order to generate various fluid flows over the graduated plate for the calibration purpose, the rotor speed was altered to vary the flow. Following the rotor speed changes, enough time was given to let the flow reach steady state. Then, data were collected using both the DIV and PIV. Figure 4.4 illustrates a few sequences of a video recording the transport of dye in the flume. At each step, the dye was injected multiple times and the averaged elapsed time was considered for velocity calculations. The whole process, including changing rotor speed, multiple injections and PIV was repeated three times. Figure 4.5 contains an image of the velocity and vector fields resulting over the plate. The image is the time-averaged velocity vector field and the contours of time-averaged velocity magnitude in the horizontal plane located just above the plate (PIV plane of interest) obtained under repeatable laboratory conditions using PIV. The location of the injector

point is indicated by a circle in the schematic in Figure 4.5. The data acquisition area extended from 2 cm downstream from the injector point (the right vertical boundary of the plot) and 18 cm downstream from the injector point (the left vertical boundary of the plot.) The velocity plot shows gradients of velocity across the top of the plate both in the streamwise and the transverse directions. These gradients can lead to errors in the case of very high flows, as discussed below.

Eleven data points in the second round and 10 data points during each of the other rounds were collected, making the total number of the data points equal to 31. The calibration curve of the DIV for all of the data was obtained and shown in Figure 4.6a. The R^2 value of the calibration curve is more than 0.98, indicating a successful calibration and that the instrument can be reliably used to measure flow velocities.

Comparing the velocity values estimated by the DIV and PIV, it was found that the DIV overestimated the velocity, for likely two reasons. First, due to turbulence and unsteady flow velocity in the dye pathline, the travel time that is recorded is the time for the fastest particles in the dye stream. Second, the dye is injected just above the plate and the DIV camera, which is located above the dye injector, observes the dye stream and plate beneath it from an angle that becomes more and more skewed as the dye progresses with the flow stream. This angle leads to a velocity overestimation and is illustrated in Figure 4.7. At the moment in time shown in Figure 4.7, DIV estimates the travelled distance to be equal to L2, whereas, the actual travel distance is L1 (and $L1 < L2$). This causes an underestimation in the dye travel time, which results in overestimation of flow velocity.

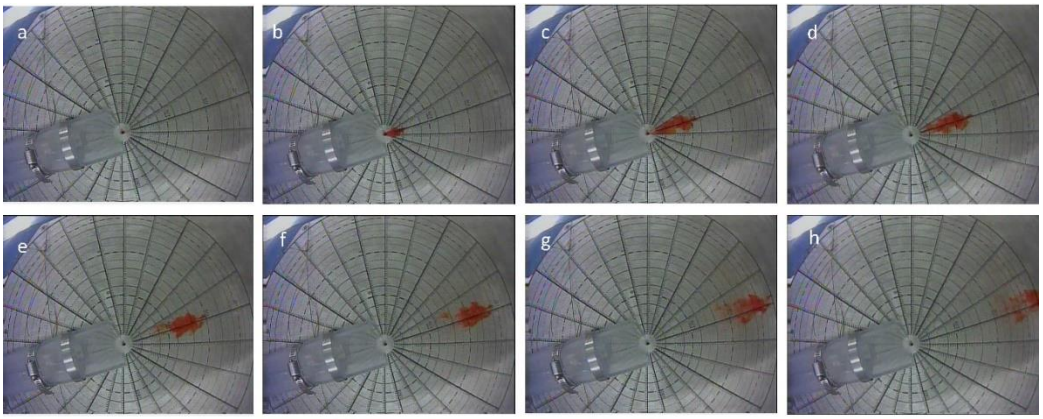

Figure 4.4 Transport of dye at an estimated speed equal to 0.14 m/s (prior to calibration) at (a) t = 0; (b) t = 0.380 s; (c) t = 0.619 s; (d) t = 0.710 s; (e) t = 0.928 s; (f) t = 1.244 s; (g) t = 1.520 s; and (h) t = 1.839 s

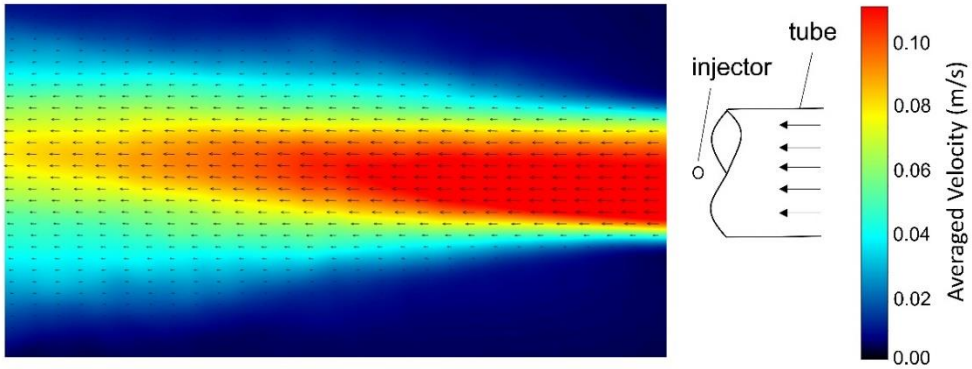

Figure 4.5 Particle image velocimetry (PIV) calculated velocity contour and vector field over the plate at a flow speed = 0.102 m/s

The velocity target range had originally been set between 0.01 and 0.2 m/s and the low end of the target range was properly detected. However, no proper data was collected at flow velocities higher than 0.1566 m/s due to dye dispersion. This may have occurred because of the high velocity gradient present in the flume at high flow velocities, as shown in Figure 4.5. Hence, the DIV was calibrated for a velocity range between 0.0094 and

0.1566 m/s. Figure 4.6b shows the deviation of estimated velocity. The highest deviation from the calibration curve occurred at 0.0174 m/s and 0.0591 m/s, which were equal to +0.0094 m/s and −0.0145 m/s, respectively. Therefore, the accuracy of the instrument can be calculated as +6.3% and −9.8% of the output span. Higher uncertainties were observed near the low end of the detection range, with the highest equal to 28.7% corresponding to the low end of the range. As the flow velocity increased, the uncertainty decreased. For flow velocities higher than 0.06 m/s, 0.08 m/s and 0.1 m/s, the uncertainty was less than 15%, 10% and 5%, respectively.

The injection of the dye might induce some turbulence to the main flow that may contribute to a loading error. However, the calibration, through which the dye was injected multiple times, in separate, statistically independent tests, provides assurance that this effect is taken into account and its impact thereby reduced. In addition, the flume, in which the calibration tests were performed, was not able to generate very low flow velocities that fit the intended application. Therefore, low flows were generated using a rotor pump and tube added to the flume. However, the fluid flowed only locally and thus high velocity gradients existed at the periphery of the resulting jet flow. The turbulence due to the high velocity gradients is a source of calibration error and made it difficult to keep track of the dye and measure flow velocities higher than 0.1566 m/s. Therefore, it is believed that testing the DIV in a flume that is able to generate low velocity flows would not only result in a calibration with lower deviations but also might expand the calibration velocity range.

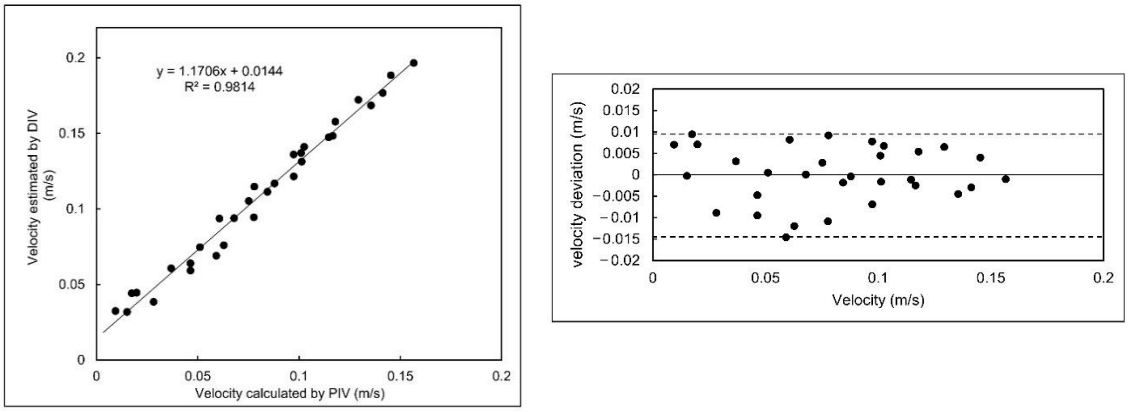

(**a**) (**b**)

Figure 4.6 (a) Calibration curve; (b) plot of deviation data for Dye Injection Velocity (DIV) calibration.

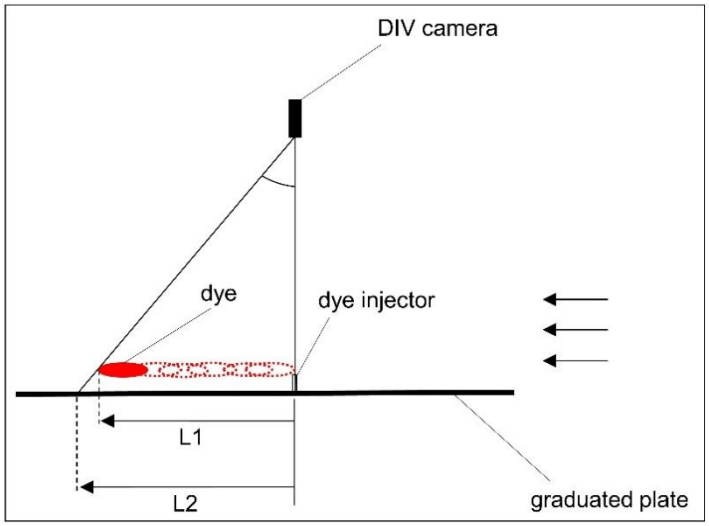

Figure 4.7 Actual distance travelled by the dye vs. the DIV camera estimation.

4. 3.2. Uncertainty Analysis

There is some uncertainty associated with the recorded video of the DIV and how this uncertainty propagates to a final estimate of velocity can be calculated using error analysis. The distance that the dye traveled and the associated travel time were found by analyzing the video. The recorded video had a resolution of 720 × 288 pixels and 50 fps of frame rate.

That corresponds to 0.5 mm and 0.02 sec of distance and time uncertainty, respectively. These uncertainties propagate to the final estimate of velocity and this propagation is computed below. Velocity was calculated using Equation (4-2). The uncertainty in velocity due to the propagation of distance and time uncertainties can be calculated by Equation (4-3).

$$V = \frac{d}{t} \qquad (4\text{-}2)$$

$$\sigma_V = \pm \sqrt{\left(\left(\frac{\partial V}{\partial d}\right)\sigma_d\right)^2 + \left(\left(\frac{\partial V}{\partial t}\right)\sigma_t\right)^2} \qquad (4\text{-}3)$$

where V, d and t are velocity, distance and time associated with the travel of the dye; and σ_V, σ_d and σ_t are the velocity, distance and time uncertainties, respectively. Equation (4-4) is the simplified form of Equation (4-3) with the appropriate substitution for the derivatives.

$$\sigma_V = \pm \sqrt{\left(\left(\frac{1}{t}\right)\sigma_d\right)^2 + \left(\left(\frac{-d}{t^2}\right)\sigma_t\right)^2} \qquad (2\text{-}4)$$

The uncertainty of velocity due to the propagation of distance and time uncertainties was found to be between $\pm (6 \times 10^{-4})$ m/s and $\pm (3.9 \times 10^{-3})$ m/s.

In addition, the velocity uncertainty can be analyzed with regard to the collected data. There are two kinds of uncertainty involved in the experiment, namely random and

systematic uncertainties. The random uncertainty is calculated using Equation (4-5) (Wheeler and Ganji, 2004):

$$P_V = \pm t \frac{S}{\sqrt{M}} \qquad (4\text{-}5)$$

where P_V is the random uncertainty in velocity; t is the appropriate value of the *t*-distribution given the confidence level of the calculation; S is the standard deviation; and M is the sample size. The total uncertainty was calculated with Equation (4-6):

$$W_V = \sqrt{B_V^2 + P_V^2} \qquad (4\text{-}3)$$

where W_V is the total uncertainty; and B_V is systematic uncertainty, which can be calculated from the accuracy of the instrument (Wheeler and Ganji, 2004). The data corresponding to the flow velocity of 0.0777 m/s after calibration were selected for uncertainty analysis because it has the largest sample size equal to 19. The random uncertainty for the mean value of the samples was calculated to be 0.0026 m/s with a 95% confidence level. The maximum systematic uncertainty was calculated by multiplying −9.8% by the full scale and found to be 0.0144 m/s. In general, the total uncertainty was calculated as 0.0146 m/s and this shows that the systematic uncertainty has a larger impact on the total uncertainty in the experiment as compared to the random uncertainty.

4. 3.3. Validation with the ADV

Validation was performed in the Inverness stormwater pond and the results were compared with the results obtained from an ADV. The dye was injected multiple times and the velocity was averaged at each location. During the validation, flow direction was

recorded as well as corresponding magnitude and the data were compared with that measured by the ADV. Figure 4.8 shows measured velocity magnitude results before averaging as estimated by both devices. Velocity data were collected from seven different spatial locations. However, the velocity magnitude at P4 was lower than the calibrated range and thus, the DIV was only used to find flow direction at this location.

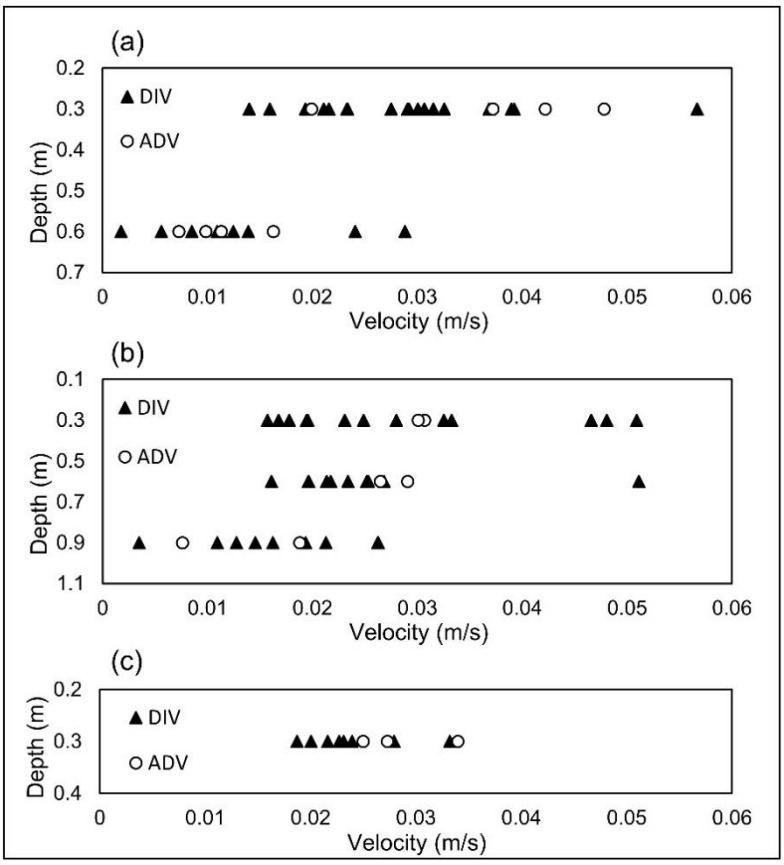

Figure 4.8 Validation tests results for flow velocity at (a) P1; (b) P2; and (c) P3.

In order to compare the velocity magnitude data measured by the DIV and ADV, a Mann-Whitney test was performed. The *p*-value obtained for the difference in velocity magnitudes was larger than 0.05 in all of the spatial points; thus, indicating that the

differences between the data are not statistically significant. In addition, the averaged values were compared and good agreement was observed. The lowest deviation between the averaged DIV and ADV occurred at the highest velocities recorded at P1 and P2 at both a 0.3 m depth. The percentage of those deviations are the lowest as well; equal to 4% and 5%, respectively. Conversely, the highest deviation between the averaged DIV and ADV measurements was equal to 0.0048 m/s, which occurred at location P3 at depth 0.3 m. However, the highest percentage in deviation was associated with P2 at a depth of 0.9 m and was equal to 27%. The velocity at this spatial point was close to the low end of the detection range and high uncertainty at the low end of the range was to be expected (Wheeler and Ganji, 2004). In addition, at this spatial point, the flow direction data were the most relatively dispersed as shown in Figure 4.9b. At low velocities, even small eddies can change velocity direction substantially. Therefore, low velocities may include higher random errors.

There were other sources of systematic and random error involved in the validation tests. For example, during data collection, the data were not collected with the DIV and ADV simultaneously in order to avoid any interaction. However, specific attention was paid to shorten the time it took to switch from one device to another by as much as possible. While the flow in a medium to large water body like the Inverness Stormwater pond does not change instantly, it is possible that in the time it took to switch devices over the same collection point, the flow velocity may have changed, particularly in low velocity flows; thus adding to the random error. In addition, the boats were not perfectly still during data acquisition and they moved slightly with large waves or strong wind gusts. Furthermore,

the boats might have had a loading impact on the flow by changing the velocity vector immediately around the boats. It should be noted that the structure held the DIV in the gap between the boats at a point equally distant from each boat in order to minimize the effects of the boats.

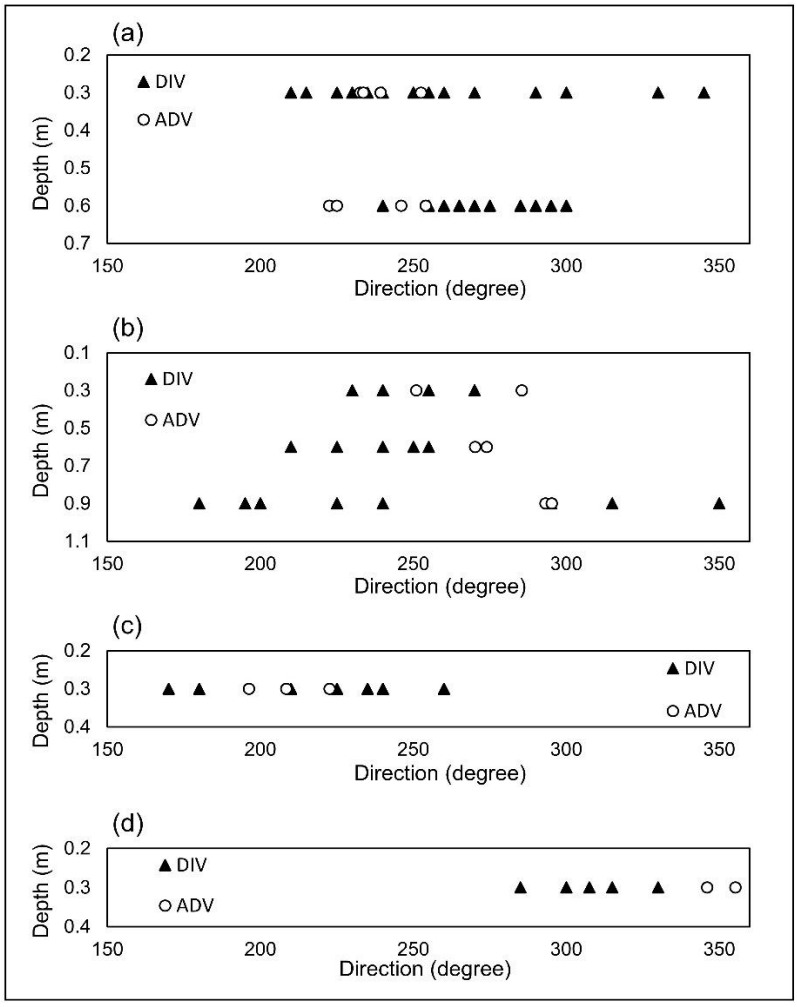

Figure 4.9 Validation tests results for flow direction at (a) P1; (b) P2; (c) P3; and (d) P4.

4.4 Conclusions

An efficient and easy to use Dye Injection Velocity meter was designed and built to measure fluid flow velocity magnitude and direction in medium to large water bodies at a relatively low cost. The DIV was calibrated for flow velocities between 0.0094 and 0.1566 m/s in a flume equipped with a PIV. An R^2 value of 0.98 was obtained for the calibration curve and the accuracy of the instrument was calculated as between +6.3% and −9.8% of the output span. It was found that the uncertainty decreases with increasing velocity. Following the calibration tests, the DIV was validated against an ADV in a large stormwater pond and good agreement was achieved. Velocity magnitudes estimated by the DIV showed no statistically significant difference with those of ADV. The deviation between flow velocity measured by the DIV and that of ADV decreased with increasing velocity. During the validation tests, velocity direction was also measured. Although the difference between the flow direction measured by the DIV and ADV at two spatial points were significant, the deviation of the averaged values did not exceed 14% at any of the points. The results of the tests proved that the DIV can be used as a tool for velocity measurements in the range indicated here. However, further calibration tests in a flume that can generate very low velocities is recommended to provide better calibration accuracies.

5. Influence of Environmental Factors in Hydrodynamic Modelling of Bacterial Distribution in Stormwater Ponds

5.1 Introduction

Reusing stormwater for overcoming water scarcity problems due to urbanization and climate change is becoming more prevalent in water resources management plans (Rodríguez-Sinobas et al., 2018; He et al., 2008). Stormwater may be considered an alternative resource for applications requiring less than pristine water quality; and therefore, stormwater retention ponds are the most viable sources of stormwater for large scale reuse (He et al., 2008). Several studies have been conducted regarding stormwater reuse (Goonetilleke et al., 2017; Hammes et al., 2018; National Academies of Sciences and Medicine, 2016; Allafchi et al., 2019; Zhang et al., 2015); however, pathogens in stormwater are still a source of public health concern (Mankad, et al., 2019). Therefore, in most jurisdictions, the stormwater must meet local guidelines for water quality depending on the end-use. If reusing stormwater suggests that a potential exposure to bacteria and pathogens is possible, knowledge that guideline or regulation levels are never exceeded is necessary for reliable stormwater reuse. This knowledge is either ascertained through measurement or through modelling.

Assessing the bacteria and pathogen levels through measurement is often not practical for a variety of reasons including accessibility, spatial scale (physical size of the pond), and the variability in each of the multitude of environmental factors that may affect bacteria

and pathogen levels over space and time. Therefore, computational models offer more practical solutions and studies have been developed to simulate bacteria fate and transport in large ponds with the intention of identifying the optimal location for water withdrawal (Allafchi et al., 2019; Allafchi et al., 2021). Bacteria and pathogenic related water quality is often indicated through Fecal Indicator Bacteria (FIB) because FIB exist in abundance in warm-blooded animal intestines and are easily detected/measured (Borrego and Figueras, 1997). *E.coli* is the most common FIB and is currently used as a standard indicator bacteria (Tallon et al., 2005) for many jurisdictions. The source of FIB in stormwater ponds would arise from animal sources in the drainage area that are washed off, or added directly into the pond (from waterfowl, for example).

The literature includes numerous models developed for simulating water quality of runoff from watersheds (Vanaei et al., 2021; Shrestha and Wang, 2019) including the fate and transport of FIBs in watersheds. These models generally involve integrating a hydrological model with a bacteria fate model (de Brauwere, et al., 2014a) and are primarily 1-dimensional for a variety of reasons including data availability issues (Aguilera et al., 2018). They can provide a low-cost approach to simulating bacteria fate and transport over large areas where only one dimension or only one direction is a reasonable assumption in the modelling. Water quality modelling of water bodies like stormwater ponds requires the additional integration of hydrodynamic concepts. Hydrodynamics is used in many studies of water quality in water bodies, but many are 1- or 2-dimensional treatments (Wang et al., 2018; Zheng et al., 2011; Babaeyan-Koopaei et al., 2003) that may involve large uncertainties depending on the circumstances.

There are a handful of 3-dimensional models that use Computational Fluid Dynamics (CFD) for simulating bacteria in water bodies. CFD models have been shown to be capable of determining spatial and temporal bacteria concentration in large water bodies such as stormwater ponds (Allafchi et al., 2019). While computationally expensive, they are sophisticated modelling systems that can provide a wider array of outcomes and possibilities for engineering design, while avoiding the inaccuracies of 1- and 2-dimensional treatments to real-world applications. A CFD model was developed to simulate the fate of *E.coli* in a stormwater pond arising from a variety of processes including attachment and settling (Vergeynst et al., 2012). The authors assumed that there was no convection and the importance of attachment in the bacterial decay process was highlighted. Shilton and Mara (2005) modelled the transport of *E.coli* in large waste stabilization ponds with different configurations using a 3-dimensional CFD model that incorporated a first order decay model (a commonly used fate model). The model focused on the bacteria concentration in the inlet and outlet and implemented a bacteria decay model according to the residence time calculated by the CFD. Similarly, fecal coliform levels in various waste stabilization ponds were also simulated using 3-dimensional CFD models (Shilton et al. 2008; Shilton and Harrison, 2003; Shilton, 2000), thus, highlighting the capability of CFD models for simulating fate and transport of bacteria. Wu and Chen (2011) also incorporated a first order kinetic decay model in a 3-dimensional CFD model to simulate biological oxygen demand (BOD) in an anaerobic lagoon with good success.

While the movement of water in water bodies is observed to be inherently wind driven (Abbasi et al., 2016), all of the above mentioned studies neglected wind effects. Moreover,

all of the transport models assumed steady state conditions, which may only be appropriate in a few circumstances. In most real-world situations, conditions are rarely steady state. Allafchi et al. (2021) developed an Integrated hydrological-CFD model (IHCFD) to simulate bacteria fate and transport in the Inverness stormwater pond, in Calgary, Alberta, Canada, that incorporated wind and unsteady conditions. The model had two components: a hydrological component and a CFD component. The hydrological component calculated the stormwater runoff discharging into the pond from the catchment, which provided inputs to the CFD model to simulate the bacteria in the pond in three dimensions. The model was also used to find the optimal location for water withdrawal for reuse.

There are two main challenges associated with the models simulating bacteria fate and transport. First, as it is highlighted in previous studies (Allafchi et al., 2019; de Brauwere et al., 2014a), due to a lack of data, model verification is very challenging and thus, often neglected. Second, modeling fate and transport is a highly parameterized endeavour, and due to the general lack of information on all these parameters, numerous assumptions are made in order to develop a functioning model. These assumptions, if left invalidated, lead to inherent uncertainty in the output. In this paper, both of the aforementioned problems are considered in the further development of the IHCFD model. The IHCFD was modified in this work by adding a non-settling particulate-attached bacteria concept, introducing alternate attachment rates and varying sediment sizes. In this research, IHCFD was verified using bacteria concentration data and fluid flow data (Allafchi et al., 2020) collected in a variety of locations spatially and with depth, that were compared with those data predicted by the model at these locations. In addition, the impact of several important assumptions

made in IHCFD on bacteria distribution were studied. Moreover, in an attempt to decrease dependability on on-site collected data for design purposes, the model's capacity to provide a reasonable bacteria distribution without actual data was also studied.

5.2 Methodology

5.2.1 Study Site

The Inverness stormwater pond is a T-shaped, large urban stormwater pond located in a residential area in the Southeast quadrant of the City of Calgary. On average, it is approximately three meters deep and has seven inlets and two outlets (see Figure 5.1). The inlets discharge stormwater runoff from a catchment that is approximately 415 ha in surface area.

Figure 5.1 The study site: (a) aerial view of the City of Calgary; and (b) the locations of inlets (I1~I7), outlets (O1 and O2) [50º54'40.07"N 113º57'45.18"W at the centre of the map]

5.2.1.1 Data Collection Campaigns

A wide variety of data have been collected at the study site over a near 15-year period (He et al., 2015; He et al., 2010; He et al., 2010; He et al., 2011; He et al., 2011b; He et al., 2008; Allafchi et al., 2020) primarily during the irrigation seasons. Data were collected in the pond in 2004 to 2007, 2017, 2018 and 2020 through surface grab samples, stormwater runoff samples, on-site meteorological data and flow field velocity measurements. The surface grab samples were collected from the pond in a depth equal to 10-20 cm below the surface. They were collected from 6 sampling locations during between 2004 and 2007 and this sampling was repeated for 4 locations in 2017. The locations in the first sampling campaign were selected to be greater in number and distribution throughout the pond because the goal was to understand bacteria distribution in the pond, and to identify the optimal location for water withdrawal. However, the second sampling campaign was aimed to further verify the model regarding the developments in the catchment between 2007 and 2017. Therefore, the samples were collected from a fewer number of locations in the second campaign. Figure 5.2 shows the grab sampling locations. Samples were tested for several water quality indicators including *E.coli*. The data was collected in 26 and 24 days during the first and second campaign, respectively, with no attempt to favor rainy or dry days. The stormwater runoff sampling included flowrate and *E.coli* concentration. To be specific, flowrates of inlet I5 and outlet O2 were measured at a 5-minute interval. In addition, an autosampler, triggered by a rain gauge, was placed in a manhole before the inlet I5 in order to measure *E.coli* concentrations. The stormwater runoff sampling scheme was scheduled to collect more samples (namely at shorter time intervals) in the beginning of the events in

order to catch the first flush effect. The meteorological data includes 5-minute rain data in a time period between 2004 and 2007 as well as 5-minute wind data collected on August 29, 2020. Flow field velocity data were also collected from multiple locations in the pond in 2020. Further details on the collection and use of these data for verifying the IHCFD model components are given below.

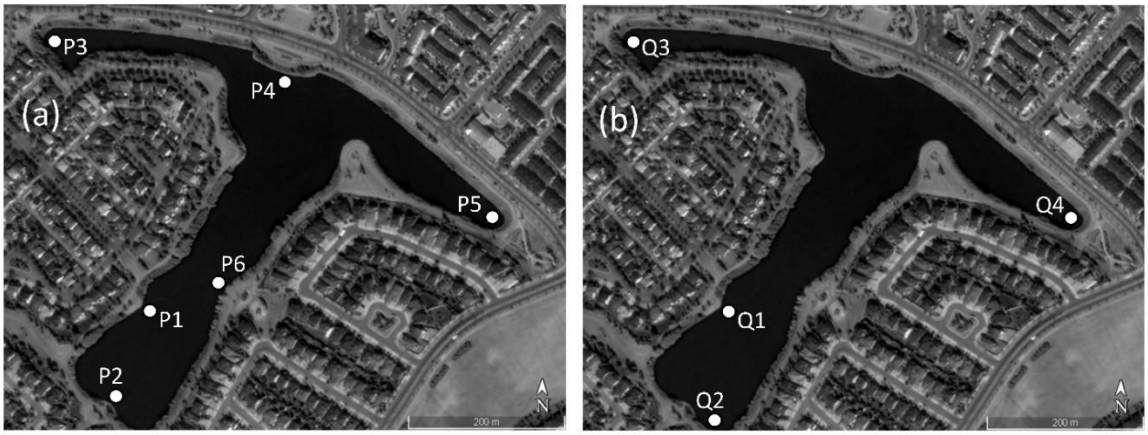

Figure 5.2 Grab sampling locations for the data collection campaigns performed in a) 2004 to 2007; b) 2017

5.2.2 Hydrological and Hydrodynamic Bacteria Fate and Transport Modelling

The developed model has two components: a hydrological component, a CFD component with a bacteria fate model embedded in.

5.2.2.1 Hydrological Model

The hydrological component involves HEC-HMS (U.S. Army Corps of Engineers. Hydrological Modeling System HEC-HMS, User's manual 2016), which calculates stormwater runoff using the SCS curve number method based on landuse data. HEC-HMS

was previously calibrated and verified for the drainage catchment to the pond (Allafchi, et al. 2019) using data in the field campaigns that took place from 2004 to 2007. This component provides stormwater runoff generated by the catchment's subbasins transported through the inlets of the pond as input to the CFD component.

5.2.2.2 CFD Model

The CFD model with inputs from the hydrological model simulates pond hydrodynamics leading to a simulated bacterial distribution in the pond. For this purpose, conservation equations are numerically solved where the equations are discretized over a grid that is generated according to the Fractional Area/Volume method (FAVOR^{TM}), which enables the equations to recognize the boundaries without the need to necessarily make a body-fitted grid. Equation (5-1) shows the conservation of mass, in FAVOR (Savage and Johnson, 2001).

$$\frac{\partial\left(u_j A_j\right)}{\partial\left(x_j\right)} = \frac{R_s}{\rho} \qquad (5\text{-}1)$$

where j = 1,2,3 indicates the three directions of 3D domains; u_j and A_j are the velocity and the fractional area open to flow in the three directions, respectively; R_s is a mass source term; and ρ is the density of the fluid. Equation (5-2) shows Reynolds-Averaged Navier Stokes equation (RANS), which represents the conservation of momentum.

$$\frac{\partial u_k}{\partial t} + \frac{1}{V_F}\left(u_j A_j \frac{\partial u_k}{\partial x_j}\right) = -\frac{\partial P}{\rho \partial x_k} + G_k + f_k - \frac{R_s}{\rho V_F}\left(u_k - u_{sk}\right) \qquad (5\text{-}2)$$

where t is the time; k = 1,2,3 indicate different directions; V_F is the fractional volume open to flow; P is pressure; G_k is the body force; u_{sk} is the injection velocity of fluid; and

f_k represents viscous stresses for which a turbulence model is required for closure. The renormalized group k-ε turbulence model is used for modeling the turbulence.

The free surface is tracked by solving the Volume of Fluid (VOF) equation, Equation (5-3) (Hirt and Nichols, 1981).

$$\frac{\partial F}{\partial t}+\frac{1}{V_F}\left[\frac{\partial}{\partial x_j}\left(FA_j u_j\right)\right]=0 \qquad (5\text{-}3)$$

where F represents the fraction of cell filled with fluid. Using the Finite Volume Method, the equations are discretized over an orthogonal structured grid which has over 4 million meshes. A 3-dimensional sketch of the pond was generated using AutoCAD Civil 3D based on bathymetric data that was collected during a survey performed on August 30, 2016. The equations are solved for unsteady state in the time period from half an hour before the start of the rain events to 24 hours after the end of the events. The time step is determined to keep the Courant number less than unity (Flow Science, 2018), but not to exceed 0.25s.

The inlets are modelled with disk-shaped mass and momentum sources, for which the input values are obtained from the hydrological component as noted earlier. The hourly wind data was obtained from the meteorological station at the Calgary International Airport. The wind is modeled as shear stress acting on the top layer of the grid using Equation (5-4).

$$\tau=\rho_{air}C_D\left|\vec{W}\right|\vec{W} \qquad (5\text{-}4)$$

where τ is the shear stress; ρ_{air} is the density of the air; $\vec{W}$ is the wind vector; and C_D is the drag coefficient, which is 0.0026 (Foreman and Emeis, 2010) in the model.

5.2.2.3 Bacteria Transport

The transport of bacteria heavily depends on attachment. Regarding the transport of bacteria, three types of bacteria, including free-floating bacteria, settling particulate-attached and non-settling particulate attached bacteria, were used in this study. It was assumed that the biological movement of bacteria is negligible and that the bacteria have a negligible effect on the flow field. Thus, the free-floating bacteria move with the water and are modeled as a passive scalar. The non-settling particulate-attached bacteria transport is similar to that of free-floating. However, their fate is different from the free-floating. Both the free-floating and non-settling particulate-attached bacteria transport are modeled using equation (5-5).

$$\frac{\partial F_b}{\partial t} + \frac{1}{V_F}\left(u_j A_j \frac{\partial F_b}{\partial x_j}\right) = \frac{1}{V_F}\left[\frac{\partial}{\partial x_j}\left(A_j D \frac{\partial F_b}{\partial x_j}\right)\right] + F_b^{sor} \quad (5\text{-}5)$$

where F_b is bacteria concentration, D is diffusivity and F_b^{sor} is the bacteria source term. Similar to previous studies (Wu and Chen, 2011; Allafchi et al., 2019), it was assumed that the diffusion of bacteria is negligible compared to convection.

A sediment transport model was integrated into the main model in order to simulate the transport of settling particulate-attached bacteria. All types of the aforementioned bacteria are transported with the fluid flow, with an exception of the settling particle-attached bacteria that settle once following the fluid flow. In other words, that type of bacteria has

an extra component of velocity downward. Equation (5-6) shows the extra downward component of velocity related to the settling particulate-attached bacteria.

$$u_{settling} = \frac{v_f}{d}[(10.36^2 + 1.049d_*^3)^{0.5} - 10.36] \qquad (5\text{-}6)$$

with d is the grain diameter and d_* equal to the dimensionless grain diameter.

According to the City of Calgary (The City of Calgary Water Resources, 2011), stormwater runoff of the region carries a wide range of sediment size. However, it was assumed that *E. coli* attach to particles smaller than 2 μm (Muirhead et al., 2006). Similar to previous studies (Bai and Lung, 2005; Allafchi et al., 2019; Wu et al., 2009), it was assumed that half of the bacteria are attached to sediment particles.

5.2.2.4 Bacteria Fate Model

Once the transport of both free-floating and particulate-attached bacteria is determined, a field function implements the first order decay of bacteria on them separately and calculates the total number of bacteria in each computational cell. Similar to previous studies (Wu et al., 2009), it was assumed that the decay rate of the attached bacteria is a quarter of that of free-floating bacteria. Equation (5-7) shows the first order kinetic decay.

$$C_t = C_0 e^{(-\eta t)} \qquad (5\text{-}7)$$

where C_t and C_0 are the concentration of bacteria at the time of t and $t = 0$, respectively; and η is the bacteria decay rate. The temperature is the dominant parameter affecting survival of bacteria (Wang et al., 2018). The decay rate of free-floating *E. coli* is modelled by Equation (5-8), which has been used in many studies (de Brauwere et al., 2014b; Beaudeau et al., 2001; Ouattara et al., 2013).

$$\eta_{E.coli} = k_{20} \frac{e^{\left[-\frac{(T-25)^2}{400}\right]}}{e^{\left[-\frac{25}{400}\right]}} \qquad (5\text{-}8)$$

where k_{20} is decay rate of *E. coli* at 20°C. In this paper, similar to Ouattara et al. (2013), a value of 1.25×10^{-5} is used for k_{20}.

5.2.3 CFD Model Verification Data

Specific details on what data were used, and how, to verify the IHCFD model's velocity flow field and predicted bacteria concentrations are given below.

5.2.3.1 Flow Field Velocity Data

On August 29, 2020, flow field velocity magnitudes and directions were measured in multiple locations within the pond from two canoes deployed near the centre of the pond. Figure 5.3 shows the canoe setup and locations where the data were collected. At each location, the canoes were secured using 4 anchors and a weight sent to the bottom with a winch held between the boats. Also, specific attention was paid to position the canoes in the wind direction in order to minimize the impact of the canoes on the flow near the data collection locations. The data were collected at different depths and with two instruments: an Acoustic Doppler Velocity meter (ADV) and a Dye Injection Velocity meter (DIV) (Allafchi et al., 2020). However, due to the limitations in the devices, in some locations the data were acquired with only one instrument. The ADV cable did not allow measurements deeper than 1.8 m. In addition, DIV had limitations in measuring flow field velocity when in very low speeds (Allafchi et al., 2020). The wind driven flow field in the pond was simulated using the wind data collected from a meteorological station installed on the

Northwest side of the pond. The collected data and the simulation results were compared for the purpose of model verification. The flow field was measured at V1 on August 27, 2020; however, the meteorological station was not working properly on that day. Therefore, the data on that location was not used for the verification.

Figure 5.3 Data collection on August 29, 2020 a) canoe setup; and b) data collection locations (the aerial map was acquired from Google earth)

5.2.3.2 Bacteria Concentration Data

The bacteria concentration in the inlet I5 was measured during several storm events in 2007. The bacteria concentration in the other inlets was obtained based on the landuse in other subbasins and by knowing the relationship between the landuse and concentration of bacteria in the stormwater (Schoonover and Lockaby, 2006). TSS were also measured during the data collection campaign. TSS of other inflows was assumed to be the same as that of I5. In addition to the data collected from the I5 inlet, *E.coli* data from grab samples data collected from 10-20 cm below the surface in six locations inside the pond (P1~P6 in

Figure 5.2) in 2007 were also used. *E.coli* data collected in 2017 from the four locations sampled that year were also used.

5.2.4 Verification and Assessment Methods

A sensitivity analysis was conducted to assess the assumptions used in the model. The Basis of Comparison (BOC) from which the sensitivity analysis was made is from three storm events: one on September 20, 2007; another on May 28, 2007; and the third on August 26, 2007. The IHCFD model was setup to simulate the pond's response and resulting bacterial distribution during and after each of these storms, which served as the BOC. The impact of some of the model assumptions on the bacteria distribution was assessed through the *sensitivity* of bacteria concentrations at 7 locations (the six locations P1 to P6 and the withdrawal location) by modifying specific model assumptions and comparing the results to that of the BOC. To be specific, bacteria distribution in the 7 locations after the events were computed for different assumptions of: (i) attachment rate of bacteria; (ii) sediment particle size that the bacteria attach to; (iii) rain hyetograph; (iv) wind direction; and (v) wind magnitude. As well, a sixth set of simulations involved determining the average wind during the irrigation season and the simulations were run with that wind in order to assess the predictability of the bacteria distribution during average wind and zero wind conditions. The time period of the simulations was half an hour before the start of the events until 24 hours after the end of events. Irrigation is generally unnecessary during and right after (e.g. within 24 hours) rain events. Therefore, the bacteria distribution in the pond 24 hours after the end of the events, when possibly starting irrigation, was of interest. Herein, the term "after event" refers to 24 hours after

the end of the event. Numerous simulations were run for this paper, however, particular attention was paid to change only one assumption/input at a time.

The attachment study was performed only for the event on September 20, 2007. However, the other assumptions were assessed for all of the three events. Attachment to four particle sizes was simulated and the distribution of bacteria in the pond was obtained. In addition, bacteria distribution was found for 3 different attachment rates, namely 25%, 50% and 75%. The impact of rain was also assessed by generating four synthetic hyetographs for each event and then run the model in order to find the bacteria distribution after the events. Comparing the resultant bacteria distribution with that of the actual rain would provide insight into the role of rainfall patterns on the predictability of bacteria distribution in the pond. Also, a comprehensive assessment was performed to find the impact of wind on the bacteria distribution. The actual wind, which changed direction and magnitude every hour (according to the data), was rotated from -90 to +90 degrees. To be specific, the actual event's wind magnitude was left untouched, however, all of the wind direction data points were shifted by a constant value. During the study of wind, rain hyetographs, attachment rate and all other settings remained the same as those of the BOC. It should be noted that the studies on the rain and wind were performed introducing a non-settling sediment, for which the decay of particulate-attached bacteria was taken into account, but the settling was neglected. This type of sediment was used in the aforementioned studies due to the high numerical costs associated with the sediment transport models. Using a non-settling sediment type made it practical to run the copious number of simulations. Similarly, to assess the assumptions and impacts of wind

magnitude, only the wind's magnitude was changed while all other assumptions and inputs remained unchanged. The wind magnitude data, which are separate data points, was changed by ±25%, ±50%, ±75% and 100%. The process was performed for all of the three storm events. In other words, the wind blowing over the pond during each event was changed and its impact on the bacteria distribution was found if the wind was stronger or weaker. Finally, with regard to average wind conditions, the recorded wind data in the region was obtained and the wind during the irrigation season was averaged. Wind magnitude data since 1971 and wind direction data since 2014 were obtained (Canada Weather Stats, 2020) and the average was calculated. The events were simulated with the average wind as well as ±1 standard deviation of the average wind. This set of simulations was performed to assess the predictability of bacteria distribution without having the wind data of the event. The simulations were performed using FLOW-3D 12u1 CFD commercial code. The simulations were run on 3 nodes, equal to 128 computational cores, of Cedar, which is a high performance computer run by Compute Canada.

5.3 Results and Discussion

Figure 5.4 shows the bacteria distribution on the surface of the pond at the end of storm events on 28 May, 2007 and 26 August, 2007 as well as during 24 hours after the end of the event that occurred on September 20, 2007 as an example. The highly contaminated stormwater was discharged into the pond through the inlets and distributed throughout the pond. After 24 hours from the event, still bacteria was not evenly distributed and some parts of the pond were more contaminated than other parts. The middle of the pond near

the surface, where the three wings join, were already determined as the optimal location for withdrawal for reuse because it has the lowest concentration of bacteria, comparatively (Allafchi et al., 2021). The withdrawal location is shown by a cross sign in Figure 5-4a.

5.3.1 Verification of Flow Velocity Vectors

The important role of fluid flow field in the hydro-environmental models was previously emphasized (Allafchi et al., 2019). Therefore, in an attempt to validate the model with respect to fluid flow field, velocity data were collected from the pond and the model was run for the same day. Figure 5.5 demonstrates the collected data from the pond as well as the simulation results for the corresponding day. The model slightly underestimated velocity magnitude. It might be associated with the wind tunnel effect due to the trees and buildings around the pond which can increase wind velocity over the pond, particularly over the South wing. On the other hand, wind obstruction by the buildings might have caused underestimation of wind by the on-site meteorological station. In general, good agreement was observed for both velocity magnitude and direction. The deviation of the simulated flow direction from the measured flow direction is relatively high in three locations, including V2 and V3 at a depth equal to 2.6 m and V4 at a depth equal to 0.3 m. At these locations, the measurements are associated with high random error because the flow velocity is comparatively low, in which even small eddies could change the flow direction (Allafchi et al., 2020). The flow near the surface at V2 and V3 were in nearly opposite directions to the directions at these locations near the bottom. It suggests that the circulation of the wind-driven flow in the pond was reasonably approximated by the model.

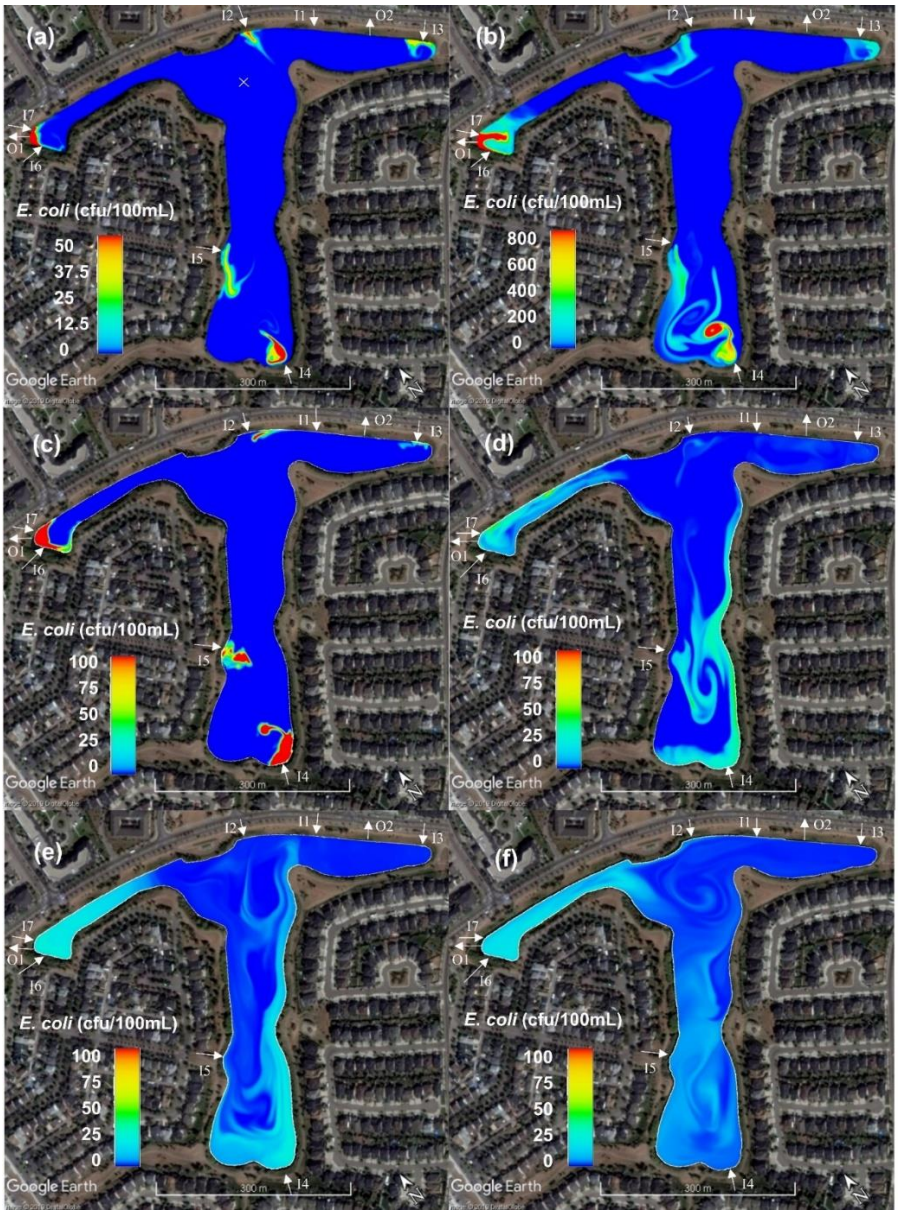

Figure 5.4 Modeled *E.coli* concentration on the surface of Inverness pond on a) May 28, 2007 at 1:05 am (end of storm event); b) August 26, 2007 at 3:20 pm (end of storm event); c) September 20, 2007 at 9:40 pm (end of storm event); d) September 21, 2007 at 3:40 am; e) September 21, 2007 at 3:40 pm; and f) September 21, 2007 at 9:40 pm. Note the difference in the color bars and the withdrawal location is shown by a white cross sign in Figure 5.4a

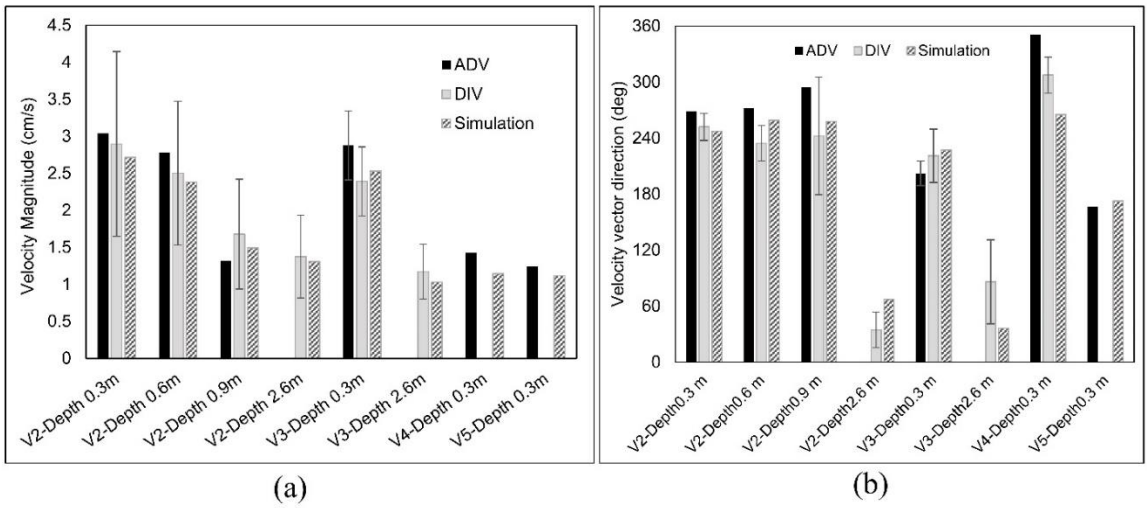

Figure 5.5 Comparison of simulation results with observations on August 29, 2020, a) flow velocity magnitude; and b) flow direction

5.3.2 Verification of Bacteria Distribution

It should be noted that the bacteria data collected in the pond during the campaign between 2004 and 2007 were collected over a period of 26 days with no attempt to favour rainy or dry days; however, 7 out of the 26 days happened to be within three days after a rain event. In addition, during another campaign in 2017, similar data was collected in 24 days but from four different locations in the pond. Similarly, 6 and 4 days were within two and one days after a storm event, respectively.

The *E.coli* concentrations were normalized by dividing the observed concentration by the maximum concentration observed in all locations for the day. For example, the location that has the maximum *E. coli* concentration would have a normalized *E. coli* equal to one. The normalized *E.coli* at each location was averaged for each category separately. The simulated bacteria concentration was also normalized with a similar approach. Figure 5.6a and 5.6b show the normalized bacteria collected in the first and second campaign,

respectively. In spite of the change that occurred in the land use between the year 2007 and 2017, the most contaminated part of the pond did not change. The data collected from both campaigns shows that the tip of the West Wing had the highest concentration of bacteria compared to the other locations. Figure 5.6b demonstrates that after rain events, the tip of the West wing was likely the most contaminated part of the pond. Following the West wing, the South wing was the second most contaminated wing of the pond. Comparing Figure 5.6a with 5.6b, both of the South and East wings became slightly more contaminated during the time between 2007 to 2017, particularly after rain events. The reason might be the developments (turning farms into residential areas) during that time on the East and South side of the catchment from which the stormwater drains into the pond through I3 and I4, respectively.

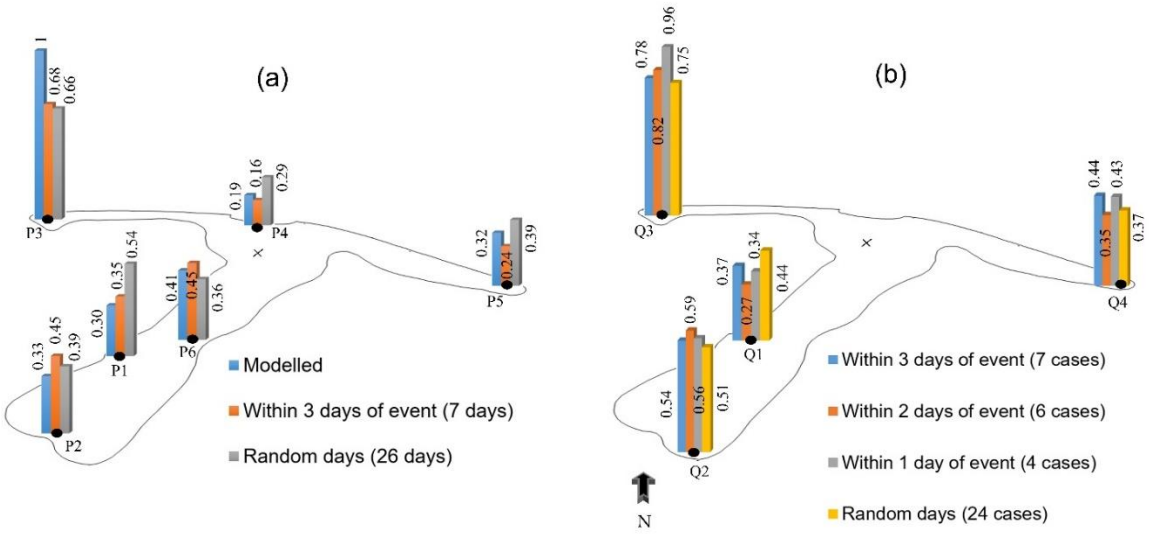

Figure 5.6 Normalized *E.coli* at the Inverness pond; data collected during the campaign a) between 2004 and 2007; and b) in 2017

5.3.3 Impact of Model Assumptions

5.3.3.1 Impact of Bacteria Attachment Assumptions

In the model developed for the pond, it was assumed that half of the bacteria attach to sediment particles. To be specific, half of the *E.coli* were assumed to be attached to particles smaller than 2 μm, as Muirhead et al., (2006) found. It should be noted that other particle sizes, which *E.coli* predominantly attach to, were also proposed in the literature. For example, Anna et al., (2005) found that more than 90% of *E.coli* attach to particles smaller than 30 μm (Anna et al., 2005). The impact of both assumptions, namely the attachment ratio and particle size, on the bacteria distribution in the pond was studied. Figure 5.7 shows the impact of attached particle size on the bacteria concentration at the withdrawal and the six locations. In general, changing the particle size did not change the relative distribution of bacteria. In other words, the most and the least contaminated locations and the ones in between did not change. However, increasing the particle size decreases bacteria concentration near the surface. The change is quite substantial replacing sediment size smaller than 2 μm with 2 to 10 μm. However, the change in bacteria concentration was negligible when the particle size was increased from 10-20μm to 20-50 μm. The reason is that settling of particles that are smaller than 2 μm was not considerable (Allafchi et al., 2019), but larger particle sizes are associated with more settling which decreases bacteria concentration in the study locations that are situated near water surface. On the other hand, reduction in bacteria concentration by increasing the particle size occurred only to an extent. Once most of the attached bacteria are already settled, increasing attached particle size does not further decrease bacteria concentration. This can

be observed comparing the bacteria concentration for the attached particle of 10-20 μm and 20-50 μm.

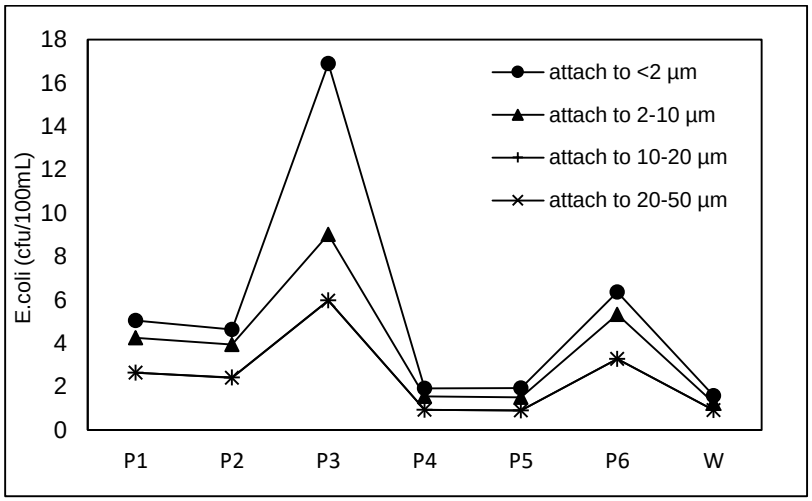

Figure 5.7 Impact of particle size attachment on bacteria distribution after the event on September 20, 2007. The 'W' on the horizontal axis refers to the withdrawal location.

5.3.3.2 Impacts of Settling Sediment

In addition, the attachment rate was studied and in this study, it was assumed that *E.coli* attach to particles smaller than 2 μm. Since the settling of such particles is found to not be considerable (comparatively speaking), two sediment types were considered for this study, namely sediment with settling and sediment without settling. The results from the two sediment types are shown in Figure 5.8. The sediment with settling was modeled integrating the sediment transport model into the main model; however, sediment without settling was modeled with passive scalars. In both cases bacteria concentration reduced with decreasing attachment rate at P3, the most contaminated location. Figure 5.8b, which

is associated with the non-settling sediment type, shows that decreasing the attachment rate decreases the bacteria concentration in all of the locations. However, in the settling-sediment type, bacteria concentrations were not necessarily decreased by reducing attachment rate (see Figure 5.8a). Attachment protects bacteria from some lethal environmental factors, and thus, decreases the decay rate. That explains why in the non-settling sediment type, decreasing attachment rate decreases bacteria concentration. However, it is harder to predict the change in bacteria distribution with settling-type sediment because the effect of settling and the effect of protection on the changes in bacteria concentration effectively neutralize each other. However, in the settling type sediment, the bacteria concentration reduced by decreasing attachment rate only at P3 and remained nearly the same at other locations. The passive scalar model used for non-settling sediment, requires much less numerical time compared to the sediment transport model. Therefore, it became practical to further conduct the sensitivity analyses on the factors influencing the bacteria distribution in the pond with it, particularly factors that the attachment does not play a role in, such as wind and inlet flowrates. Hence, the case with 50% attachment to the non-settling sediment is used as part of the BOC benchmark in the rest of this chapter to run the model numerous times that study the effect of multiple factors on the bacteria distribution.

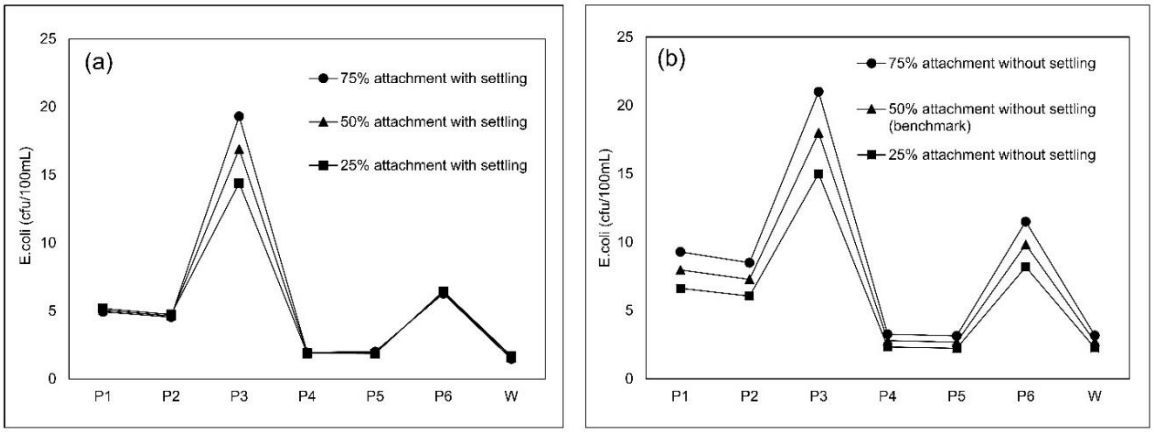

Figure 5.8 Impact of attachment rate on *E.coli* distribution for a) sediment with settling; and b) sediment without settling. The 'W' on the horizontal axis refers to the withdrawal location.

5.3.3.3 Impact of Rain Distribution and Flowrate

In order to find the impact of inflow flow rates on the distribution of bacteria, four synthetic rains were generated and fed to the hydrological model. Three Chicago hyetographs (American Iron and Steel Institute, 2010) and a triangular hyetograph (Ellouze et al., 2009) was modeled and the resultant bacteria distributions were compared with that of the actual event. The Chicago hyetographs are distinguished by the peak factor varying from 0.3 to 0.5. The synthetic hyetographs were designed to have the same total volume and duration of rain compared to the actual events. They were also set to occur at the same time as the actual event. Figure 5.9 demonstrates the synthetic hyetographs generated for the event occurring on September 20, 2007.

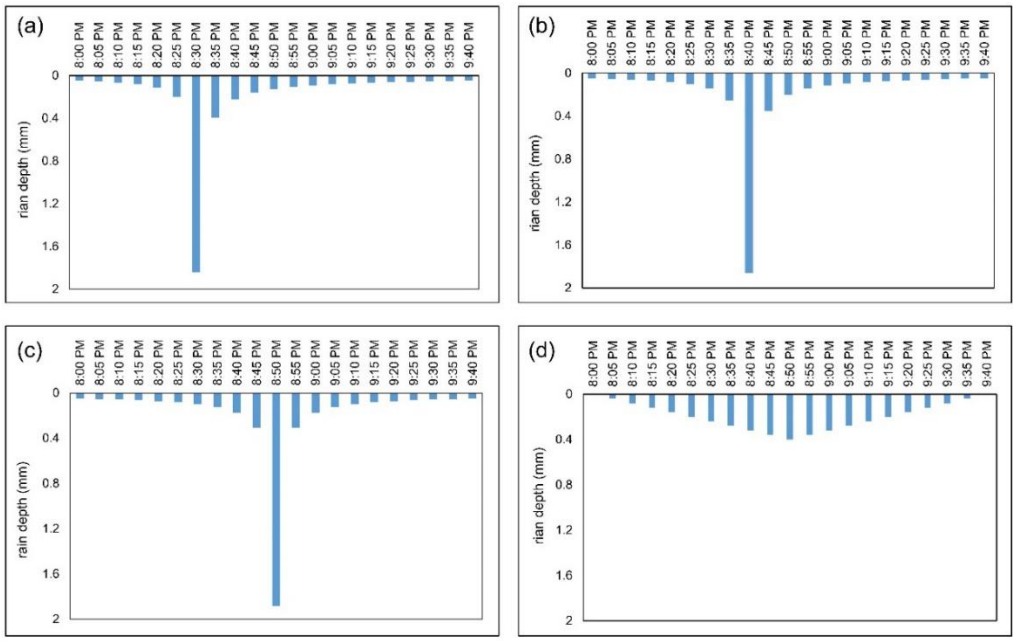

Figure 5.9 Synthetic hyetographs to model the storm event on September 20, 2007, a) Chicago hyetograph Y=0.3; b) Chicago hyetograph Y=0.4; c) Chicago hyetograph Y=0.5; d) triangular hyetograph

Once the flowrates were found running the hydrological model, the CFD model was run to find the bacteria distribution under different rain conditions. All other settings and conditions including bacteria pollutographs of the inlets and wind at each day was the same as the actual event day. The distribution of bacteria in the six locations using the synthetic hyetographs was obtained and compared to that of the BOC for each of the three events (see Figure 5.10). In almost all of the cases, the bacteria concentration was underestimated. However, the most contaminated location of the pond, P3, did not change by altering the hyetograph in any of the events. It is to be expected that the total number of bacteria changes with changing hyetograph because the bacteria pollutograph, of the inlets did not change during this study. Therefore, depending on the timing of pollutograph and flowrate

peaks, the total number of bacteria in the pond can be overestimated or underestimated. In addition, the pattern of bacteria concentration from P1 to P6 was almost repeated with all of the hyetographs. Only the triangular hyetograph on September 20, 2007 showed a slightly different pattern. Moreover, the withdrawal location appeared to be the least contaminated location of the pond even with different hyetographs. The concentration of bacteria at only the withdrawal location with different hyetographs is shown in Figure 5.11. This Figure also confirms that the withdrawal location would still be the optimal location for water withdrawal for reuse because it would have the lowest bacteria concentration. It can be concluded that synthetic hyetographs, particularly the Chicago hyetograph, can be used to find the most contaminated and the optimal withdrawal location of a stormwater pond for design purposes or when actual rain data is not available.

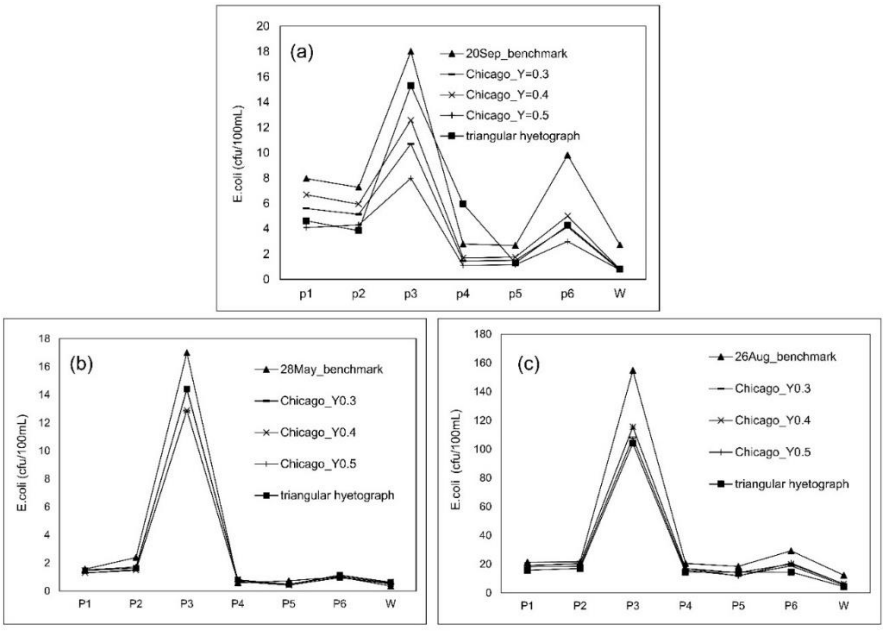

Figure 5.10 Impact of hyetograph on bacteria distribution after the event occurred on a) September 20, 2007; b) May 28, 2007; and c) August 26, 2007. The 'W' on the horizontal axis refers to the withdrawal location.

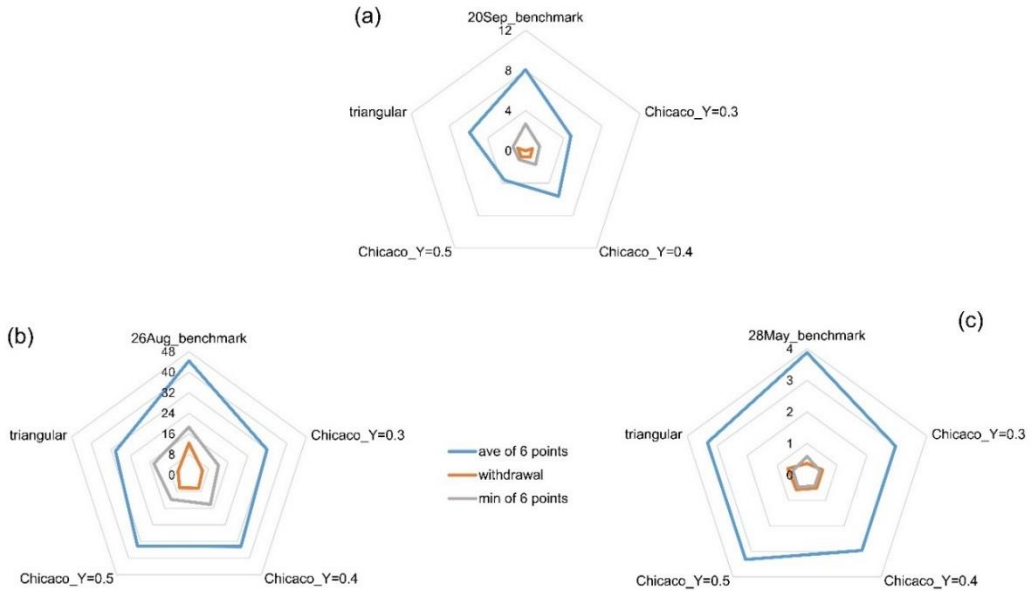

Figure 5.11 Impact of hyetograph on the bacteria distribution at the withdrawal location after the event on a) September 20, 2007; b) August 26, 2007; and c) May 28, 2007.

5.3.3.4 Impact of Wind Direction

A set of simulations was run to study the effect of wind direction on the bacteria distribution of the pond. Accordingly, all other parameters such as rain hyetograph, bacteria concentration in the inlets and wind magnitude were the same as those of the actual event. It should be noted that the wind data (magnitude and direction) at the time was recorded on an hourly basis. For studying the impact of wind direction, the actual wind data, in which wind direction and magnitude change hourly, was modified and used for the simulations. The direction is basically an angle, and constant values were added or subtracted to it. In this paper the wind directions are handled on a trigonometric basis. For

example, adding 90 degrees to a North wind would turn it into a West wind. Figure 5.12 shows the bacteria distribution after the three events if the wind is rotated by certain angles. The wind was rotated from -90 to +90 degrees with smaller intervals at the middle of the range. Figures 5.12a shows that if the direction of wind at the event on September 20, 2007 was changed, in most cases the pattern of the bacteria distribution 24 hours after the event (bacteria concentration from P1 to P6) would generally follow the pattern of the BOC. In other words, P3 experienced the maximum concentration of bacteria and P6 in the South wing was the next highly contaminated location. However, Figure 5.12b shows that the pattern was not followed in three out of four cases. To be specific, in the -90^{o} case, the bacteria concentration at P6 was the lowest among all the locations. Also, in the -22.5^{o} and -11.25^{o} cases, concentration of P1 was larger than that of P6. The bacteria distribution after the event occurred on May 28, 2007 changed substantially with the change in wind direction, but it generally followed the pattern of the BOC (see Figure 5.12c and 5.12d). The bacteria distribution after the event on August 26, 2007 had some exceptions that did not follow the pattern, see Figures 5.12e and 5.12f. For example, in the $+90^{o}$ case, P3 was not the most contaminated case anymore. Also, in the -90^{o} case, P6 located at the South wing was not the second most contaminated location. However, Figure 5.12f shows a pattern in the bacteria distribution at P3. In general, Figure 5.12 shows that study of wind direction is both event specific and location specific and it is not practical to make a general prediction about the impact of wind direction on the bacteria distribution throughout the pond. The reason is that the shape of the pond and the high number of inlets make it difficult

to predict the fluid flow, which is 3-dimensional and unsteady. Also, the wind is changing over time.

However, studying the impact of wind direction more closely on the withdrawal location shows that by changing wind direction, the withdrawal location might not be the optimal location anymore. The reason is that in some cases the bacteria concentration in the other locations happened to be lower than that of withdrawal location. Interestingly, some of those cases occurred when the wind direction changed slightly as seen in Figure 5.13. It should be noted that the bacteria concentration at the withdrawal location remained below that of the average of the six locations in all of the cases regarding the change in wind direction. Both Figures 5.13 and 11 show the impact of an environmental factor, namely wind direction and rain, respectively, on the bacteria distribution of the withdrawal location and compared with that of other locations. Therefore, despite the difference in the nature of those environmental factors, comparing the figures might enable us to assess the relative importance of different environmental factors. Originally the withdrawal location had been determined because it was the optimal location for withdrawal for reuse. In other words, it had shown the lowest bacteria concentration throughout and after the events. The withdrawal location remained optimal with different rain hyetographs (see Figure 5.11). However, it was not optimal location anymore in several cases when the wind direction changed, (see Figure 5.13). This might indicate a larger impact of wind direction on bacteria distribution, particularly in the withdrawal location, than rainfall distribution. However, due to the difference in the nature of the environmental factors and their impact on the total number of bacteria in the pond, greater study is recommended.

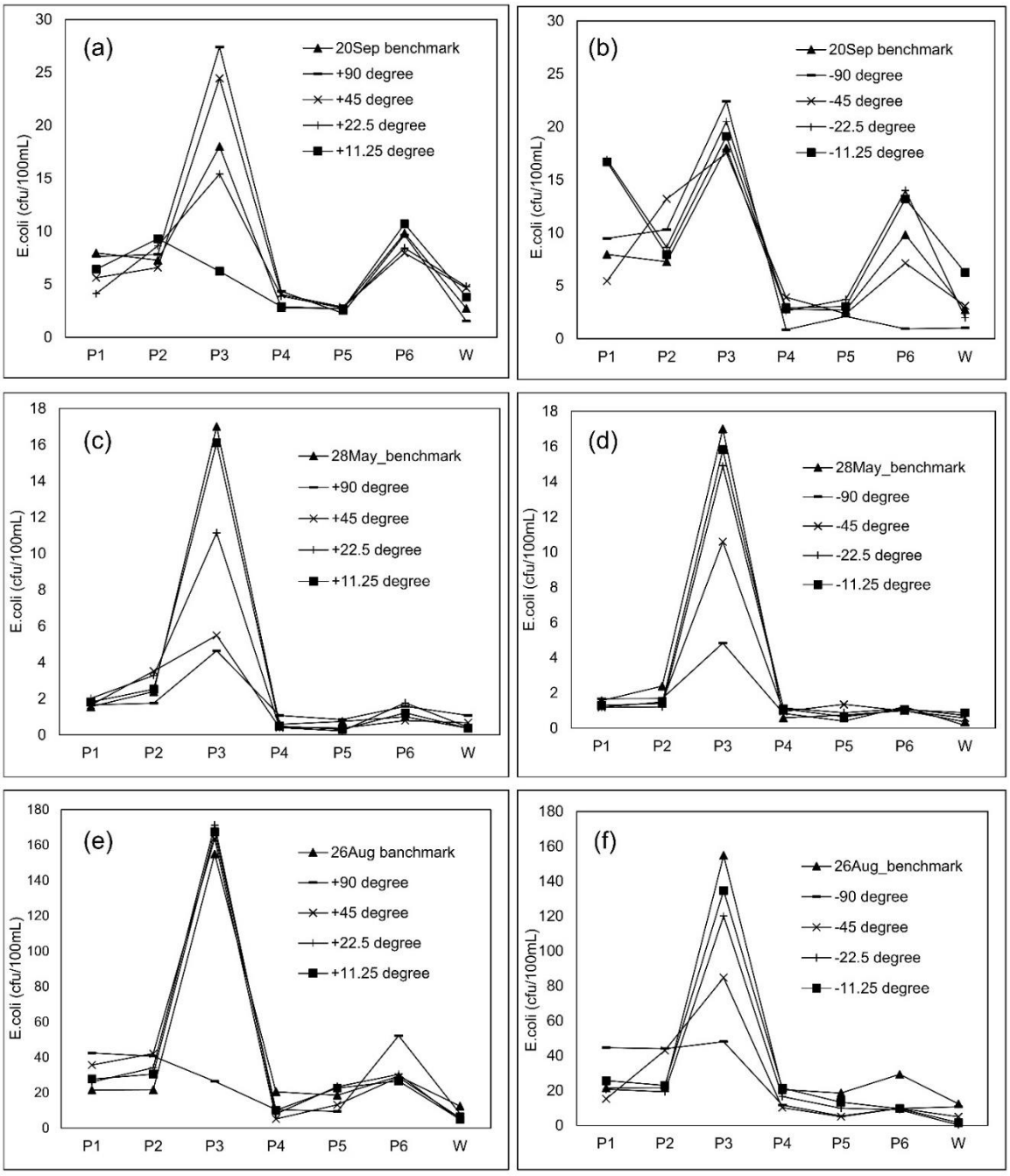

Figure 5.12 Impact of wind direction on bacteria distribution after the event on a and b) September 20, 2007; c and d) May 28, 2007; e and f) August 26, 2007. The 'W' on the horizontal axis refers to the withdrawal location. The 'W' on the horizontal axis refers to the withdrawal location.

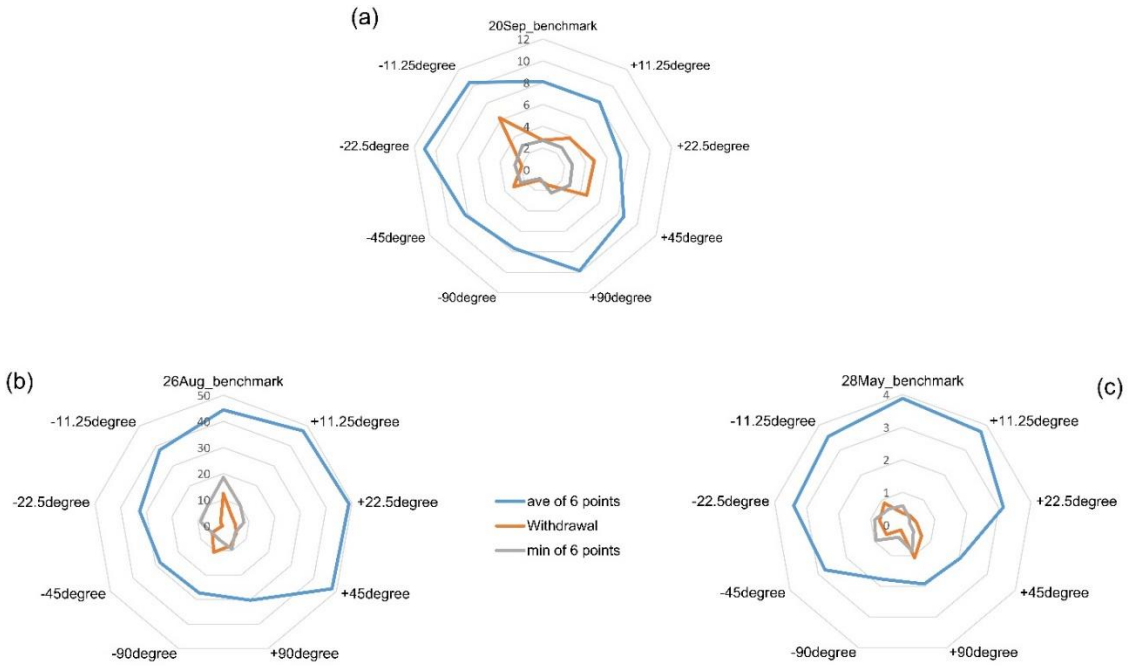

Figure 5.13 Impact of wind direction on the bacteria distribution at the withdrawal location after the event on a) September 20, 2007; b) August 26, 2007; and c) May 28, 2007.

5.3.3.5 Impact of Wind Magnitude

Similar to the wind direction, wind magnitude during and after the events was changing on an hourly basis. In this section, the impact of wind magnitude on bacteria distribution is studied by changing the hourly wind magnitude data points. For example, simulating the pond with a wind magnitude half of the wind in actual event shows the bacteria distribution if the wind would have been half of what it was, denoted by wind-50% in Figure 5.14. In all of the three events, when the wind magnitude increased, the bacteria concentration pattern from P1 to P6 was generally followed. In addition, it can be observed that increasing wind magnitude caused an underestimation in bacteria concentration at P3, the most contaminated location of the pond. The reason is that P3 is located at the tip of the West

wing and the highly contaminated stormwater entered the pond from the nearby subbasins has only one way to get transported to the other parts of the pond. In the process of transporting bacteria from this location to the rest of the pond, wind plays the primary role. Therefore, increasing the wind magnitude accelerated transportation of highly contaminated stormwater from this region, and thus, the bacteria concentration dropped in this area. The maximum drop occurred in the case of doubling the wind (wind+100%) after all of the three events. However, decreasing the wind magnitude during and after the actual events does not necessarily decrease or increase the bacteria concentration at P3. In addition, the pattern of bacteria concentration from P1 to P6 was not followed in the cases that wind magnitude was lower than that of actual events, see Figures 5.14b, 5.14d, and 5.14f.

The effect of diffusion of bacteria in the transportation of bacteria was assumed to be negligible compared to that of convection in the model. The effect of diffusion on the transport is more highlighted when the wind magnitude is minimal. Therefore, decreasing wind will increase spatial sensitivity of the model because the main factor that played role in distributing bacteria was decreased, and thus, the gradient of bacteria concentration near the inlets increases. In other words, the contaminated stormwater that was discharged into the pond during the storm would not get dispersed and would remain as a plug that moves slowly. Then, if the grab sampling location (P1~P6) and withdrawal location happen to be near the periphery of the plug, the high sensitivity of the model would appear in the bacteria concentration. This effect can be observed in Figures 5.14b, 5.14d, and 5.14f.

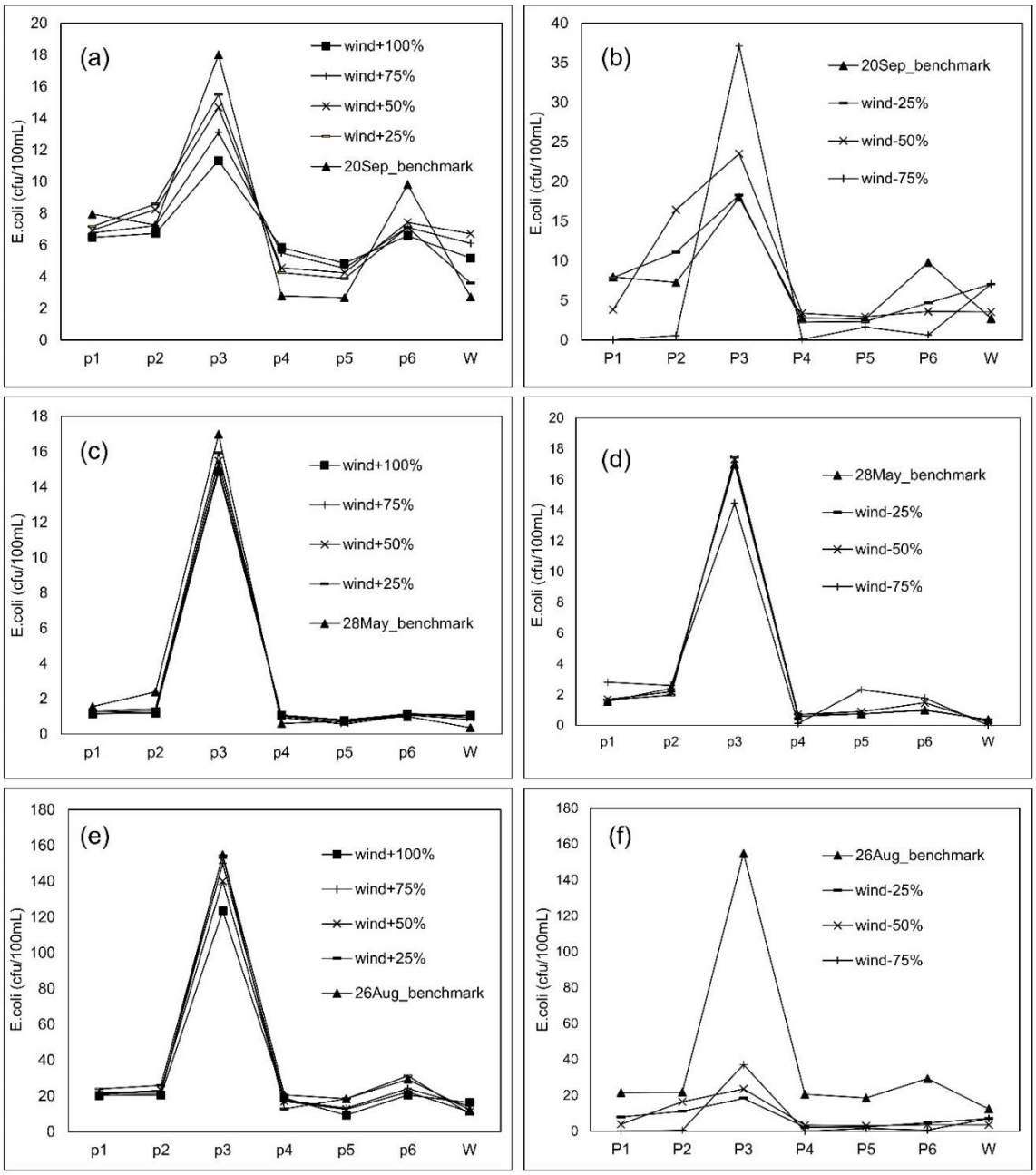

Figure 5.14 Impact of wind magnitude on bacteria distribution after the events occurred on a and b) September 20, 2007; c and d) May 28, 2007; e and f) August 26, 2007. The 'W' on the horizontal axis refers to the withdrawal location.

The modeled concentration of bacteria in the withdrawal location after the three actual events were compared with that of stronger and weaker wind. Figure 5.15 shows the comparison. The modeled bacteria concentration at the withdrawal location in all of cases was lower than the average of that of the six locations. However, in most of the cases the concentration in the withdrawal location was higher than the minimum of the six locations. Therefore, the withdrawal would not be the optimal location anymore. This might indicate the large impact of wind magnitude on the bacteria distribution in the pond.

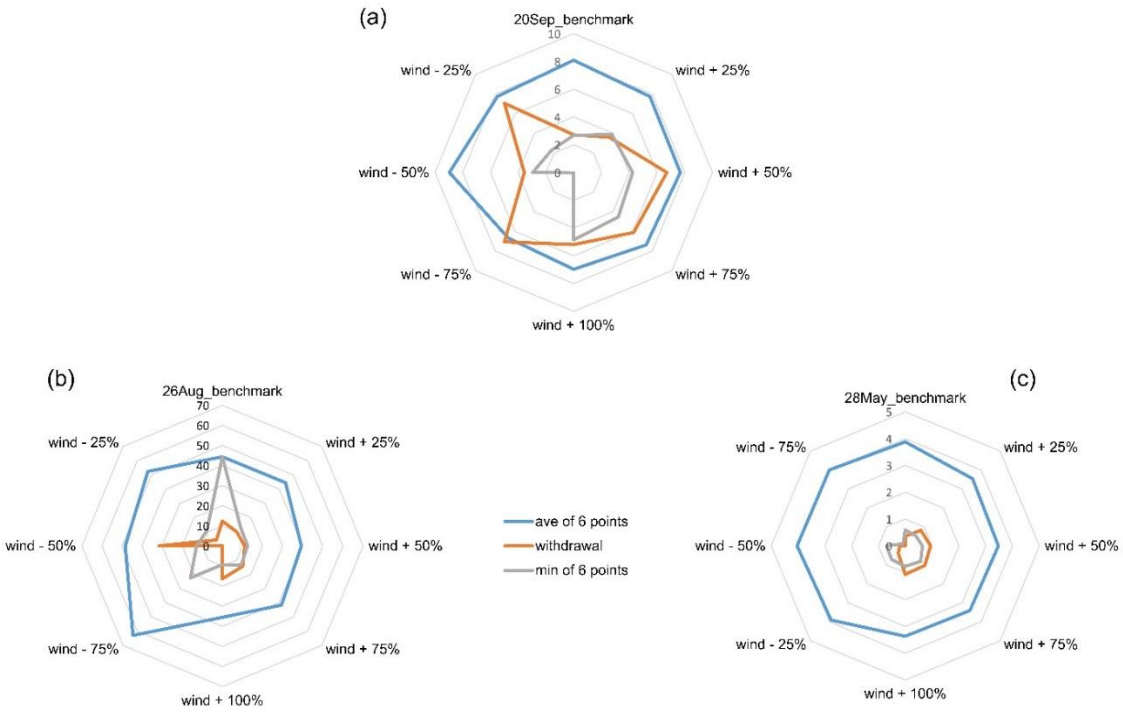

Figure 5.15 Bacteria concentration at the Withdrawal location on a) September 20, 2007; b) August 26, 2007; and c) May 28, 2007.

5.3.3.6 Impact of Averaged Wind

In an attempt to further assess the predictability of the bacteria distribution in the pond, the averaged wind during the irrigation season was obtained and the pond was simulated with that wind. The wind magnitude in Calgary, which has been recorded since 1971 on an hourly basis (Canada Weather Stats, 2020), was averaged for irrigation seasons (beginning of May to the end of September). Similarly, hourly wind direction data has been recorded since 2014, and it was averaged as well. The averaged wind magnitude and direction in irrigation season were found to be 14.5 km/h and 178^{o} angle, respectively. The pond was simulated with that wind and the modeled bacteria distribution was compared with that of the actual event. Moreover, the pond was simulated with two other wind magnitudes equal to the averaged wind ±1 standard deviation of the wind. The pond was simulated with a constant wind, in which neither wind magnitude nor wind direction changes. Other inputs and parameters, such as inflow flowrates and bacteria pollutographs of the inlets, remained the same as those of the actual event. Figure 5.16 shows the bacteria distribution at the six grab sampling locations considering the averaged wind. None of the cases corresponding to September 20, 2007 nor August 26, 2007 followed the bacteria concentration pattern of the actual event, and only one case corresponding to May 28, 2007 followed the pattern. In addition, the difference between the bacteria concentration corresponding to the actual event and that of the averaged wind was relatively high. Therefore, predicting the bacteria distribution with a constant wind is not considered practical.

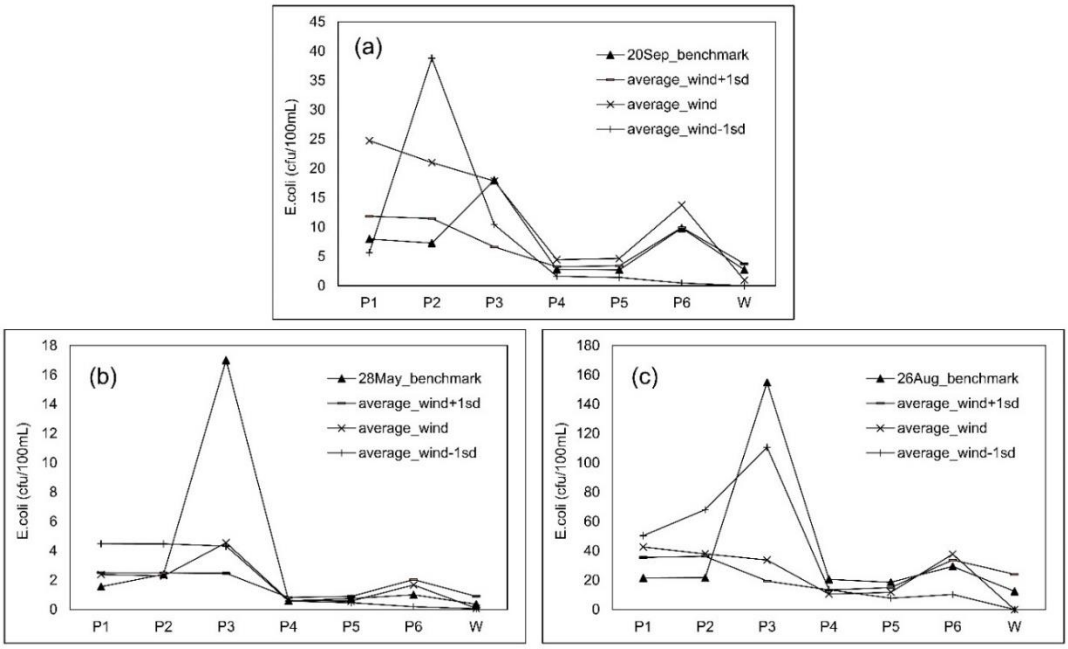

Figure 5.16 Impact of averaged wind on the bacteria distribution in the pond on a) September 20, 2007; b) May 28, 2007; c) August 26, 2007. The 'W' on the horizontal axis refers to the withdrawal location.

5.4 Conclusions

The integrated hydrological and CFD model (IHCFD), which was initially developed to simulate bacteria fate and transport in the Inverness stormwater pond, Calgary, AB, Canada for the purposes of reusing the stormwater, was further modified, verified and studied for sensitivity in this work. The model was verified for both fluid flow and bacteria distribution against the data collected from the pond. The fluid flow verification was performed for a wind-driven flow, and good agreement was observed. The bacteria distribution data showed some parts of the pond became more contaminated between 2007 and 2017; however, the tip of the West wing was found to be the most contaminated location of the pond. The model results showed a good agreement with the collected data. Once verified,

the model's assumptions were assessed using a sensitivity analysis. IHCFD was run a copious number of times to assess the impacts of different inputs on the bacteria distribution in the pond. The impacts were more closely studied for the withdrawal location, which was determined as the optimal location for pulling stormwater from the pond for later reuse. The particle size that *E.coli* predominantly attach to was one of the assumptions studied and it was found that increasing particle size generally decreases the bacteria concentration in the grab sampling locations due to the settling. However, no noticeable difference was found in the bacteria distribution at the study locations when the attached particle size was increased from 10-20 μm to 20-50μm. Attachment rate was also studied and it was found that with non-settling sediment, the bacteria concentration decreases in all study locations with decreasing the attachment rate. However, with settling-sediment this decrease only occurred at the most contaminated location. The impact of rainfall distribution was also assessed by comparing bacteria distribution in the pond arising from 4 different synthetic rainfall distributions with that produced by the actual rain. It was found that for design purposes or if there is a lack of collected data, synthetic hyetographs could be used to determine pond hot spots - locations with the highest level of contamination - as well as the optimal location for withdrawal. In addition, the model was run for several wind directions and wind magnitudes. Results revealed that the impact of wind direction is event specific and location specific. Changes in wind magnitude resulted in changes to the optimal withdrawal. In general, wind was found to play a critical role in the bacteria distribution of the pond.

6. Conclusions

All of the findings in the previous chapters are summarized in this chapter. The research objectives that were outlined in the introduction are briefly discussed and the way they are addressed throughout this dissertation is discussed in this chapter. In addition, the novel contribution of this study is discussed separately.

6.1 Summary of Objectives and Research Achieving the Objectives

The first objective of this research was to develop a modelling approach to simulate bacteria in stormwater ponds. This objective was addressed in Chapter 2 in which a modelling approach was developed to simulate bacteria fate and transport in stormwater ponds. The model was applied to investigate bacteria distribution in the Inverness stormwater pond, in Calgary, Alberta, after rain events as a test case. The model has two components and is called the Integrated Hydrological and CFD model (IHCFD). The hydrological component of the model was calibrated and validated using the runoff data collected from inlet I5. The validation showed good agreement with the measured data. Results from the hydrological component were fed to the CFD component as input boundary conditions. The CFD component simulated the distribution of *E.coli*, the most commonly used indicator bacteria, in the pond both during the rain events and the next 24 hours after the events. The efficiency of sediment traps with regard to bacteria was investigated. It was found that only one of the sediment traps performs efficiently in

trapping bacteria due to its configuration. Other sediment traps were found ineffective in trapping bacteria. In addition, the study of bacteria distribution at different depths showed that bacteria concentration changes with depth and it is affected by wind.

A non-dimensional number was introduced allowing a comparison between the modelled bacteria concentration and the available data that was collected from multiple locations throughout the pond. The averaged normalized bacteria concentrations at the end of the simulation time – 24 hours after the end of events - in six locations were compared with that of measured data that was collected on September 11, 2005. This day was selected because of the heavy rain that occurred in the previous day. Comparison showed reasonable agreement and the South wing was initially found the most contaminated wing of the pond.

The second objective of the research was to improve the model in order to simulate other bacteria. This objective also includes trying to improve water quality at the withdrawal location. This objective is addressed in Chapter 3, in which incorporating sediment transport and a VOF model into the main CFD component is discussed. In this improved model, similar to the original CFD component, the free-floating bacteria had a higher decay rate compared to attached bacteria. However, the transport of particulate-attached bacteria was now governed by the sediment transport model. Since the collected data was available for both *E.coli* and FC, separately, they were modelled as separate bacteria with different fate and transport characteristics. Moreover, a VOF model was integrated into the CFD component in order to take into account the movement of the water surface. The results of the model with the upgraded CFD component were compared with measured data. However this time, FC was included as well as *E.coli*. The comparisons were performed

using the previous locations but collected in 26 days. Comparison showed good agreement and included more data collection days in the comparison giving a stronger validation, which is attributed to the VOF and sediment transport model. The West wing was found as the most contaminated wing of the pond following by the South wing. The middle of the pond (the joint of the three wings) was found to be the optimal location for water withdrawal for reuse due to its lowest concentration of bacteria. In addition, the vertical investigation of the bacteria concentration at the withdrawal location showed that closer to the surface was more appropriate for water withdrawal.

Trees can obstruct wind which is the main factor in driving the flow in the pond after the storm events. A separate set of simulations was performed that simulates only the West wing. The results from this set of simulations were verified, and then, used to simulate the wing with the trees planted on the north bank of the wing. Strategic tree planting was found to be a solution to mitigate transport of highly contaminated stormwater from the West wing to the withdrawal location.

The third objective of this research was to develop a validation scheme for the model. This objective was mainly achieved in Chapter 5. However, Chapter 4 facilitated achieving the objective. Flow field plays a crucial role in the distribution of bacteria in the pond. Therefore, it is important to validate the hydrodynamic component of the model separately. However, no affordable and easy-to-use device was found on the market that could be used for this purpose. Thus, a velocity meter was designed and built in order to measure fluid flow velocity magnitude and direction that are experienced in medium to large water bodies. Chapter 4 is only dedicated to the design, calibration and validation of the velocity

meter which is called Dye Injection Velocity meter (DIV). DIV was calibrated in a fluid visualization flume that was equipped with a PIV system. An R^2 value of 0.98 was obtained from the calibration curve, with higher uncertainties near the low end of the range. Once calibrated, the DIV was deployed to the Inverness pond for validation against an ADV. Both velocity magnitude and direction was measured using both of the instruments. Good agreement was achieved indicating that DIV can be used for flow field measurements in the calibrated range.

During the fluid flow measurements onsite wind data were also collected allowing the modelling of the wind-driven flow in the pond with IHCFD (the developed model) for validation purposes. In Chapter 5 it is discussed how the modelled flow field velocity magnitude and direction at multiple locations and depths were compared with those of measured with DIV and ADV. Good agreement was observed for both fluid flow velocity magnitude and direction. Moreover, wind-driven circulation in the pond, which was observed in the field, was modelled reasonably well by IHCFD.

In the literature, it was discussed that validating mechanistic hydro-environmental models is challenging due to the lack of data. This issue is even more problematic with IHCFD because it models stormwater ponds after rain and collecting grab samples from the pond immediately after rain is often not practical due to the randomness of storm events occurrence. However, introducing the non-dimensional number, referred to as “normalized bacteria”, allowed for validating the model results against the available data. The normalized bacteria number is an indicator of the relative bacteria concentration. The number was separately calculated for the modelled events (3 events) and collected data (26

days). The comparison showed good agreement. In addition, the normalized bacteria were calculated in four locations in which the data were collected during a campaign in 2017. In spite of the change in land use between 2007 and 2017, the most contaminated location of the pond did not change. However, the South and East wings became more contaminated during 2007 and 2017, probably due to the developments on the east and south sides of the pond during that period of time.

Another common issue associated with mechanistic models is the numerous number of assumptions that need to be made. As a result, the fourth research objective was to assess the impact of major assumptions and factors on the modelling results. This objective is addressed in Chapter 5 and some of the IHCFD assumptions and important inputs were investigated through a sensitivity study. To be specific, the impact of attachment rate, attached sediment size, rain hyetograph and wind on bacteria distribution in the 6 sampling locations was studied. The impacts on the withdrawal location were studied more closely. It was found that with non-settling sediment, the bacteria concentration decreases in all grab sampling locations with decreasing attachment rate. However, with settling-sediment the concentration of bacteria only decreases in the most contaminated location. The model was also run with different particle sizes that *E.coli* predominantly attach to. It was found that with increasing particle size, bacteria concentration in the grab sampling location decreases in general. However, the difference in the bacteria concentration is not noticeable when particle size is increased from 10 ~ 20 μm to 20 ~ 50 μm. The reason is due to the sedimentation of most of the particulate-attached bacteria. The impact of rainfall was also assessed for design purposes or in the case of lack of rain data. The model was run for

multiple synthetic hyetographs. It was found that synthetic hyetographs could be used to identify the optimal location for withdrawal for reuse as well as the most contaminated locations. The impact of wind magnitude and direction on the bacteria distribution in the pond was also assessed. As a result, wind was found to play a crucial role in the bacteria distribution of the pond. It was found that the impact of wind direction is event specific, and changes in wind magnitude can result in changes to the optimal location for withdrawal.

6.2 Novel Contributions

The primary novelty of this work is the developed modelling approach in order to simulate bacteria in stormwater ponds to identify the optimal location for water withdrawal for reuse. The model simulates bacteria fate and transport in ponds 3-dimansionally. It integrates a hydrological component which feeds to a CFD component simulating the ponds 3-dimensionally. It considers the free surface, employs a VOF and sediment transport model within IHCFD and this has not been done before for stormwater ponds and particularly for this type of application.

In the literature, a challenge in developing process-based models was identified to be a lack of data. However, the developed model in this work requires minimal amount of data. As an example, if runoff data is not available for one or some of the inlets, the hydrological component can generate them, and the CFD component would be run accordingly to simulate bacteria. Moreover, it was found that if rain data are not available or the pond is

not built yet and it is being designed with stormwater recycling in mind, synthetic hyetographs can be used as input rain data for the model to find the withdrawal location as well as the most contaminated location. Also using the model, strategic tree planting was shown to be useful in reducing transport of highly contaminated stormwater to the withdrawal location.

Lack of data makes validating of hydro-environmental models challenging. In this study, this challenge was overcome with two approaches. First, an affordable and easy-to-use velocity meter was built, calibrated and validated in order to quantify velocity flow fields in water bodies such as stormwater ponds. The instrument was successfully used to validate the hydrodynamics of the model, which plays a crucial role in the modelling. Second, a non-dimensional number, called normalized bacteria, is introduced that facilitates validation. Using the non-dimensional number, modelling results can be validated against the available data collected from the ponds. In addition, the impact of multiple assumptions and inputs, such as wind and attachment, on the bacteria distribution in a stormwater ponds, particularly the withdrawal location, was assessed. All of these are new contributions to the literature.

Bibliography

Abbasi, A., Annor, F.O., and van de Giesen, N. (2016). Investigation of Temperature Dynamics in Small and Shallow Reservoirs. Case Study: Lake Binaba, Upper East Region of Ghana. Water 8(3), 1–24. doi:10.3390/w8030084.

Aguilera, R., Sabater, S., and Marcé, R. (2018). A Methodological Framework for Characterizing the Spatiotemporal Variability of River Water-Quality Patterns Using Dynamic Factor Analysis. Journal of Environmental Informatics 31(2),.

Ahilan, S., Guan, M., Wright, N., Sleigh, A., Allen, D., Arthur, S., Haynes, H., and Krivtsov, V. (2019). Modelling the Long-Term Suspended Sedimentological Effects on Stormwater Pond Performance in an Urban Catchment. Journal of Hydrology 571. Elsevier 805–18. doi:10.1016/j.jhydrol.2019.02.002.

Allafchi, F., Valeo, C., Chu, A., He, J., Lee, W., Oshkai, P., and Neumann, N.F. (2020). A Velocity Meter for Quantifying Fluid Flow Velocity Vectors in Large Water Bodies. Sensors 20(24), 7204. doi:https://doi.org/10.3390/s20247204.

Allafchi, F., Valeo, C., He, J., and Neumann, N.F. In press, A Mechanistic Model for Estimating Bacteria Level in Stormwater Ponds. Journal of Hydro-Environmental Research.

Allafchi, F., Valeo, C., He, J., and Neumann, N.F. (2019). An Integrated Hydrological-CFD Model for Estimating Bacterial Levels in Stormwater Ponds. Water 11(5),. doi:https://doi.org/10.3390/w11051016.

Andradóttir, H.Ó. and Mortamet, M.-L. (2016). Impact of Wind on Storm-Water Pond Hydraulics. Journal of Hydraulic Engineering 142(10), 4016034.

doi:10.1061/(asce)hy.1943-7900.0001150.

Anna, H., Jeng, C., Englande, A.J., Bakeer, R.M., and Bradford, H.B. (2005). Impact of Urban Stormwater Runoff on Estuarine Environmental Quality. Estuarine, Coastal and Shelf Science 63 513–26. doi:10.1016/j.ecss.2004.11.024.

APHA. (1998). Standard Methods for Examining Water and Wastewater, 20th Edition.

Auer, M.T. and Niemaus, S.L. (1993). Modeling Fecal Coliform Bacteria-Field and Labratory Determination of Loss Kinetics. Water Research 27(4), 693–701.

Babaeyan-Koopaei, K., Ervine, D.A., and Pender, G. (2003). Field Measurements and Flow Modeling of Overbank Flows in River Severn, U. K. Journal of Environmental Informatics 1(1), 28–36.

Bai, S. and Lung, W.S. (2005). Modeling Sediment Impact on the Transport of Fecal Bacteria. Water Research 39(20), 5232–40. doi:10.1016/j.watres.2005.10.013.

Banner, M.L. and Peirson, W.L. (1998). Tangential Stress beneath Wind-Driven Air–water Interfaces. Journal of Fluid Mechanics 364 115–45.

Beaudeau, P., Tousset, N., Bruchon, F., Lefèvre, A., and Taylor, H.D. (2001). In Situ Measurement and Statistical Modelling of Escherichia Coli Decay in Small Rivers. Water Research 35(13), 3168–78. doi:10.1016/S0043-1354(01)00011-2.

Borrego, J.J. and Figueras, M.J. (1997). Microbiological Quality of Natural Waters. Microbiologia 13 413–26.

Canada Weather Stats. (2020). www.weatherstats.ca.

Characklis, G.W., Dilts, M.J., Simmons, O.D., Likirdopulos, C.A., Krometis, L.H., and Sobsey, M.D. (2005). Microbial Partitioning to Settleable Particles in Stormwater.

Water Research 39 1773–82. doi:10.1016/j.watres.2005.03.004.

Chen, F., Cai, Q., Sun, L., and Lei, T. (2016). Discharge-Sediment Processes of the Zhadang Glacier on the Tibetan Plateau Measured with a High Frequency Data Acquisition System. Hydrological Processes 30(August), 4330–38. doi:10.1002/hyp.10900.

Chen, H.J. and Chang, H. (2014). Response of Discharge, TSS, and E.coli to Raifall Events in Urban, Suburban, and Rural Watersheds. Environmental Science: Processes & Impacts 16. Royal Society of Chemistry 2313–24. doi:10.1039/C4EM00327F.

Chick, H. (1908). An Investigation of the Laws of Disinfections. The Journal of Hygiene 8(1), 92–158.

Clevenot, L., Carré, C., and Pech, P. (2018). A Review of the Factors That Determine Whether Stormwater Ponds Are Ecological Traps And/or High-Quality Breeding Sites for Amphibians. Frontiers in Ecology and Evolution 6 40. doi:10.3389/fevo.2018.00040.

Dalian Zero Instrument Technology Co. (2020). https://www.environmental-expert.com/products/zero-instrument-model-ls1206b-portable-water-velocity-meter-642802.

de Brauwere, A., Ouattara, N.K., and Servais, P. (2014a). Modeling Fecal Indicator Bacteria Concentrations in Natural Surface Waters: A Review. Critical Reviews in Environmental Science and Technology 44(21), 2380–2453. doi:10.1080/10643389.2013.829978.

de Brauwere, A., Gourgue, O., de Brye, B., Servais, P., Ouattara, N.K., and Deleersnijder,

E. (2014b). Integrated Modelling of Faecal Contamination in a Densely Populated River-Sea Continuum (Scheldt River and Estuary). Science of the Total Environment 468–469 31–45. doi:10.1016/j.scitotenv.2013.08.019.

Di Modugno, M., Gioia, A., Gorgoglione, A., Iacobellis, V., la Forgia, G., Piccinni, A.F., and Ranieri, E. (2015). Build-Up/wash-off Monitoring and Assessment for Sustainable Management of First Flush in an Urban Area. Sustainability 7(5), 5050–70. doi:10.3390/su7055050.

Ellouze, M., Abida, H., Safi, R., Ellouze, M., Abida, H., and Safi, R. (2009). A Triangular Model for the Generation of Synthetic Hyetographs. Hydrological Sciences Journal 6667 287–99. doi:10.1623/hysj.54.2.287.

Flow Science, I. (2018). FLOW-3D v11.2 User Manual.

Foreman, R.J. and Emeis, S. (2010). Revisiting the Definition of the Drag Coefficient in the Marine Atmospheric Boundary Layer. Journal of Physical Oceanography 40 2325–32. doi:10.1175/2010JPO4420.1.

Goonetilleke, A., Liu, A., Managi, S., Wilson, C., Gardner, T., Bandala, E.R., Walker, L., et al. (2017). Stormwater Reuse, a Viable Option: Fact or Fiction? Economic Analysis and Policy 56. Elsevier B.V. 14–17. doi:10.1016/j.eap.2017.08.001.

Gorgoglione, A., Bombardelli, F.A., Pitton, B.J.L., Oki, L.R., Haver, D.L., and Young, T.M. (2018). Role of Sediments in Insecticide Runoff from Urban Surfaces: Analysis and Modeling. International Journal of Environmental Research and Public Health 15(7), 1464. doi:10.3390/ijerph15071464.

Gosling, S.N. and Arnell, N.W. (2016). A Global Assessment of the Impact of Climate

Change on Water Scarcity. Climatic Change 134(3), 371–85. doi:10.1007/s10584-013-0853-x.

Graebel, W.P. (2007). Advanced Fluid Mechanics; Academic Press: Oxford, UK. Edited by 1st. Burlington, MA: Academic Press, 233–50.

Gu, L., Dai, B., Zhu, D.Z., Hua, Z., Liu, X., van Duin, B., and Mahmood, K. (2017). Sediment Modelling and Design Optimization for Stormwater Ponds. Canadian Water Resources Journal / Revue Canadienne Des Ressources Hydriques 42(1), 70–87. doi:10.1080/07011784.2016.1210542.

Guaraglia, D.O. and Pousa, J.L. (2014). Introduction to Modern Instrumentation For Hydraulics and Environmental Sciences. De Gruyter. doi:https://doi.org/10.2478/9783110401721.

Hamdan, S. (2009). A Literature Based Study of Stormwater Harvesting as a New Water Resource. Water Science and Technology 60(5), 1327–39.

Hammes, G., Thives, L.P., and Ghisi, E. (2018). Application of Stormwater Collected from Porous Asphalt Pavements for Non- Potable Uses in Buildings. Journal of Environmental Management 222(June),. Elsevier 338–47. doi:10.1016/j.jenvman.2018.05.094.

He, J. (2009). Reducing the Vulnerability of Water Supply under a Changing Climate: An Assessment of Stormwater Reuse. PhD Thesis, University of Calgary, Calgary, AB, Canada.

He, J., Valeo, C., and Chu, A. (2015). Variation in Water Quality of a Stormwater Pond from Diurnal Thermal Stratification. Journal of Water Resources and Hydraulic 4(2),.

The World Academic Publishing Company Limited 189–98.

He, J., Valeo, C., Chu, A., and Neumann, N.F. (2010). Characterizing Physicochemical Quality of Storm-Water Runoff from an Urban Area in Calgary, Alberta. Journal of Environmental Engineering 136(11),. American Society of Civil Engineers 1206–17.

He, J., Valeo, C., Chu, A., and Neumann, N.F. (2011a). Prediction of Event-Based Stormwater Runoff Quantity and Quality by ANNs Developed Using PMI-Based Input Selection. Journal of Hydrology 400(1–2),. Elsevier 10–23.

He, J., Valeo, C., Chu, A., and Neumann, N.F. (2011b). Stormwater Quantity and Quality Response to Climate Change Using Artificial Neural Networks. Hydrological Processes 25 1298–1312. doi:10.1002/hyp.7904.

He, J., Valeo, C., Chu, A., Neumann, N.F., and Tn, A. (2008). Water Quality Assessment in the Application of Stormwater Reuse for Irrigating Public Lands. Water Quality Research Journal of Canada 43(2/3), 93–107.

He, J., Valeo, C., and Neumann, N. (2010). Microbiological, Physical and Chemical Water Quality of Event-Based Stormwater Run-off from an Urban Residential Area. Water Environmental Research 82(12), 2333–45.

Hirt, C.W. and Nichols, B.D. (1981). Volume of Fluid (VOF) Method for the Dynamics of Free Boundaries. Journal of Computational Physics 39 201–25.

Inc., F.S., NM, S.F., and USA. n.d. FLOW-3D®. https://www.flow3d.com.

Institute, A.I. and S. (2010). HANDBOOK OF STEEL DRAINAGE & HIGHWAY CONSTRUCTION PRODUCTS. Second edi.

Jeong, J., Wagner, K., Flores, J.J., Cawthon, T., Her, Y., Osorio, J., and Yen, H. (2019).

Linking Watershed Modeling and Bacterial Source Tracking to Better Assess E. Coli Sources. Science of the Total Environment 648. Elsevier B.V. 164–75. doi:10.1016/j.scitotenv.2018.08.097.

Juntunen, J., Ropponen, J., Shuku, T., Krogerus, K., and Huttula, T. (2019). The Effect of Local Wind Field on Water Circulation and Dispersion of Imaginary Tracers in Two Small Connected Lakes. Journal of Hydrology 579. Elsevier 124137. doi:10.1016/j.jhydrol.2019.124137.

Kundu, P.K., Cohen, I.M., Dowling, D.R., and Tryggvason, G. (2016). Fluid Mechanics. Sixth. Academic Press.

Kunkel, E.A., Privette, C. V., Sawyer, C.B., and Hayes, J.C. (2013). Attachment of Escherichia Coli to Fine Sediment Particles within Construction Sediment Basins. Advanced in Bioscience and Biotechnology 4 407–14.

Labaky, W., Devlin, J.F., and Gillham, R.W. (2009). Field Comparison of the Point Velocity Probe with Other Groundwater Velocity Measurement Methods. Water Resources Research 45(March), 1–9. doi:10.1029/2008WR007066.

Launder, B.E. and Sharma, B.I. (1974). Application of the Energy-Dissipation Model of Turbulence to the Calculation of Flow near a Spinning Disc. Letters in Heat and Mass Transfer 1(2), 131–38.

LaVision GmbH. (2018). FlowMaster Product Manual.

Leclerc, H., Mossel, D.A.A., Edberg, S.C., and Struijk, C.B. (2001). Advances in the Bacteriology of the Coliform Group: Their Suitability as Markers of Microbial Water Safety. Annual Review of Microbiology 55(201), 201–34.

Lundy, L., Revitt, M., and Ellis, B. (2018). An Impact Assessment for Urban Stormwater Use. Environmental Science and Pollution Research 25(20),. Environmental Science and Pollution Research 19259–70. doi:10.1007/s11356-017-0547-4.

Mallin, M.A., Johnson, V.L., and Ensign, S.H. (2009). Comparative Impacts of Stormwater Runoff on Water Quality of an Urban, a Suburban, and a Rural Stream. Environmental Monitoring and Assessment 159 475–91. doi:10.1007/s10661-008-0644-4.

Mallin, M.A., Williams, K.E., Esham, E.C., and Lowe, R.P. (2000). Effect of Human Development on Bacteriological Water Quality in Coastal Watersheds. Ecological Applications 10(4), 1047–56.

Manickathan, L., Defraeeye, T., Allegrini, J., and Derome, D. (2018). Comparative Study of Flow Field and Drag Coefficient of Model and Small Natural Trees in a Wind Tunnel. Urban Forestry & Urban Greening 35 230–39. doi:.1037//0033-2909.I26.1.78.

Mankad, A., Walton, A., and Gardner, J. (2019). Psychological Predictors of Public Acceptance for Urban Stormwater Reuse. Journal of Hydrology 572(February),. Elsevier 414–21. doi:10.1016/j.jhydrol.2019.03.018.

Markfort, C.D., Perez, A.L.S., Thill, J.W., Jaster, D.A., Porté-Agel, F., and Stefan, H.G. (2010). Wind Sheltering of a Lake by a Tree Canopy or Bluff Topography. Water Resources Research 46(3), 1–13. doi:10.1029/2009WR007759.

McCuen, R.H., Knight, Z., and Cutter, G. (2006). Evaluation of the Nash-Sutcliffe Efficiency Index. Journal of Hydrologic Engineering 11(6), 597–602.

Melville, J.G., Molz, F.J., and Güven, O. (1985). Laboratory Investigation and Analysis of

a Ground-Water Flowmeter. Ground Water 23(4),. Blackwell Publishing Ltd 486–95. doi:10.1111/j.1745-6584.1985.tb01498.x.

Mockus, V. (1972). Hydrology. In: National Engineering Handbook, 2nd Edition, Natural Resources Conservation Service, USA. U.S. Government Printing Office, 21.2-21.49.

Moeini, M., Khorsandi, B., and Mydlarski, L. (2020). Effect of Acoustic Doppler Velocimetry Sampling Frequency on Statistical Measurements of Turbulent Axisymmetric Jets. Journal of Hydraulic Engineering 146(7), 1–17. doi:10.1061/(ASCE)HY.1943-7900.0001767.

Muirhead, R.W., Collins, R.P., and Bremer, P.J. (2006). Interaction of Escherichia Coli and Soil Particles in Runoff. Applied and Environmental Microbiology 72(5), 3406–11. doi:10.1128/AEM.72.5.3406.

National Academies of Sciences and Medicine, E. (2016). Using Graywater and Stormwater to Enhance Local Water Supplies: An Assessment of Risks, Costs, and Benefits. National Academies Press.

Oschwald, M., Bechle, S., and Welke, S. (1995). Systematic Errors in PIV by Realizing Velocity Offsets with the Rotating Mirror Method. Experiments in Fluids 18 329–35.

Ouattara, N.K., de Brauwere, A., Billen, G., and Servais, P. (2013). Modelling Faecal Contamination in the Scheldt Drainage Network. Journal of Marine Systems 128 77–88. doi:10.1016/j.jmarsys.2012.05.004.

Pachepsky, Y.A. and Shelton, D.R. (2011). *Escherichia Coli* and Fecal Coliforms in Freshwater and Estuarine Sediments. Critical Reviews in Environmental Science and Technology 41(12), 1067–1110. doi:10.1080/10643380903392718.

PRB. (2019). 2019 World Population Data Sheet. https://www.prb.org/worldpopdata/.

Raffel, M., Willert, C.E., Scarano, F., Kähler, C.J., Wereley, S.T., and Kompenhans, J. (2018). Particle Image Velocimetry: A Practical Guide. 3rd 2018.; Springer International Publishing. doi:10.1007/978-3-319-68852-7.

Rahimpour, M., Bossi, F.C., Barannyk, O., Malavasi, S., and Oshkai, P. (2018). Flow-Induced Loading on and Unsteady Flow Structure in the Wake of Bluff Perforated Plates at Zero Incidence. Journal of Fluids and Structures 81. Elsevier Ltd 712–27. doi:10.1016/j.jfluidstructs.2018.06.007.

REALtime Aquifer Services. (2020). https://www.rasinc.org/.

Rodríguez-sinobas, L., Zubelzu, S., Perales-momparler, S., and Canogar, S. (2018). Techniques and Criteria for Sustainable Urban Stormwater Management . The Case Study of Valdebebas (Madrid , Spain). Journal of Cleaner Production 172. Elsevier Ltd 402–16. doi:10.1016/j.jclepro.2017.10.070.

Rodriguez, J.F., Bombardelli, F.A., Garcia, M.H., Frothingham, K.M., Rhoads, B.L., and Abad, J.D. (2004). High-Resolution Numerical Simulation of Flow Through a Highly Sinuous River Reach. Water Resources Management 18 177–99.

Sah, L., Rousseau, D.P.L., Hooijmans, C.M., and Lens, P.N.L. (2011). 3D Model for a Secondary Facultative Pond. Ecological Modelling 222. Elsevier B.V. 1592–1603. doi:10.1016/j.ecolmodel.2011.02.021.

Savage, B.M. and Johnson, M.C. (2001). Flow Over Ogee Spillway: Physical and Numerical Model Case Study. Journal of Hydraulic Engineering 127(8), 640–49.

Schoonover, J.E. and Lockaby, B.G. (2006). Land Cover Impacts on Stream Nutrients and

Fecal Coliform in the Lower Piedmont of West Georgia. Journal of Hydrology 331 371–82. doi:10.1016/j.jhydrol.2006.05.031.

Selvakumar, A. and Borst, M. (2006). Variation of Microorganism Concentration in Urban Stormwater Runoff with Land Use and Seasons. Journal of Water and Health 4(1), 109–24. doi:10.2166/wh.2005.063.

Selvakumar, A., Borst, M., and Struck, S. (2007). Microorganisms Die-Off Rates in Urban Stormwater Runoff. In Proceedings of the Water Environment Federation, 214–30. doi:https://doi.org/10.2175/193864707786619125.

Seric, I., Afkhami, S., and Kondic, L. (2018). Direct Numerical Simulation of Variable Surface Tension Flows Using a Volume-of-Fluid Method. Journal of Computational Physics 352 615–36.

Shilton, A. (2000). Potential Application of Computational Fluid Dynamics to Pond Design. Water Science and Technology 42(10–11), 327–34.

Shilton, A. and Harrison, J. (2003). Integration of Coliform Decay within a CFD (Computational Fluid Dynamic) Model of a Waste Stabilisation Pond. Water Science and Technology 45(2), 205–10.

Shilton, A., Kreegher, S., and Grigg, N. (2008). Comparison of Computation Fluid Dynamics Simulation against Tracer Data from a Scale Model and Full-Sized Waste Stabilization Pond. Journal of Environmental Engineering 134(October), 845–50. doi:10.1061/(ASCE)0733-9372(2008)134:10(845).

Shilton, A.N. and Mara, D.D. (2005). CFD (Computational Fluid Dynamics) Modelling of Baffles for Optimizing Tropical Waste Stabilization Pond Systems. Water Science

and Technology 51(12), 103–6.

Shrestha, N.K. and Wang, J. (2019). Water Quality Management of a Cold Climate Region Watershed in Changing Climate. Journal of Environmental Informatics 35(1), 56–80. https://doi.org/10.3808/jei. 201900407.

SonTek. (2020). FlowTracker® Wading Discharge Measurement Instrument. https://www.sontek.com/flowtracker2.

Soulsby, R. (1997). Dynamics of Marine Sands A Manual for Practical Applications. 1st ed. Thomas Telford Services Ltd.

St-hilaire, A., Duchesne, S., and Rousseau, A.N. (2016). Canadian Water Resources Journal / Revue Canadienne Floods and Water Quality in Canada: A Review of the Interactions with Urbanization, Agriculture and Forestry. Canadian Water Resources Journal / Revue Canadienne Des Ressources Hydriques 41(1–2),. Taylor & Francis 277–91. doi:10.1080/07011784.2015.1010181.

Stokes, G. (1851). On the Effect of the Internal Friction of Fluids on the Motion of Pendulums. Transactions of the Cambridge Phillosophical Society 9 8–106.

Tallon, P., Magajna, B., Lofranco, C., and Leung, K.T. (2005). Microbial Indicators of Faecal Contamination in Water: A Current Perspective. Water, Air, and Soil Pollution 166 139–66.

Teegavarapu, R.S. V and Chinatalapudi, S. (2018). Incorporating Influences of Shallow Groundwater Conditions in Curve Number-Based Runoff Estimation Methods. Water Resources Management 32. Water Resources Management 4313–27.

The City of Calgary Water Resources. (2011). Stormwater Management and Design

Manual. http://www.calgary.ca/UEP/%0AWater/Pages/Water-and-wastewater-systems/Storm-drainagesystem/%0AHistory.aspx.

Todeschini, S., Manenti, S., and Creaco, E. (2019). Testing an Innovative First Flush Identification Methodology against Field Data from an Italian Catchment. Journal of Environmental Management 246. Elsevier 418–25. doi:10.1016/j.jenvman.2019.06.007.

U.S. Army Corps of Engineers. Hydrological Modeling System HEC-HMS, User's manual. (2016).

U.S. Army Corps of Engineers. Hydrologic Modeling System HEC-HMS, Technical Reference Manual. (2000).

United Nations. (2018). 2018 Revision of World Urbanization Prospects. https://www.un.org/development/desa/publications/2018-revision-of-world-urbanization-prospects.html.

Vanaei, A., Guo, X., Wu, P., Richter, A., and Ng, K.T.W. (2021). Numerical Simulation of Water Quality and Self-Purification in a Mountainous River Using QUAL2KW. Journal of Environmental Informatics 37(1),. doi: 10.3808/jei.202000435.

Vergeynst, L., Vallet, B., & Vanrolleghem, P. (2012). Modelling Pathogen Fate in Stormwaters by a Particle-Pathogen Interaction Model Using Population Balances. Water Science and Technology 65(5), 823–32. doi:10.2166/wst.2012.818.

Versteeg, H.K. and Malalasekera, W. (1995). An Introduction to Computational Fluid Dynamics: The Finite Volume Method. Longman Scientific and Technical: New York, USA. Longman Scientific and Technical.

Wang, Y., Pandey, P., Zheng, Y., Atwill, E.R., and Pasternack, G. (2018). Particle Attached and Free Floating Pathogens Survival Kinetics under Typical Stream and Thermal Spring Temperature Conditions. AMB Express 8(100),. Springer Berlin Heidelberg. doi:10.1186/s13568-018-0626-z.

Wheeler, A.J. and Ganji, A.R. (2004). Introduction to Engineering Experimentation. 2nd ed. Prentice Hall.

Wu, B. and Chen, Z. (2011). An Integrated Physical and Biological Model for Anaerobic Lagoons. Bioresource Technology 102 5032–38. doi:10.1016/j.biortech.2011.01.076.

Wu, J., Rees, P., Storrer, S., Alderisio, K., and Dorner, S. (2009). Fate and Transport Modeling of Potential Pathogens: The Contribution from Sediments. Journal of the American Water Resources Association 45(1), 35–44. doi:10.1111/j.1752-1688.2008.00287.x.

Wu, L., Gong, M., and Wang, J. (2018). Development of a DEM−VOF Model for the Turbulent Free-Surface Flows with Particles and Its Application to Stirred Mixing System. Industerial & Engineering Chemistry Research 57 1714–25. doi:10.1021/acs.iecr.7b04833.

Wu, T., Qin, B., Ding, W., Zhu, G., Zhang, Y., Gao, G., Xu, H., Li, W., Dong, B., and Luo, L. (2018). Field Observation of Different Wind-Induced Basin-Scale Current Field Dynamics in a Large , Polymictic ,. Journal of Geophysical Research: Oceans 123 6945–61. doi:10.1029/2018JC014040.

Wu, T., Zhai, C., Zhang, J., Zhu, D., Zhao, K., and Chen, Y. (2019). Study on the Attachment of Escherichia Coli to Sediment Particles at a Single-Cell Level: The

Effect of Particle Size. Water 11(4),. doi:10.3390/w11040819.

Yakhot, V. and Smith, L.M. (1992). The Renormalization Group, the E-Expansion and Derivation of Turbulence Models. Journal of Scientific Computing 7(l), 35–61.

Zhang, K., Randelovic, A., Aguiar, L.M., Page, D., McCarthy, D.T., and Deletic, A. (2015). Methodologies for Pre-Validation of Biofilters and Wetlands for Stormwater Treatment. PLoS ONE 10(5), 1–21. doi:10.1371/journal.pone.0125979.

Zhang, Z. and Eisele, K. (1995). The Two-Dimensional Velocity Shift in PIV Flow Field Measurements. Experiments in Fluids 20 106–11.

Zheng, C., Yang, W., and Yang, Z.F. (2011). Strategies for Managing Environmental Flows Based on the Spatial Distribution of Water Quality: A Case Study of Baiyangdian Lake, China. Journal of Environmental Informatics 18(2),.